CONTRIBUTION OF RC INFILLS TO THE SEISMIC
BEHAVIOR OF STRUCTURAL SYSTEMS

A THESIS SUBMITTED TO
THE GRADUATE SCHOOL OF NATURAL AND APPLIED SCIENCE
OF
THE MIDDLE EAST TECHNICAL UNIVERSITY

BY

ERDEM CANBAY

IN PARTIAL FULFILLMENT OF THE REQUIREMENTS FOR THE DEGREE OF
DOCTOR OF PHILOSOPHY
IN
THE DEPARTMENT OF CIVIL ENGINEERING

DECEMBER 2001

Approval of the Graduate School of Natural and Applied Sciences

Prof. Dr. Tayfur ÖZTÜRK
Director

I certify that this thesis satisfies all the requirements as a thesis for the degree of Doctor of Philosophy.

Prof. Dr. Mustafa TOKYAY
Head of Department

This is to certify that we have read this thesis and that in our opinion it is fully adequate, in scope and quality, as a thesis for the degree of Doctor of Philosophy.

Prof. Dr. Güney ÖZCEBE
Co-Supervisor

Prof. Dr. Uğur ERSOY
Supervisor

Examining Committee Members

Prof. Dr. Sinan ALTIN

Prof. Dr. Uğur ERSOY

Prof. Dr. Güney ÖZCEBE

Prof. Dr. Haluk SUCUOĞLU

Prof. Dr. Tuğrul TANKUT

ABSTRACT

CONTRIBUTION OF RC INFILLS TO THE SEISMIC BEHAVIOR OF STRUCTURAL SYSTEMS

CANBAY, Erdem
Ph.D., Department of Civil Engineering
Supervisor: Prof. Dr. Uğur ERSOY
Co-Supervisor: Prof. Dr. Güney ÖZCEBE

December 2001, 162 pages

A large number of reinforced concrete buildings damaged in recent earthquakes required extensive amounts of strengthening as well as repairing. In recent earthquakes in Turkey it has been realized that inadequate lateral stiffness is one of the major causes of damage in reinforced concrete buildings. Many approaches and techniques have been developed and applied in the past thirty years to strengthen the existing structures. The simplest and the most effective way of improving the behavior of such buildings, where unsatisfactory seismic behavior is inherent in the system, is to provide an adequate number of structural walls. Such walls not only increase the lateral stiffness significantly, but also relieve the existing frames from the lateral loads.

The main objective of this research was to investigate the behavior and strength of reinforced concrete infilled frames (cast-in-place reinforced concrete panels) that are commonly used in Turkey for seismic strengthening. Most of the experimental research in this area was restricted to one-bay, one-story or two-story frames where very significant improvements in strength and stiffness were observed due to the addition of infill walls. However this is not the case for a retrofitted structure in which only a few bays will be infilled. Therefore, a test set-up for a multi-bay, multi-story specimen was developed in which only one bay would be infilled. This specimen was tested in a vertical position under reversed cyclic lateral loads. The test specimen was a three-bay, two story frame. The frame was detailed and built to have the deficiencies common to the buildings in Turkey (low concrete strength, inadequate lateral stiffness, inadequate confinement, lapped splices at floor levels etc.). The test frame could be considered to be 1/3 scale of a prototype building.

The reinforced concrete infill was introduced to the middle bay, after damaging the bare frame under reversed cyclic lateral loads. The specimen with the infill was tested to failure under reversed cyclic lateral loads. Since the main objective of the test program was to observe the contribution of the frame columns to the lateral load resistance, two special transducers were designed and manufactured to measure the axial force, shear and moment the base of frame columns. Analytical tools were used to predict the behavior of the test specimen.

Strength, stiffness, energy dissipation and story drifts of the test specimens were examined by evaluating the test results. In the analytical part of the study, the simulation of reinforced concrete infills by means of limit analysis and computer programs were studied; and the calculated values were compared with the experimental results.

Keywords: Seismic Rehabilitation, Repair, Strengthening, Reinforced Concrete Frames, Reinforced Concrete Infill Walls, Cyclic Loading, Force Transducer

ÖZ

BETONARME DOLGU DUVARLARIN YAPILARIN SİSMİK DAVRANIŞI ÜZERİNE ETKİLERİ

CANBAY, Erdem
Doktora, İnşaat Mühendisliği Bölümü
Tez Yöneticisi: Prof. Dr. Uğur ERSOY
Ortak Tez Yöneticisi: Prof. Dr. Güney ÖZCEBE

Aralık 2001, 162 sayfa

Yakın geçmişimizde olmuş depremler incelendiğinde, birçok betonarme binanın hasar görmüş olduğu gözlenmektedir. Bu binaların yeniden kullanılabilmesi için güçlendirilmesi ve tamir edilmesi gerekmektedir. Türkiye'nin yakın geçmişinde olmuş depremler göstermiştir ki yapılardaki hasarın temel nedenlerinden biri, yatay rijitliklerindeki yetersizlikdir. Mevcut yapıların güçlendirilmesi için son otuz yıldır birçok yaklaşım ve teknik geliştirilmiş ve uygulanmıştır. Sismik davranışları yetersiz bu binaların iyileştirilmesi için en basit ve etkin yol yapıya yeterli sayıda betonarme dolgu duvar eklemektir. Eklenen bu dolgu duvarlar yapının sadece yatay rijitliğini artırmakla kalmazlar aynı zamanda çerçeveleri yatay kuvvetler açısından rahatlatırlar.

Bu araştırmanın amacı, Türkiye'de sismik güçlendirme için yaygın olarak kullanılan betonarme ile doldurulmuş çerçevelerin davranış ve dayanımlarını incelemektir. Bu konudaki deneysel çalışmaların hemen hepsi tek açıklıklı ve tek katlı veya iki katlı deney elemanlarından oluşmaktadır. Tek açıklıktan oluşan deney elemanındaki tek açıklığı betonarme duvar ile doldurmak, çerçevede çok büyük bir rijitlik ve dayanım artışı sağlamaktadır. Ancak gerçekte durum böyle değildir. Mimari kısıtlamalar ve mevcut kullanımın engellenmemesi koşulu, binada sınırlı sayıdaki açıklıkta dolgu duvar yapılmasına izin vermektedir. Bu nedenle bazı açıklıkları dolgu duvarla doldurulmuş deneylerin yapılması önem kazanmıştır.

Bu deneysel araştırmada, bu amaca yönelik iki katlı, üç açıklıklı, yaklaşık 1/3 ölçekte bir çerçeve üretilmiştir. Sözü edilen çerçevede, ülkemizdeki binalarda sık rastlanan kusurların olmasına özen gösterilmiştir (yetersiz yanal rijitlik, düşük beton dayanımı, yetersiz sargı donatısı ve kat düzeyinde bindirmeli ekler).

İmal edilen çerçeve, depremi benzeştiren tekrarlanır tersinir yükler altında önemli hasar gözleninceye kadar yüklenmiştir. Daha sonra çerçevenin orta gözü, betonarme bir duvarla doldurulmuş ve oluşan deney elemanı aynı tür yükler altında test edilmiştir.

Araştırmanın temel amacı, yatay yük çeşitli aşamalarda, duvar ve çerçeve kolonları arasındaki dağılımını incelemek olduğundan, çerçeve kolonlarının tabanındaki eksenel kuvvet, kesme ve momenti ölçmek üzere özel kuvvet ölçerler geliştirilmiş ve imal edilmiştir.

Deney sonuçlarının değerlendirilmesiyle elemanların, dayanım, rijitlik, enerji tüketme ve göreli ötelenme özellikleri irdelenmiştir. Analitik kısımda ise yapı, limit analizi kullanılarak çözülmüş ve paket programlarla modellenmiştir. Hesaplanan değerler deneysel verilerle karşılaştırılmıştır.

Anahtar Kelimeler: Sismik İyileştirme, Onarım, Güçlendirme, Betonarme Çerçeveler, Betonarme Dolgu Duvarlar, Tersinir yükleme, Kuvvet Ölçer

Dedicated to my daughter *Ilgın Sultan Canbay*

ACKNOWLEDGEMENTS

This study was conducted under the supervision of Prof. Dr. Uğur Ersoy. I would like to convey my sincere appreciation to him for his helpful guidance and endless encouragement throughout this thesis. It was a great honor and opportunity having a chance to work with him.

I would like to extend my sincere thanks and appreciation to my co-supervisor Prof. Dr. Güney Özcebe. Throughout my academic studies, he was much more than a professor to me. It would be impossible to complete this study without his support.

I owe special thanks to Prof. Dr. Tuğrul Tankut for his valuable suggestions and concerns especially during the calibration of the force transducers. His addendum to this study was very significant.

Special thanks are due to Prof. Dr. Haluk Sucuoğlu for his valuable suggestions and criticism.

I would like to present my deepest appreciation to Prof. Dr. Mete Sözen for his help on the analytical studies and for his constructive criticism.

I also would like to convey my thanks to Prof. Dr. Sinan Altın, Prof Dr. Polat Gülkan and Prof. Dr. Engin Keyder for their valuable helps.

I cannot forget my dear friend Dr. Musa Onur Sonuvar. He gave endless assistance throughout the experimental phase of this study.

I also would like to extend my thanks to the METU-Structural Mechanics Laboratory staff; Hasan Metin, Hasan Hüseyin Güner and Murat Pehlivan.

I would like to thank to my wife Feyhan Fethiye Canbay and Ayşegül Askan for editing this thesis.

The financial supports from the Scientific and Technical Research Council of Turkey (INTAG 563) and Middle East Technical University (AFP- 99.03.03.08) are gratefully acknowledged.

Finally, I am deeply indebted to my daughter who gave a new meaning to my life, and to my wife for her endless support, encouragement, patience and love throughout this study.

TABLE OF CONTENTS

LIST OF TABLES

TABLE

LIST OF FIGURES

FIGURE

LIST OF SYMBOLS

A	Axial Force applied on the transducer
A	Gross cross-sectional area
A_c	Area of the column section
A_G	Grid area of strain gages
b_w	Width of the wall
d	effective depth of the wall
E	Elastic modulus of concrete
F	Applied forces calculated from the load cell readings
f_c	Concrete compressive strength
f_{ctf}	Flexural tensile strength of concrete
f_y	Yield stress of steel
H	Distance between the lateral load and base of the infill wall
I, I_g	Moment of inertia of the gross concrete section
I_{cr}	Moment of inertia of the cracked concrete section
K	Gage factor of the strain gages
L	The center-to-center distance between the members
M	Moment applied on the transducer
M_{cr}	Moment corresponding to the flexural cracking of the infill wall
N	Axial load applied on the section
p	The number of calibration stages
P	The lateral load
P'_G	Grid power density of strain gages
Q_w	Strength of monolithic wall
R	Resistance
R_B	Bridge resistance
R_G	Gage resistance
S	Shear Force applied on the transducer
$[S]$	Calibration matrix
x	The quantity actually measured

T	Torque
V	Excitation voltage (supply voltage) of Wheatstone bridge
V	Shear force on the section
V_{cr}	Shear cracking strength
V_{fcr}	Shear corresponding to the flexural cracking of the infill wall
y	The quantity to be determined
y	Distance between the centroid and extreme tension fiber of the section
ΔE	Output voltage of Wheatstone bridge
ΔR	Resistance change of strain gages
δ	Lateral displacement
ε	Equivalent output strain of strain gages
ϕ	Diameter of the bars
θ	Plastic hinge rotation
σ	Stress
τ	Nominal shear stress
ν	Poisson's ratio

CHAPTER 1

INTRODUCTION

1.1 GENERAL

Damage in reinforced concrete buildings can be caused by gravity loads, imposed deformations (shrinkage, temperature change, settlement, etc.), earth or water pressure, wind or seismic loading. Damage can also be caused by what is called accidental loading; like, gas explosion, truck impact, bomb etc.

Buildings, which have suffered damage under various loads, have been rehabilitated by repairing and strengthening. Among all types of loads, earthquakes caused the most extensive damage. Therefore, seismic rehabilitation has been considered as major rehabilitation projects. In Turkey, extensive structural rehabilitation has been done after the major earthquakes, starting with 1992 Erzincan Earthquake.

As a result of these rehabilitation projects, there has been a significant increase in research related to rehabilitation. The research, especially the experimental research, has been focused on the structural rehabilitation of structures damaged by the seismic action. In recent years, rehabilitation of undamaged buildings to upgrade their seismic performance has been a popular research area.

Seismic rehabilitation can be defined as the operation to upgrade the performance of the structural system or some members to the specified level. The aim in seismic rehabilitation is to reduce the vulnerability of the structure during an earthquake.

"Seismic Repair" is the structural rehabilitation of the damaged structure or structural member to ensure satisfactory performance under the seismic action foreseen. "Seismic Strengthening" is the rehabilitation of the undamaged structure or the structural members to upgrade the performance to a specified level under the seismic action [1,2,3,4].

Until recently, the design and construction leading to strengthening of the buildings have been accomplished on the basis of experience and engineering judgment alone, since no guidelines existed. Various materials and techniques have been used in the rehabilitation of buildings. These techniques have been developed as a result of analytical and especially experimental research. In recent years, attempts are being made to draft guidelines in the light of experience gained and the research data. A good example is the attempt made by FEMA in USA [65].

1.2 SEISMIC REHABILITATION STRATEGY AND TECHNIQUES

The main objective of the seismic rehabilitation can be:

- to bring the structural performance to the level before the damage,
- to upgrade the seismic performance of the structure to a level which will ensure satisfactory performance under the seismic action specified,
- to reduce seismic response, to reduce the vulnerability under the seismic action specified.

Before rehabilitation, the performance of the structure, as it is, should be established. If there is damage, cause or causes of the damage should be correctly established. The rehabilitation should aim to correct the deficiencies in the building and the added strengthening elements should be able to work together with the existing ones. The repair/strengthening technique should not create major problems during construction and the new elements should not interfere with the function of the building.

In Figure 1.1, basic strategies and operations for seismic rehabilitation has been summarized. This figure is taken from Sugano's work [4].

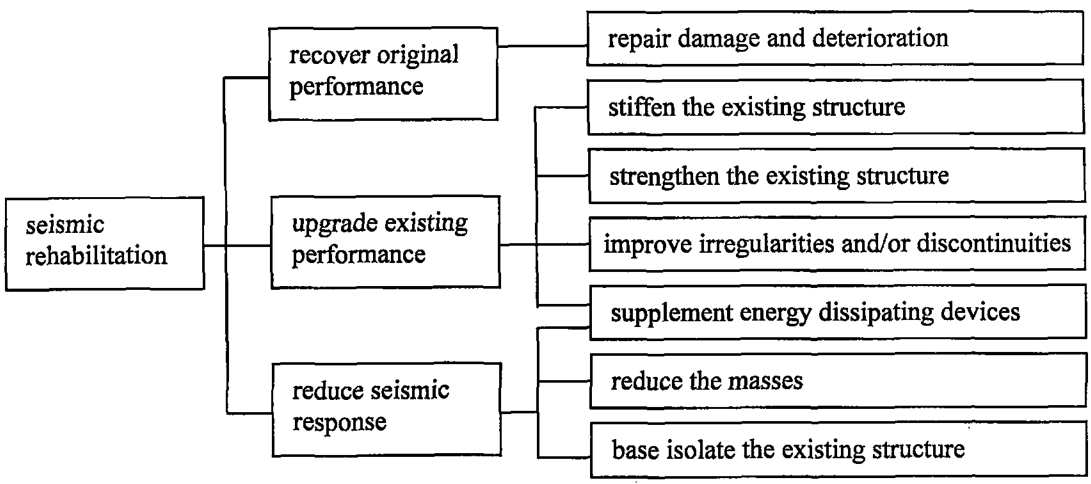

Figure 1.1 Seismic rehabilitation strategy and measures (Sugano [4])

The aims of seismic strengthening can be; (a) to increase the lateral strength and stiffness, (b) to increase the ductility and (c) to increase both strength and ductility. The aims outlined can be reached either by repair/strengthening of individual members or by improving or chancing the lateral load resisting system. In Turkey, second one is more commonly used since the main problems are:

- the building does not have adequate lateral stiffness,
- members are not ductile (lack of confinement),
- detailing is bad,
- concrete quality is low.

To summarize, the existing frames in buildings are not suitable to resist lateral loads. Therefore, in what is called "System Improvement", a new lateral load resisting system composed of structural walls is formed.

Figure 1.2, which is taken from Sugano [4], summarizes the most commonly used strengthening methods.

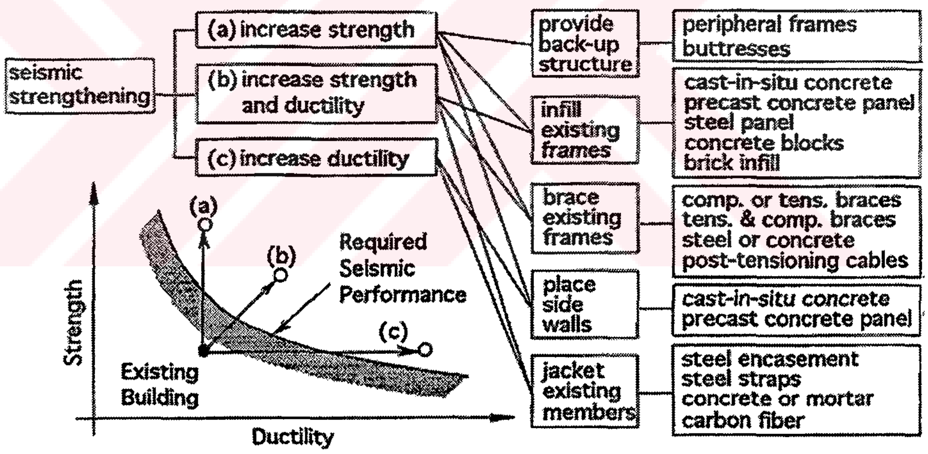

Figure 1.2 Commonly used strengthening methods (Sugano[4])

Turkey is a country having a high earthquake risk, i.e., 89% of population, 91% of land, 98% of the industry, and 92% of the dams are located in seismically active zones [5]. In recent earthquakes, it has been realized that inadequate lateral stiffness is the major cause of damage in buildings in Turkey. Undesirable seismic behavior due to well-known weaknesses of the structural system, such as strong beam-weak column, soft story, short column etc. have also led to considerable damage. Many approaches and techniques have been developed and applied in the past to strengthen existing structures. The simplest and the most effective way of improving the behavior of buildings, where unsatisfactory seismic behavior is inherent in the system, is to provide an adequate number of structural walls. Such walls not only increase the lateral stiffness significantly, but also relieve the existing frames from the lateral loads, so that the weaknesses in frames such as soft story, short column etc. cannot lead to undesirable behavior.

Seismic provisions in Turkey, like in most modern building codes, are designed to provide adequate stiffness, strength and ductility to the structure. The structure should posses adequate stiffness to resist minor earthquake without any architectural or structural damage. The structure should possess adequate strength to resist moderate earthquake with some architectural damage but without any significant structural damage. The structure should possess adequate ductility to prevent collapse during a major seismic event. But this design philosophy does not necessarily apply to important structures like hospitals, fire stations, power stations, communication centers, or public buildings, which should be functional after the seismic event. However, if the performance of such buildings in the previous major earthquakes are investigated, it will be seen that the many of them were unfunctional after the earthquakes. In Erzincan Earthquake (1992), all the hospital buildings collapsed, and in İzmit Earthquake (1999) one of the major hospital buildings of Turkey was severely damaged and became unoperational after the earthquake.

The characteristics of typical buildings in Turkey include flexible columns, soft stories, non-ductile detailing and strong beam – weak column systems. The main design deficiencies inherent in the columns are due to inadequate lap splice or insufficient transverse reinforcement or both. Lap splice lengths in most concrete columns are often inadequate to develop the yield strength of the spliced bars in tension. In addition, in the absence of adequate confinement, the bond strength of these lap splices in plastic hinge regions starts to degrade once the cover concrete is damaged. Insufficient transverse reinforcement and poor reinforcement detailing cause inadequate flexural ductility. Due to these simple but very important deficiencies, above-mentioned buildings sustained severe damage in recent earthquakes.

Upgrading the stiffness and strength is the most used approach in the seismic rehabilitation of low to medium-rise buildings. Even if sufficient ductility is provided, adequate strength is required to reduce inelastic displacements. The improved resistance should be designed not only to prevent collapse but also to limit lateral displacements so that architectural and mechanical elements within the building will not be severely damaged, since the non-structural damage (infills, plaster suspended ceilings, windows, doors, electric and sanitary infills, etc.) amounts to a high percentage in the total cost of the damage.

1.3 Object and Scope of the Study

In Turkey, rehabilitation of buildings damaged in earthquakes by introducing reinforced concrete infills, has been commonly used in the last decade.

First application of infilled frames as seismic rehabilitation by the METU group was in 1970, after the Bartın earthquake. Experimental research on infilled frames was initiated at METU right after this application. Initial tests were performed on one bay two story frames, in which the frames were designed and constructed following the current seismic code. In recent years, research initiated by METU and carried on at METU and Boğaziçi University included frames which had the common weaknesses encountered in buildings in Turkey. These were:

- insufficient lateral stiffness,
- weak column-strong beam connections,
- insufficient reinforcement detailing which included inadequate anchorage length for beam bottom bars, inadequate lap length of column longitudinal bars made at the floor level and inadequate confinement at the ends of beams and columns,
- poor and low strength concrete.

In all test specimens, both bottom and top stories were infilled. In some tests the infill was introduced to undamaged frame whereas in others the infill was applied to damaged frames.

The tests made at METU provided very valuable data with regard to the behavior, strength and stiffness of frames infilled with reinforced concrete cast in panels connected to the frame with proper dowels.

In practice, only selected bays of the frame are infilled. In the rehabilitation of structures after the earthquakes, METU group usually did not repair the moderately damaged columns and beams assuming that these frame members would not be subjected to critical moments and shears due to the presence of the infills which would act as structural walls.

Although test data is available on the behavior of individual infilled frames, no test data is available on the behavior of frames in which only selected bays are infilled.

The main objective of this study was to observe the behavior of frames in which only some of the bays are infilled. For this purpose a two story, three bay frame was tested under reversed cyclic lateral load. In the test specimen only one bay was infilled. The frame members had some of the common weaknesses encountered in buildings in Turkey. It was intended to study the behavior of such structures, emphasizing on the distribution of the lateral forces between the wall and the columns.

The infill was applied to the frame, which was damaged under reversed-cyclic lateral load. Special transducers were developed to measure the axial load, moment and shear at the bases of the two exterior columns.

The scope was limited to testing and analyzing one type of structure designed and built at the Structural Mechanics Laboratory of METU. The design of a force transducer for accurately measuring the internal forces of the first story columns of the test specimen was the most important phase of the research. This study involved the design, fabrication, calibration and installation of the force transducer.

CHAPTER 2

LITERATURE SURVEY

There are many different repair and strengthening methods as mentioned in previous chapter. The results of considerable amount of experimental research have been reported in literature. In these research programmes, the behavior of reinforced concrete and steel frames, infilled with brick or concrete blocks or with reinforced concrete panels were investigated in a more or less systematic way. The main parameters investigated were [6]:

- Aspect ratio of infills
- Number of stories and bays of the frame
- Detailing of columns
- Reinforcement in infills
- Connection of infill to the surrounding frame
- Number of panels
- Axial load level of columns
- Type of loading (monotonic or reversed cyclic)
- Dimensions and location of openings in the infill
- Relative stiffness of bare and infilled frames
- Material strength of the infill

Since the main objective of this study is reinforced concrete infill walls, literature survey is concentrated on such infills. The purpose of this review part was to determine the level of knowledge related to reinforced concrete infilled frames. In the following pages the review related to reinforced concrete infilled frames will be presented in chronological order.

Ersoy and Uzsoy (1971) [7] published a report presenting their experimental results and analytical studies on reinforced concrete frames infilled with cast-in-place reinforced concrete panels. They tested nine one-story, one-bay frames with reinforced concrete infills under monotonic loading. They concluded that the presence of the infill increased the lateral load capacity of the frame by approximately 700% and reduced the lateral displacement at failure by 65%. They also concluded that connection between the infill and the frame was not so important under monotonic loading. For the analytical study, the infills were modeled with struts having a width equal to thickness of the infill.

Higashi and Kokusho (1975) [8] published a report investigating three retrofit techniques; addition of infill walls, addition of wing walls and concrete jacketing of columns. Later on, effectiveness of each method was assessed in relation to strength and ductility. For the case of infill walls, two frames were tested. In the first frame, wall was cast monolithically with the beams and the columns; whereas in the second frame, perimeter of the wall was jointed by concrete shear keys. In both cases, the wall reinforcement was not anchored to the surrounding frame. According to the test results, the strength of the infill wall was close to the strength of the monolithic wall. The monolithic wall failed in bending; whereas, the infilled wall failed by shear failure of the columns following the failure of the shear keys.

Kahn and Hanson (1979,1980) [9,10] investigated three strengthening techniques for framed structures which were; monolithically cast wall, single precast panel wall, cast-in-place wall and multiple precast panel wall. They also tested a reference reinforced concrete frame with no infilled wall. Each infilled wall greatly strengthened and stiffened the single story reinforced concrete frame. The cast-in-place wall demonstrated nearly the same nominal ultimate shear stress as the monolithically cast wall. The cast-in-place wall failed at its connections to the overhead beam that led to a shear failure of the columns. Therefore, the cumulative energy dissipation of this specimen was one-half of the monolithic structure. The columns failed in shear. To minimize this column shear problem, column confinement by special reinforcement may be considered (Higashi and Kokusho [8]).

Higashi et al. (1980) [11] studied 13, one third scale, one-bay,one-story reinforced concrete frames (with inadequate ties in columns) using 10 different types of strengthening methods. The methods were as follows; infilled with reinforced concrete cast in place wall, precast concrete wall panels, precast concrete wall panels with door openings, steel bracing, steel frame, and steel truss. The lateral load carrying capacities of all strengthened specimens came between that of the pure frame and that of the monolithic wall. Particularly, the strength of specimens infilled with reinforced concrete cast-in-place walls or with precast concrete panels without opening behaved well. Authors also suggested an analytical model for the analysis of the frames. In this model, the columns and beams were considered to be rigidly connected to the frame and the infill walls or precast concrete panels were idealized as compressive bracing or, compressive bracing plus tensile bracing. Both ends of these bracing members were assumed to be pin connected with or without springs. The area of the bracing depended on many factors as given in the paper.

Adachi and Nakanishi (1980) [12] tested twenty framed shear wall models of reinforced concrete. Influences of load history and hoop reinforcement were shown by means of the tests. It was observed that, a gradual decrease in load capacity could be maintained provided that sufficient hoop reinforcement was employed. The object of the paper was to discuss "force-deformation" hysteresis curves of reinforced concrete shear walls referring to the test results. Main parameters were the height of wall (2m & 3m), the thickness of wall (5 cm to 10 cm), longitudinal reinforcing bars in columns, web reinforcement ratio in the column (0.22 to 1.02%) and reinforcement ratio of the wall (0.23 to 0.70%).

Experimental study revealed that the ductility of shear wall subjected to monotonic loads was different from that subjected to cyclic loads, and the hoop reinforcement of the surrounding columns was effective to keep the horizontal and vertical load capacities beyond the maximum.

Sugano and Fujimara (1980) [13] tried to determine the seismic behavior of reinforced concrete frames strengthened by using various types of infilling and bracing techniques. For this purpose, they tested ten one-story, one-third scale frames. Test results showed that all these techniques improve the earthquake resistance of existing structures.

The authors concluded that the aims of aseismic strengthening should be:

- *to increase lateral force capacity*: It is effective for low and middle-height buildings. However, it requires large amount of lateral force capacity so that they may resist the considerably high seismic forces.
- *to increase the ductility and toughness*: For this purpose, adequate strength may also be required to avoid extensive inelastic displacement even if the ductility or toughness of the building is satisfactory.
- *to balance the stiffness and strength of structural elements*: It can be simultaneously satisfied when the first one is accomplished by means of an appropriate design.

Five of the frames were strengthened using different infilling techniques; two frames with bracing techniques, one bare frame, and two frames with monolithic walls. The last three specimens were reference specimens.

- According to test results, reinforced concrete infilled frames behaved similar to shear walls. They provided highest strength and stiffness. The degradation of strength after the maximum load was moderate.
- Steel elements did not provide as much strength as infilled walls. Braced frames had the advantage of great energy absorption and/or displacement ability, while the steel walls indicated higher strength but significant loss of capacity due to the failure of joints. The authors concluded that more attention must be paid to the joints so that steel elements may sufficiently develop their capacities.
- All the strengthened frames finally failed by the failure of columns.

- Generally the smaller the increased capacity, the larger the displacement capacity is.
- It is desirable to provide connectors all around the existing frame.

Ohki and Bessho (1980) [14] tested five one-story, one-bay, one-half scale reinforced concrete frames in order to obtain design data for aseismic strengthening of the existing Morioka Station building of the Japanese National Railway (JNR). Two of the test frames were strengthened with reinforced concrete infilled walls, and in the other one, the existing columns alone were strengthened with steel plate encasing.

For the old Morioka Station building, the strengthening method was studied considering not only the seismic resistance, but also the functionality and ease of construction. Finally, methods of aseismic strengthening proposed were:

- introduction of additional infilled walls in a part of the existing frame in order to increase the aseismic strength of the entire frame
- strengthening of all independent columns with steel plates in order to improve the ductility of the entire frame

The shear force acting on the infilled walls was transferred by means of mechanical anchors. Hereupon, the column at the story level could punch the walls. The punching shear became more severe with the decreasing shear force transfer of the mechanical anchors. As a result, they concluded that:

- The connection of infilled wall to the existing frame should have sufficient strength and ductility.
- Top and bottom of the column should be sufficiently reinforced to prevent shear failure.
- The shear walls should be thick enough and reinforced for shear sufficiently to prevent failure by stress concentration.

For the strengthening of columns with steel plate encasing, initially, finishing materials were removed. Then, existing column was encased with relatively thin steel plates, with the seams between the plates being spot-welded and the clearances between the existing column and the plates being grouted with mortar. This method, which was intended only for shear strengthening of columns, served to improve the ductility of the entire frame without changing the strength and stiffness of the existing frame considerably.

Hayashi, Niwa and Fukuhara (1980) [15] worked on the strengthening techniques to increase strength, stiffness or ductility. The study presented had two schemes; infill walls and column jacketing. Infill walls increased strength and stiffness, whereas column jacketing increased the ductility. Both methods proved to be effective.

It has been recognized that frames with infills have more strength and stiffness than the frames without infills. Hence, six one-bay, one-story frames with infilled walls were tested. First two specimens were the reference specimens with no infills and the monolithic wall with the surrounding frame. The connections between the frames and walls of the remaining specimens were provided by the following techniques; small concrete shear keys, steel pieces anchored to beams with roughened surfaces, steel pieces anchored to inner surfaces without roughening the columns and beams and steel pieces anchored to inner surfaces and roughening.

At large displacements, steel pieces sheared out. Their load capacities were 0.5-0.72 times that of the monolithic specimen. It was concluded that infilled walls could be remarkably effective for strengthening of the existing reinforced concrete buildings, which lack of strength and stiffness. According to experimental results, infilled walls increased the lateral resistance and stiffness of buildings, whereas column jacketing increased shear strength and ductility. Column jacketing has been applied by means of mortar and welded wire fabric.

Sugano (1980) [16] who worked on infilled frames, proposed the following guidelines from the viewpoint of increased strength of infilled frames with proper dowel connections.

- when the required shear strength was more than 60% of that of the monolithic wall dowels should be designed to have a strength of more than 1 MPa,

- a wall should have the strength more than $0.4Q_w$ or $0.31\sqrt{f'_c}$ (MPa) even without any connection in between the infill and the frame,

Based on the experimental data related to infilled frames, Sugano reached to the following conclusions:

- A very large variety of materials (reinforced concrete, clay bricks, reinforced concrete precast panels, lightweight concrete panels) were used for infilling. Infills were either plain or reinforced, while several techniques of connection between infill and frame were used. In case of reinforced concrete frames infilled with reinforced concrete infills, a lateral resistance of approximately 5 times that of the bare frames was recorded.
- The presence of infills caused considerable increase of the lateral stiffness. According to the tests, the stiffness of frames infilled with reinforced concrete walls was several times higher than the stiffness of frames infilled with brick or concrete blocks.
- In all cases, very pronounced pinching effect was observed. Therefore, the area under the hysteresis loops was small.

Higashi, Endo and Shimuzu (1982) [17] have studied the effects of strengthening on one-story and three-story frames with infilled shear walls or wing walls. They investigated the effect of partial strengthening on multiple bay structures. The experimental results of strengthening schemes utilizing both precast and post-cast infilled walls and wing walls were presented. Totally, eight frames were tested: four one-bay, three-story specimens and four two-bay, three-story specimens. Two strengthening techniques were used; (a) addition of infilled shear walls and (b) addition of wing walls. For each type of specimens, a bare frame and monolithic frame-wall were tested as reference specimens. According to test results:

- specimens, strengthened with an infill wall had a behavior similar to that of monolithic walls,

- the specimen with one-bay yielded in flexure, whereas the specimen with two bays failed in shear. The wall panel finally split along the anchor bolts and then the column failed in shear,
- specimens strengthened with wing walls experienced mortar crushing at large displacements.

A numerical analysis was made for each of the test structures. The beams and columns were modeled as frame members while walls were modeled as diagonal braces. Overall, the analytical results were satisfactory to predict the behavior under monotonic loading.

Higashi, Endo and Shimuzu (1984) [18] reported tests on eight three-story, one-bay frames. They used six strengthening methods that proved to be effective in a previous study of thirteen one-story, one-bay specimens.

In the experiments, an axial load was applied to each column. Lateral loads applied at each level were the same. The original specimen was detailed with inadequate transverse reinforcement. Each single-bay, three-story frame with poorly detailed column reinforcement were infilled with either precast concrete panels, with steel bracing or by introducing steel frame or post cast walls. The effects of these infilling techniques were investigated through the tests under lateral cyclic loading. The joints between the precast panels and the existing frames were filled with expansive mortar, and precast panels and steel members were attached to existing beams by steel pieces. At the end of the test program, the following conclusions were reached:

- three-story, full-width walls failed in flexure, whereas one-story full-width walls failed in shear. The reason was the increased moment arm of three-story system,
- post cast walls resulted in the greatest increase in initial stiffness, then comes the precast walls, steel braces, and steel frame,
- there was no appreciable increase in strength for the specimen retrofitted with precast wing walls. However increase in displacement capacity was significant,

- the specimens with steel-frame, steel-braces and four precast concrete panels showed not only high strength but also improvement in ductility.

Aoyama, Kato, Katsumata and Hosokawa (1984) [19] studied the behavior of frames with post cast reinforced concrete walls, used for strengthening. The improvement in post casting construction methods resulted in increase in strength and decrease in deformation capacity.

Totally, twelve specimens were tested. All specimens were single story, single bay walls with a very stiff top girder, to simulate the confining effect of multi-story shear walls (although overturning effects are not simulated). Through the tests, following parameters were considered; boundary column width (wider columns to simulate adjacent panel), amount of column reinforcement, size and location of openings in post-cast wall, type of anchor (wall to frame connection).

In all specimens, flexural cracks occurred at the column base, and shear cracks were observed on the infills. Bond cracks were observed on columns along the spliced bars. Walls with an opening suffered extensive shear cracks on both sides of the opening. At the maximum load, all specimens had extensive shear cracks in the wall. Specimens with weak columns developed extensive flexural cracks at the column base. The failure mechanism for the specimens were in the manner of pulling-out of spliced bars at the base of the wall or shear compression / direct sliding shear. Walls with an opening failed by direct shear on both sides of the opening, failure extending into adjacent columns.

Chemical anchors seemed stronger than the mechanical anchors, which were observed to be weak, particularly in tension. From the test results, following conclusions were drawn:

- shear strength increased with the confining effect for both post cast and monolithic walls. The confining effect in the form of increased flexural strength was more effective than that in the form of increased stiffness of the side columns,

- the shear strength of post-cast walls was less than that of the corresponding monolithic shear walls,
- post-cast walls may fail by sliding along the interface of the old and new concrete,
- behavior of chemical anchors was generally satisfactory, and it was superior to the mechanical anchors particularly in tension.

Liauw and Kwan (1985) [20] developed a plastic analysis for infilled frames with three types of interface conditions. Their study was based on tests and nonlinear finite element analysis. In the analysis; stress redistribution towards collapse and conditions at the infill frame interface were considered. The following assumptions were made:

- for fully-integrated infilled frames, the collapse load is governed by the strength of the infilled frame, and interface,
- for semi-integral infilled frames, the collapse load is normally governed by the strength of interface,
- for non-integral infilled frames, the collapse load is governed only by the strength of the frame.

Jirsa and Kreger (1989) [21] summarized tests on retrofitting schemes including infill walls. They tested four one-bay, one-story specimens with infill wall. Although the strength of the frame was increased by the addition of the infill wall, the failure mode of all the three specimen was brittle. In specimens with full infills, failure occured in the columns at regions where column bars were spliced. In specimens with door openings, tension failure occured along the length of each wall. In the infill with window openings, failure was controlled by concrete crushing near the corners of the openings and by shear failure in the column.In the last specimen, three longitudinal bars adjacent to each of the columns was placed to supplement the column reinforcement. Both the strength and ductility of this retrofit scheme was greater than that of the other specimen with the door opening.

Altın, Ersoy and Tankut (1990,1992) [22,23,24] tested fourteen one bay, two story specimens to investigate the behavior and strength of reinforced concrete frames strengthened by reinforced concrete infills. Infills were introduced to undamaged frames, which were properly designed, detailed and constructed according to the seismic code. Main variables were the pattern of infill reinforcement, the connection of the infill to the frame, effect of axial load and strength of the frame columns.

All specimens were tested under reversed cyclic lateral loads. As a result of the tests, the following conclusions were reached by the authors:

- the infills, which were properly connected to the frame members, increased both the strength and the stiffness significantly.
- column strength and axial load on the column improved the behavior and increased the strength of the specimens.
- the most important problem faced in practice was the connection of the infill to the existing frame. The connection detail should not only provide satisfactory behavior but also should be economical and practical.

Valluvan, Kreger and Jirsa (1993) [25] reported an experimental investigation on improving the behavior of frames with spliced bars at the floor levels. The benefit of strengthening the nonductile concrete frames might be limited by the failure of splices in the existing column. For this problem, various techniques were employed to provide continuity and confinement along the splice region.

Jirsa et al. tested twelve specimens. One of the specimens was not strengthened to provide reference; the other eleven were strengthened by either providing continuity of the splices or improving confinement. Testing involved applying a tensile load followed by the application of a compressive load of equal magnitude. The splices were located at the midheight of the specimen. Continuity was provided over the splice region of two specimens by welding the bars together with a #3 bar serving as a filler.

The column without additional ties displayed unstable loops (90-degree hook opened at the onset of spalling of the concrete). The behavior of the second specimen with proper hooks in the ties was very satisfactory. Three specimens were strengthened using steel angles and straps, whereas other three specimens were confined with external ties made of U-shaped bars spaced at some distance on centers and with overlapping legs welded. Lastly, one specimen was provided with additional internal ties. For this purpose, cover was chipped of at some spacing, and U-shaped bars were lap welded, and cover was replaced with a non-shrink grout.

According to the test results, welded splices with additional ties, steel angles and straps (grouted), external ties (grouted) seemed superior as compared to others. Grouting seemed to be essential.

Miller and Reaveley (1996) [26] performed feasibility studies on different methods of seismic upgrading. The results indicated that adding new concrete structural walls would provide the most economical method for upgrading without significant impact on the interior floor plan of the building. Three methods of seismic upgrading were investigated as a part of this feasibility study:

- addition of new structural steel braced frames incorporating the existing steel frame of the building
- base isolation
- addition of reinforced concrete infill walls

The feasibility study indicated that first method would be quite costly. Cost estimates indicated that the base isolation method for upgrading was significantly more expensive than the other methods considered. So, it was decided to add new concrete shear walls. The thickness of the wall varied from 250 mm at the roof of the building to a maximum 800 mm at the lower levels of the building.

Gregorian and Gregorian (1996) [27] presented the strength evaluation of two VA Hospital Buildings, which were planned to undergo major renovations. Various options were considered for seismic strengthening of the two existing R/C frame structures built in 1930's without any seismic load design considerations. Two alternatives were studied:

- adding interior structural walls, exterior buttresses, steel cross bracings, and base isolation proved to be complex, costly, and undesirable for architectural reasons,
- use of peripheral shear walls, attached to existing concrete frames was considered as a final solution for strengthening.

Prior to final design, they reviewed the following options.

- adding of buttresses at various locations at the periphery of the building. The buttresses would create an unappealing architectural image, and distinguish the two buildings as being the only ones retrofitted from 63 structures on the site. So, this solution was not accepted by the architects for aesthetic reasons.
- base isolation proved to be technically complex and costly,
- use of "K" or "X" steel bracings was also considered, and not selected due to nonuniformity created by combination of steel and concrete elements for transfer of horizontal loads from the bracings to the floor. The reason for rejection was cost.
- adding exterior concrete structural walls was selected as the final solution. Interior or peripheral structural walls were also considered. Interior walls cause loss of space and create permanent walls disrupting functional use. It was not possible to locate areas where shear walls could be continuous in all floors without causing major changes in spaces in use. This solution created numerous problems in the interior space planning and was canceled,
- reinforcing the exterior walls: Concrete peripheral structural walls could be placed in existing walls without the inconveniences of permanent interior walls. Dowels were installed in to drilled holes through sides of columns and top and bottom of exterior beams. The wall would be continuous from top floor down to the basement wall. It was recommended to use epoxy-anchored dowels instead of expansive anchors. The epoxy-anchored dowels would maintain a better grip under cyclic loading of the shear walls during earthquake motion.

Shear walls were distributed in a symmetrical pattern in both directions of building. Symmetrically positioned shear walls of equal and symmetrical shape, helped to minimize the effect of planar torsional stresses.

Addition of concrete shear walls to existing concrete frame structures is an economical and relatively inexpensive solution; especially, if there is space to locate the new shear walls behind existing facade walls. Compared to steel bracings, which will need attachment of steel elements all around to columns and beams and creating complex forms at window openings, the concrete shear walls are less complex and less expensive.

Phan and Lew (1996) [29] developed hysteresis failure models and incorporated into computer program IDARC for assessing seismic performance of strengthened lightly reinforced concrete frames. They selected a total of fifty five specimens and performed multiple-variable regression analysis to obtain empirical expressions for stiffness degradation, strength degradation and pinching factor in terms of the physical properties (material, geometric properties and reinforcement details) of the specimens. The comparison of the results obtained from computer program and results of the experiments were satisfactory. They conducted also a parametric study to assess the sensitivity of the thickness of the wall, the amount of wall reinforcement and the area of connecting anchor to the seismic behavior of lightly reinforced concrete frames. They concluded that the maximum story drifts of infilled frames decreased with increasing the wall thickness. But after the wall thickness exceeds 3/5 of the column width, story drift remained at 4%. The maximum shear strength increased parabolically with increasing wall thickness. Neither the story drift nor shear strength are affected by increasing the infilled wall reinforcement ratio. The maximum shear force appears to increase slightly as the anchor area is increased. Story drift increases at different rates as the anchor area increases.

There has been a tremendous increase in recent years of strengthening buildings for improved seismic performance in regions of high and moderate seismicity, both after and in anticipation of strong Earthquakes. So many structural engineers need guidance on the art of strengthening existing buildings. **Wyllie (1996)** [31] intended to give simple and straightforward guidance to engineers on the advantages and disadvantages of various strengthening strategies and directions to follow.

The selection of a seismic strengthening scheme depends on many factors. The scheme must correct the identified deficiencies in the existing building's seismic resisting system and the new strengthening elements must be structurally compatible with the existing structural system. It must be functionally and sometimes aesthetically compatible and complimentary to the existing building.

Existing columns with short compression splices may become a weak link. A strengthening solution must correct the identified deficiencies in the existing structural system, to satisfy the established performance criteria of the owner and be compatible with functional and other building-specific criteria. Economy is best achieved by finding solutions with minimal disruption to building system and ease of construction.

Türk (1998) [63] conducted an experimental study to investigate the effect of adding cast-in-place reinforced concrete infills to the damaged frames. Totally, nine one-third scale, one-bay, two-story specimens were tested under reversed cyclic loading. Following main conclusions were presented by the author:

- Success of the reinforced concrete infills depends mainly on the efficiency of connection between infill and frame. Success of the connecting dowels mainly depends on the workmanship at the site.
- Inadequately confined lapped splices at the story levels decrease strength and stiffness of the infilled frames.
- The level of damage in the frames seemed not to have much effect on the behavior of the reinforced concrete infill walls.

- The lateral strength of the infilled frames was about 8 to 13 times greater than that of the bare frame. The initial stiffness of the infilled frames was 19 to 24 times that of the corresponding bare frames.
- Amount of column reinforcement seemed to be effective in the behavior since the failure modes first initiated in terms of flexure.

Sonuvar (2001) [59] tested five two-story, one-bay, 1/3 scale reinforced concrete frames under reversed cyclic loading to examine the behavior of repaired frames. Heavily damaged bare frames were rehabilitated by cast-in-place R/C infill walls. In the construction of bare frames, the following common weaknesses were considered; lack of confinement, poor concrete quality, strong beams - weak columns, inadequate lapped splices, poor details for beam bottom reinforcement and ineffective ties.

- The introduction of infill walls to the damaged frames significantly increased both the stiffness and strength of the test frames.
- The local strengthening techniques applied in addition to reinforced concrete infills were quite effective. Partial steel jacketing improved the performance of the lapped splice region. Considering the performance, economy and ease in construction, introduction of boundary columns to the infills, seemed to be better solution compared to the concentrated boundary reinforcement.
- The quality of the frame concrete is influential on the anchorage of the connecting dowels.
- The magnitude of the story drift index was significantly reduced as a result of the rehabilitation studies.

In the experimental research reported in this thesis, it was intended to measure the forces at the column bases. Therefore, a literature survey was performed to find out information about force transducers, which could measure shear, moment and axial load. Information on the transducers given in papers in the literature is very simple. Therefore, research reports are examined carefully for detailed information about the design, manufacturing and calibration processes of force transducers. In the following paragraphs, it is not intended to summarize to whole report but to give information about the force transducer used in the experimental research.

Sozen et al. (1959) [57] conducted quarter scale model tests on reinforced concrete floor slabs. Floor slabs consisted of a continuous plate supported on columns. Each column of the test structure was supported on a steel ball. These balls were in turn supported on tripod reaction dynamometers. These dynamometers consisted of three legs which form a triangular pyramid. Each leg of the dynamometer itself was a load cell. The legs joined the ball at the top and a thick stiff plate at the base. The joints were assumed pin connected. Therefore, the legs did not take any moment.

Tankut (1969) [58] developed a similar dynamometer by improving the earlier models. He used these dynamometers to measure the reaction at the bottom of the slab specimens.

Hidalgo and Clough (1974) [32] conducted an experimental research on earthquake simulator for a reinforced concrete frame. They design a force transducer to provide the flexural moment, the shear force, and the axial force time histories at the mid-height section of the columns. These transducers consist of a narrow, 4" long, steel I section. This I section has height of 7½" and width of 2". The thickness of the web and flanges are 1/8" and 3/16" respectively. This I section was welded to its 1" thick top and bottom plates. Strain gages were mounted on the flanges and web of the I section. Each force transducer was calibrated for axial compression force (compression calibration), for shear and flexural moment (cantilever calibration). The data was obtained from at least three load cycles over the calibration ranges and seven points within this range were used to derive the linear behavior of the force transducer.

Oliva (1980) [33] reported shaking table tests of a reinforced concrete frame with biaxial response. He designed a force transducer to provide the actual flexural moment and shear histories along the two column axes at the mid-height. The individual transducers were made of hollow rectangular steel sections. This square tube was connected to the 1" steel top and bottom plates by a full penetration fillet weld.

Bending was monitored by a half bridge strain gauge circuit comprised of one gauge mounted in the direction of compression stress on the compression flange and a second in the tensile direction on the tension flange. Shear was monitored by a full bridge circuit with two gauges mounted at 90 degrees to each other on each of two shear webs. A constant correction factor for exact shear strain should be applied to eliminate cross sensitivity if shear strain is desired.

The transducers were subjected to a rigorous calibration procedure including various combined loadings of shear, moment and axial load applied simultaneously. Data from the calibration was analyzed graphically and through a statistical multiple regression to define prime and cross sensitivities directly in moment or shear units as a function of voltage output from the prime circuit and three other secondary circuits.

Aktan and Bertero (1981) [34] carried out experimental research to study the seismic resistant design of R/C coupled structural walls. Special force transducers were designed to monitor the axial force, shear force, and bending moment at the midspan of the connecting beams. The basic approach in the design was to idealize a beam segment by various axially loaded fibers (force bars), which could be instrumented by strain-gages and wired so that individual internal force channels, which do not interact with each other, could be obtained. Totally twelve force bars are welded to the left and right end steel plates. These plates have a dimension of 21"×11"×2". The circular bars have a diameter of 1.8". Their 2" region at the midspan are reduced to a diameter of 1.2". Four horizontal bars are treated for axial force measurement, four other horizontal bars for bending moment, and four inclined bars for shear force measurement.

In the transducers, the total number of force channels, twelve altogether, were monitored by the primary data acquisition system. It was possible to compute the internal force at any cross section of any member of the subassemblage with the information obtained from the force transducers and the load cells, as the components of the subassemblage were rendered statically determinate with this information. The force transducer thus yields vital information to assess the overall behavior of the subassemblage, namely, the shear and flexural redistributions that occurred between the walls, and the axial load in each wall.

Aktan, Bertero, Chowdhury and Nagashima (1983) [35] conducted an experimental research to predict experimentally and analytically the mechanical characteristics of a 1/5-scale model of a 7-story R/C frame-wall building structure. In this research, a special force transducer was designed to measure the internal forces at the mid-height of the columns. Sause and Bertero (1983) [36] provided detailed information regarding the design, fabrication (machining, welding, heat treating, and tempering), electronic instrumentation, calibration, and installation of the force transducers.

The main criteria considered in the design of the transducers were:

- The transducer was required to be sensitive enough and remain linearly elastic while monitoring the strains induced by the possible lower and upper bounds of axial force, flexure, and shear force in the columns and to enable the simultaneous recording of these internal forces independently;
- The discontinuity in the stiffness and mass introduced at the mid-height of the first-story columns was required to be sufficiently small so as not to alter the responses of these elements at any of the response limit states. Since the stiffnesses of a column would change during different response limit states while the transducer should remain linearly elastic, the axial and flexural stiffnesses of the transducer were designed to correspond to estimated average values of the corresponding column stiffnesses.

Aluminum, 6061, with a minimum yield of 35 ksi and a modulus of elasticity of 10500 ksi, was selected. A 4" long hollow tube was welded to two plates, and the two sides of the tube were machined in order to increase the sensitivity of the transducer in shear. Three strain gage bridges were used to pick up the strains corresponding to shear, axial force, and flexure independently.

CHAPTER 3

TEST SPECIMENS AND EXPERIMENTAL TECHNIQUE

3.1 GENERAL

The Earthquake Engineering Research Center of Middle East Technical University has been operational as a teaching, research and consulting institute attached to the Civil Engineering Department since 1971 [51]. After every moderate or severe earthquake in Turkey, requests are made to make use of the expertise available at the Center. The center has cooperated with the Ministry of Public Works and Settlement after these earthquakes. METU center has acted as adviser and consultant for establishing the strategies, pertaining to the rehabilitation of moderately damaged buildings and for the overall technical supervision of such rehabilitation, once the relevant contracts have been awarded to the concerned contractors. In all these rehabilitation projects infilled frames have been used. Design criteria and construction techniques of such infilled frames have been developed at METU as a result of the experimental research carried out at the Structural Mechanics Laboratory of METU since 1970.

Faculty members of the Civil Engineering Department of METU have gained extensive field experience in structural damage assessment and disaster evaluation after the 1970 Gediz, the 1971 Burdur and Bingöl, the 1975 Lice, the 1976 Çaldıran, the 1983 Narman, the 1992 Erzincan, the 1995 Dinar, the 1998 Adana-Ceyhan, the 1999 Kocaeli and the 1999 Düzce earthquakes.

The first tests on infilled frames at Middle East Technical University date back to 1970 [7]. One-bay one story infilled frames were tested under lateral loads. The main objective of these tests was to observe the strength and the behavior and assess the adequacy of infilled frames used for strengthening some buildings after the 1970 Bartın Earthquake. Subsequently, infilling of frames by means of cast-in-place reinforced concrete infills have been widely used by METU group for the seismic rehabilitation of framed structures. In 1986, another experimental research project was initiated at METU Structural Mechanics Laboratory to investigate the behavior of infilled frames in which different techniques were used to connect the infills to the frames [22, 23, 24]. At the end of this research program it was concluded that connecting the panel to the frame by using dowels, which were embedded into the frame elements proved to be the most successful technique. Based on the satisfactory behavior observed in these tests, the same technique was used by the METU group to rehabilitate reinforced concrete framed buildings damaged in Erzincan (1992), Dinar (1995) and Ceyhan (1998) earthquakes. The main objective of the third experimental research program initiated at METU jointly with Boğaziçi University in 1994, was to observe the behavior of infilled frames in which infills have been introduced to damaged frames which suffered most of the common weaknesses encountered in practice [52]. Here the term "weakness" refers to poor concrete quality, poor reinforcement detailing, strong beams-weak columns, connections.

The results of these tests were discussed in Chapter 2.

In all the tests conducted at METU Structural Mechanics Laboratory, either one-bay one-story or one-bay two-story frames were used as test specimens. The main objective of the research reported in this thesis was to study the behavior of framed structures in which reinforced concrete infills have been introduced only to a few bays. To fulfill this objective, test specimens consisted of three bay, two story frames, in which only the interior bay was infilled. The other difference between this project and the former ones is that specimens in this project have been tested vertically by using the reaction wall and the strong floor; whereas, the preceding ones were tested horizontally on the floor. Furthermore, in this research program, a new transducer had to be designed to measure end forces in the columns. The force transducer enabled recording of three forces simultaneously, namely axial force, shear force and moment, in the frame direction at column base.

Since system testing is expensive and time consuming, test specimens had to be designed and detailed carefully, construction of the test specimens had to be planned considering all the details and instrumentation had to be designed considering the main objectives for this experimental research.

In the design of the test specimens and the instrumentation, the following points were considered:

- Dimensions of the frame and the frame members should not be very different from those used in the individual infilled frame tests at METU.
- Similar to the experimental research initiated at METU and Boğaziçi in 1994, frame members had to be damaged before the introduction of the infill and the frames had to have the common deficiencies encountered in buildings in Turkey.
- Instrumentation should be designed considering the objectives of this research program. Special transducers had to be designed to measure the axial force, moment and shear force at the bases of the columns in order to study the load-displacement behavior of the system. Also, curvatures on the columns and shear deformations in the wall had to be measured.

The experimental study conducted by the author was a part of a research program sponsored by National Science and Technical Research Council of Turkey (TUBITAK-INTAG 563) and by Middle East Technical University (AFP-99.03.03.08).

3.2 TEST SPECIMENS

3.2.1 General

Two tests were carried out in this study. A bare frame was constructed first. Then, the frame was damaged under reversed cyclic loading simulating the seismic forces. This first test was identified as "B1". Holes were drilled on the inner faces of the members of the middle bay of the damaged frame. Following the cleaning process of the holes, dowels (deformed bars) were inserted into the epoxy-injected holes. Finally, two layers of mesh reinforcement were placed and the infill wall was cast. This specimen represented a repaired frame. This frame was designated as "R1". The letters in these designations describe the structure; "B" is for the **B**are frame, "R" is for the **R**epaired frame.

3.2.2 Dimensions of the Test Specimens and the Formwork

All specimens were cast vertically by using steel forms. The steel formwork was manufactured from 1.5 mm thick steel plates. Steel plates were assembled with bolts, forming the formwork. The dimensions of the test specimen are given in Figure 3.1. The right and left bays of the frame have a width of 1600 mm. The middle bay, which would be infilled by reinforced concrete wall, is 1000 mm in width. The height of the first story is 1500 mm and the second story 1000 mm. The columns were 110 x 110 mm and beams were 110 x 150 mm. The steel forms of this frame were manufactured with an error of 1/10 of one millimeter. The forms were stiff enough to avoid any deformations during the molding process. The top of the steel forms of the beams was open. During molding of concrete, this part had a tendency to open up. Therefore, only the middle top part of the beams was clamped to prevent opening of the forms. The dimensions of the formwork of the bare frame are given in Figure 3.2.

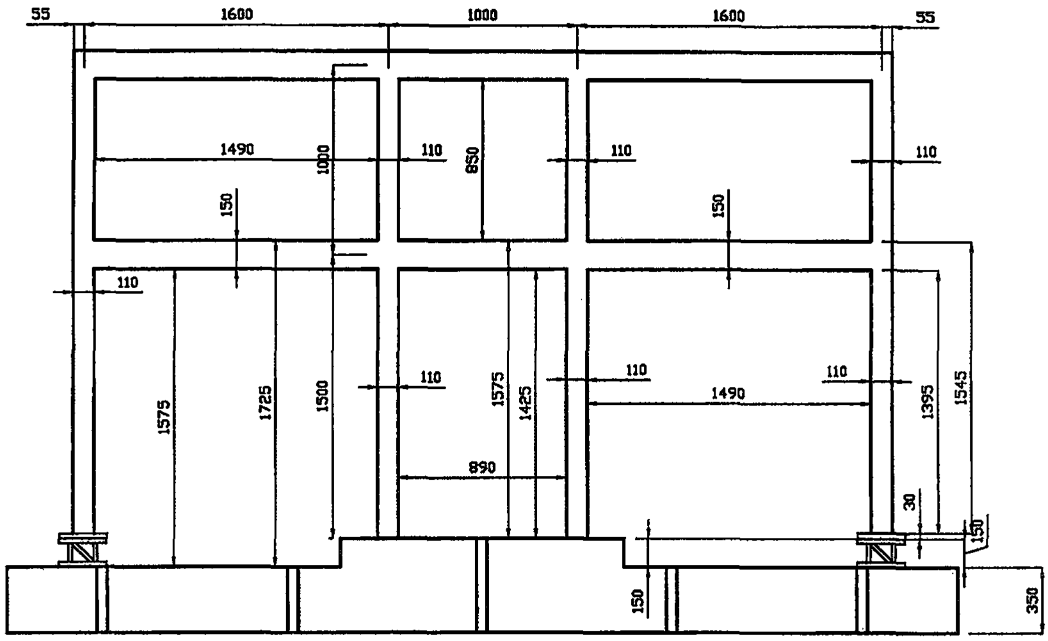

Figure 3.1 Dimensions of the test specimen (All dimensions are in mm)

The thickness of the infill wall was 70 mm. Considering these dimensions, the ratio of the wall area to the floor area at the base was approximately 1% (for the calculation of the tributary floor area, the width of the slab is assumed as 1600 mm). Figure 3.3 shows the details of the formwork of the infill wall. The first story forms were manufactured in two parts to make the forms stiffer against out of plane bending. But during the molding of concrete of the infill wall, the out of plane stiffness against bending was not sufficient and they began to bend outwards. Therefore, they were supported with timber joists. After molding of first specimens, these forms of the infill wall were strengthened by means of steel angles to prevent swelling of the form.

Figure 3.4 and Figure 3.5 show a general view of the first and second story formworks respectively.

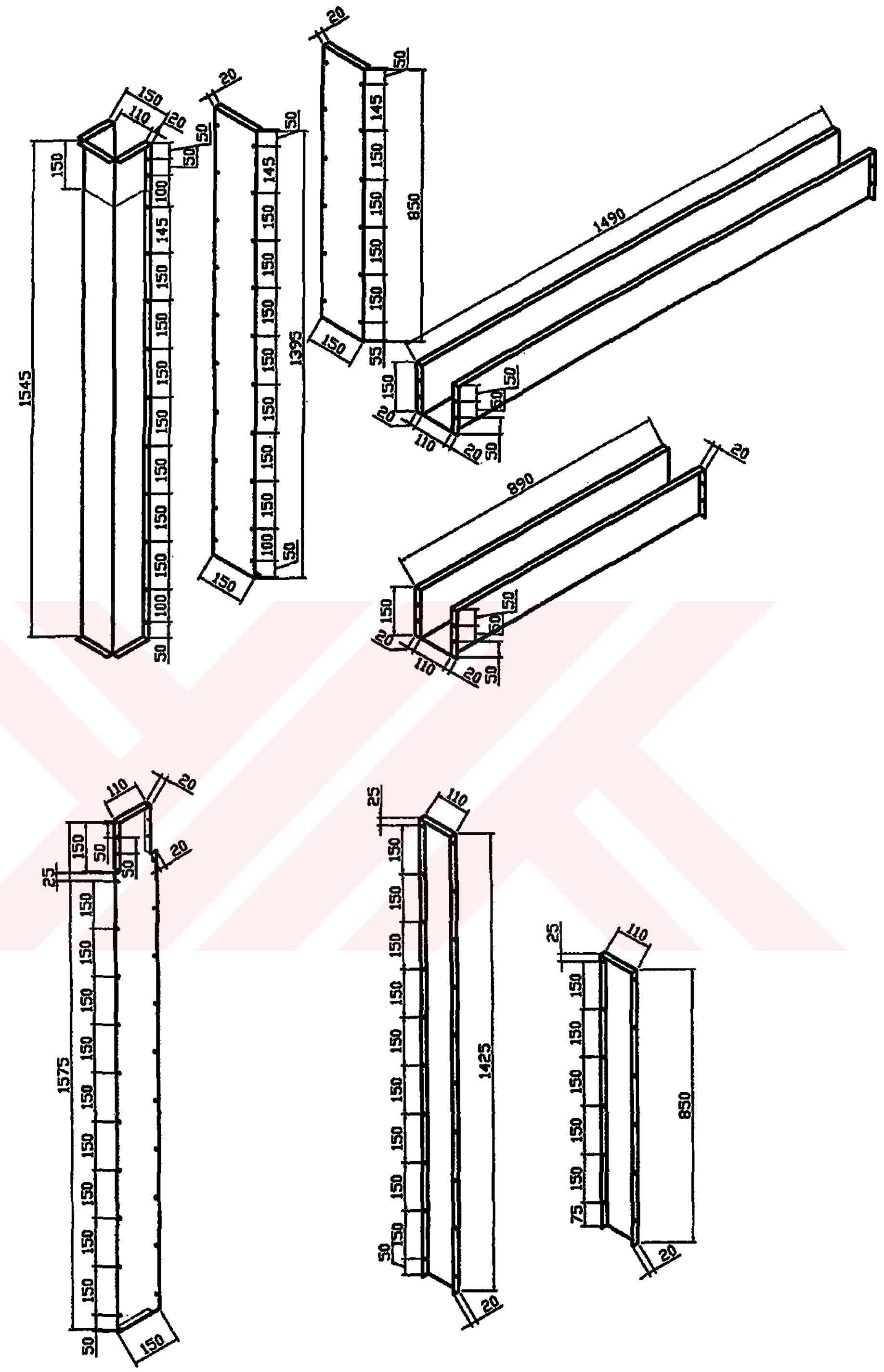

Figure 3.2 Details of the formwork of the bare frame (All dimensions are in mm)

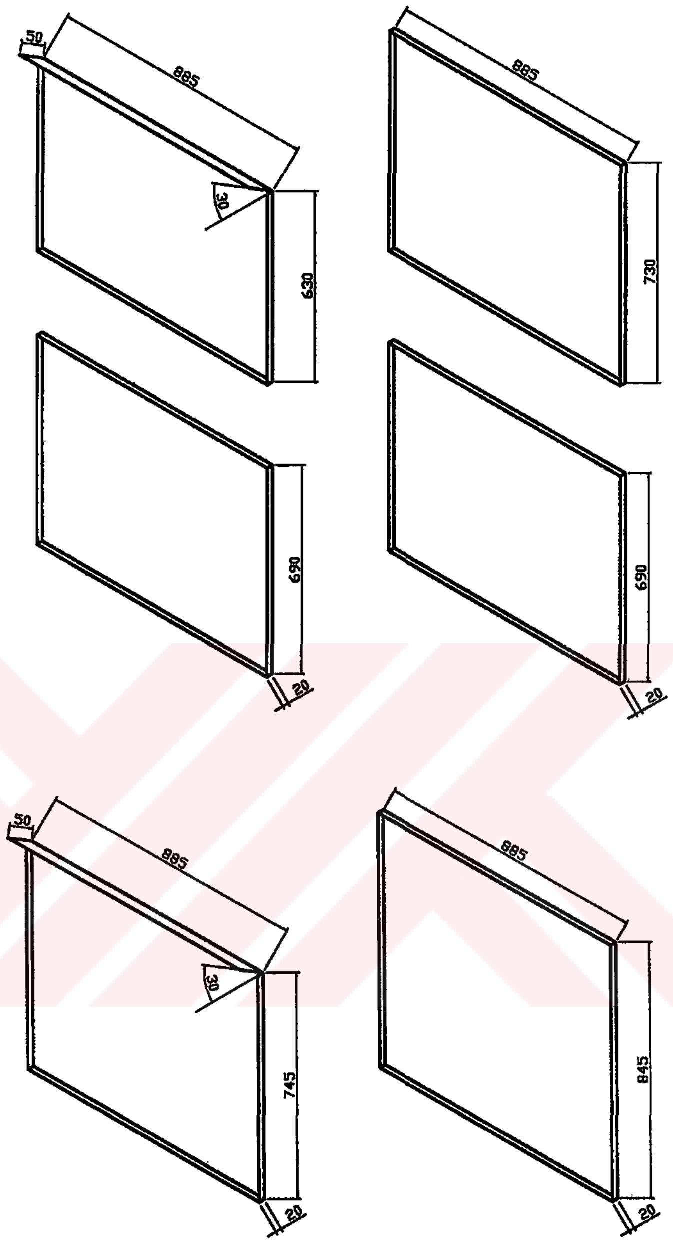

Figure 3.3 Details of the formwork of the infill walls (All dimensions are in mm)

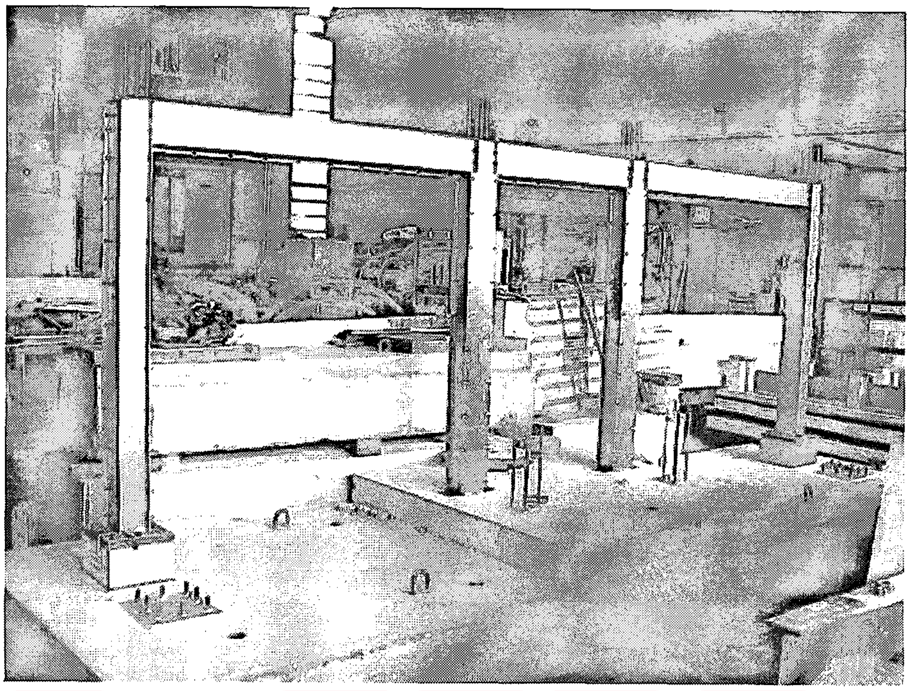

Figure 3.4 A general view of the first story formwork

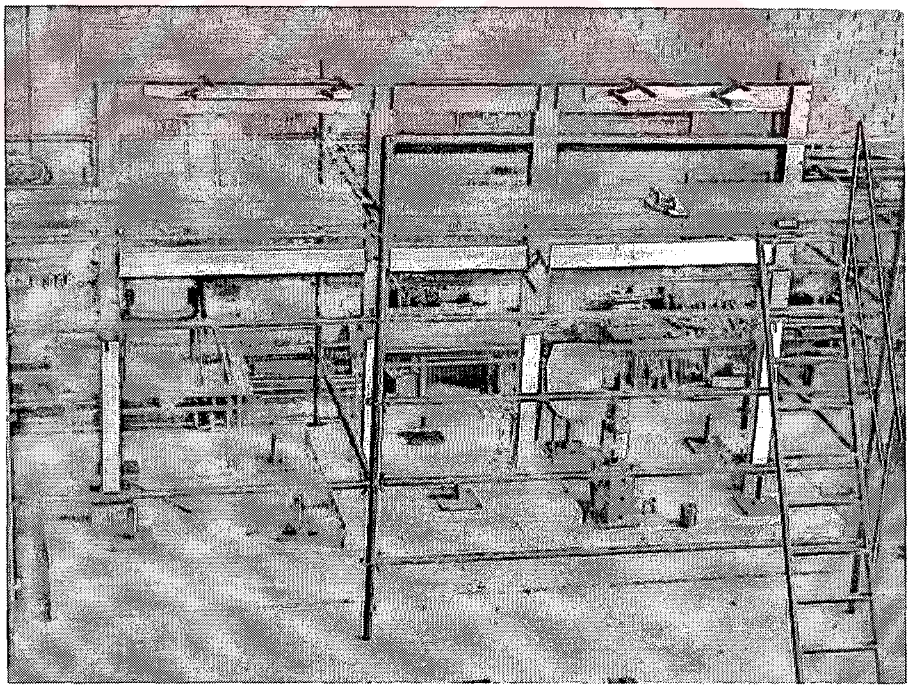

Figure 3.5 A general view of the second story formwork

3.2.3 Details of the Test Specimens

Dimensions of the test specimens were given in Section 3.2.2. As mentioned before dimensions and detailing of the reinforcement were chosen to reflect the common deficiencies encountered in practice in Turkey.

In both beams and columns, 4ϕ8 plain bars were used as longitudinal reinforcement. Figure 3.6 shows the reinforcement details of the column and the beam. The longitudinal reinforcement of the beams was one piece going through the three beams. This means that beam reinforcement was not spliced. The beam top reinforcement was extended into the exterior column and bent 90° downward. The beam bottom reinforcement was extended into the external column and its ends were just hooked. The column longitudinal reinforcement was spliced at floor levels with a splice length of 20ϕ (160 mm). The longitudinal reinforcement of the two interior columns spliced at foundation level. 4ϕ8 dowels cast with the foundation had a length of 40ϕ (320 mm). Longitudinal reinforcement of the interior columns was lapped with these bars. At exterior columns, force transducers were placed at the foundation level in order to measure the column end forces. Therefore, there were no dowels extending into the foundation to transmit column forces. The top surface of the force transducer has been roughened to provide better bonding between steel plate and concrete. Also 4ϕ8 L-shaped bars extending 50 mm into the column were welded to the top of the steel plate. The column longitudinal reinforcement was welded to these bars with 50 mm weld length. No splice problem was faced during the experiments at those locations. The reinforcement pattern of the specimens is given in Figure 3.7.

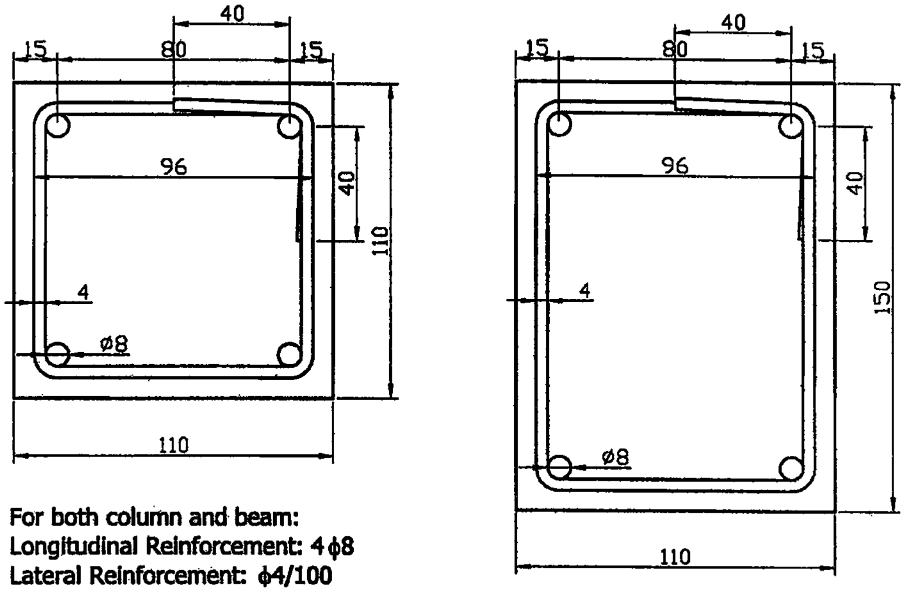

Figure 3.6 Reinforcement detail of column and beam sections

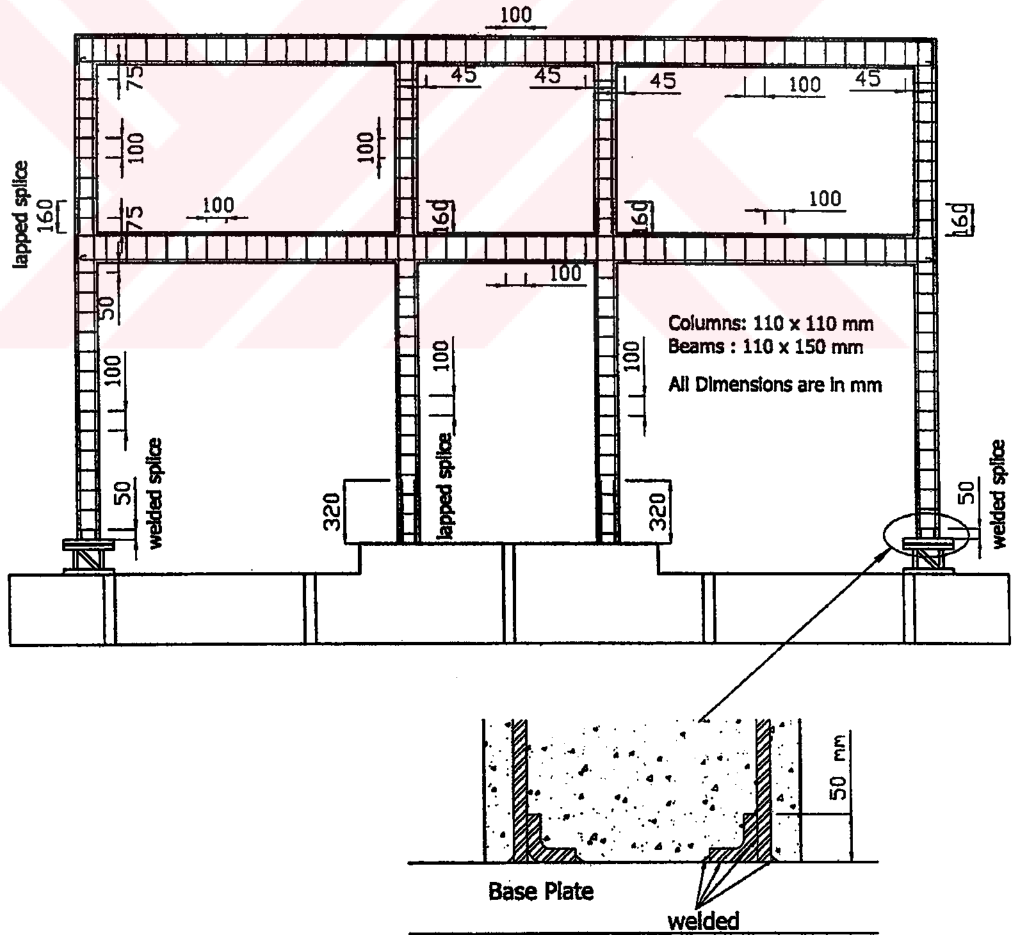

Figure 3.7 Reinforcement pattern of the specimens

The same lateral reinforcement was provided in columns and beams. Plain bars with a diameter of 4 mm were used as ties. The tie spacing was 100 mm both for columns and beams. The ends of the ties had 90° hooks. The straight portion of the hook was extended ten bar diameters.

The force transfer between the infill wall and existing frame was achieved by means of dowels. Dowels were made of ϕ10-deformed bars. These dowels were embedded into the column and beams. The holes for the dowels were drilled with a small inclination to prevent epoxy flow out from holes. The configuration of the dowels is given in Figure 3.8. The spacing of dowels was 100 mm at the foundation level, 150 mm in columns and 200 mm in beams. The dowels extended 200 mm (20ϕ) into the infill wall, except for the foundation dowels. Foundation dowels extended 300 mm (30ϕ). The depth of the drilled holes in the columns was 100 mm (10ϕ). Thus, a 10 mm un-drilled portion was left on the outer face of the column in order to prevent crushing of the concrete. The top beam was also drilled 100 mm (10ϕ). The holes in the first story beam went all the way through the depth of the member. In the foundation, length of the embedded dowels was 150 mm (15ϕ). Figure 3.9 shows a detailed view of the epoxy-injected dowels.

The mesh reinforcement of the infill wall consisted of ϕ6-plain bars. Bar spacing in horizontal and vertical directions were 150 mm. The reinforcement was placed on both faces of the wall. The thickness of the wall was 70 mm. The ratio of the wall reinforcement was 0.00545 in the vertical direction (ρ_v) for both stories. The ratio of the wall reinforcement in the horizontal direction (ρ_h) was 0.00567 and 0.00570 for the first and second stories respectively. Figure 3.10 shows the detailed drawing of the wall mesh reinforcement. A general view of the mesh reinforcement of the second story infill wall is given in Figure 3.11.

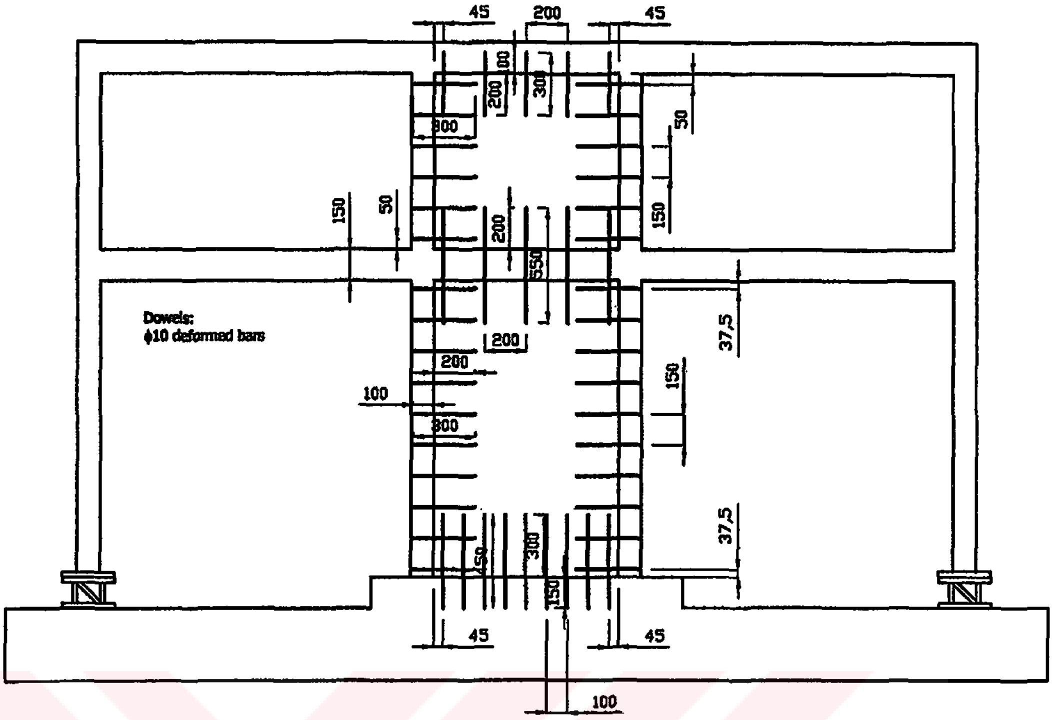

Figure 3.8 Configuration of infill dowels

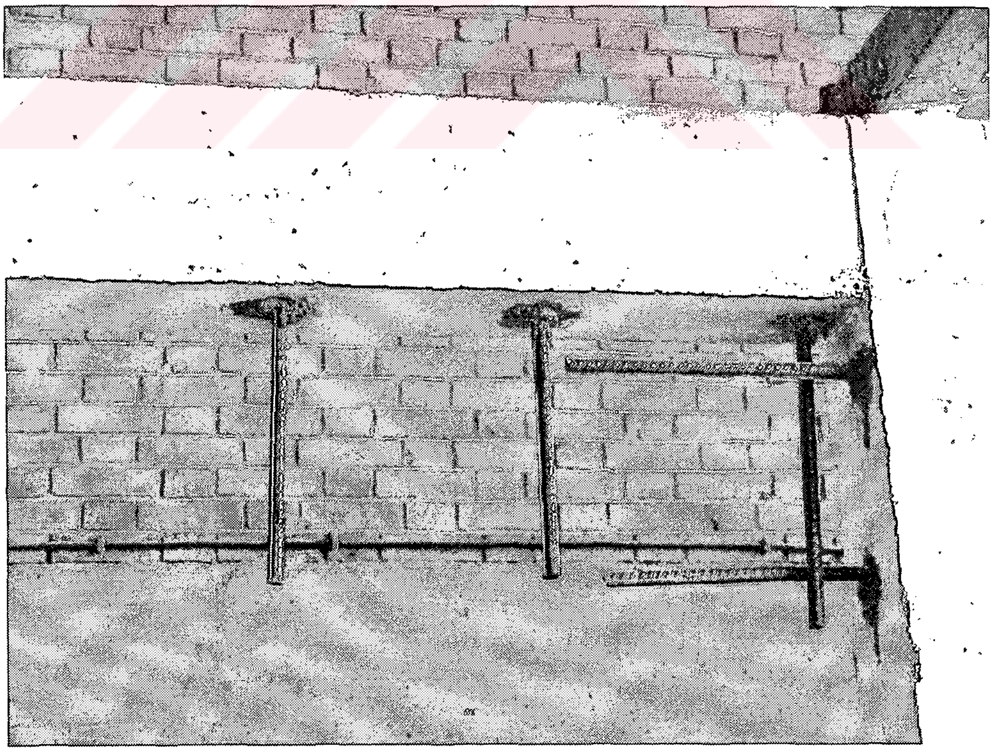

Figure 3.9 Details of the epoxy-injected dowels

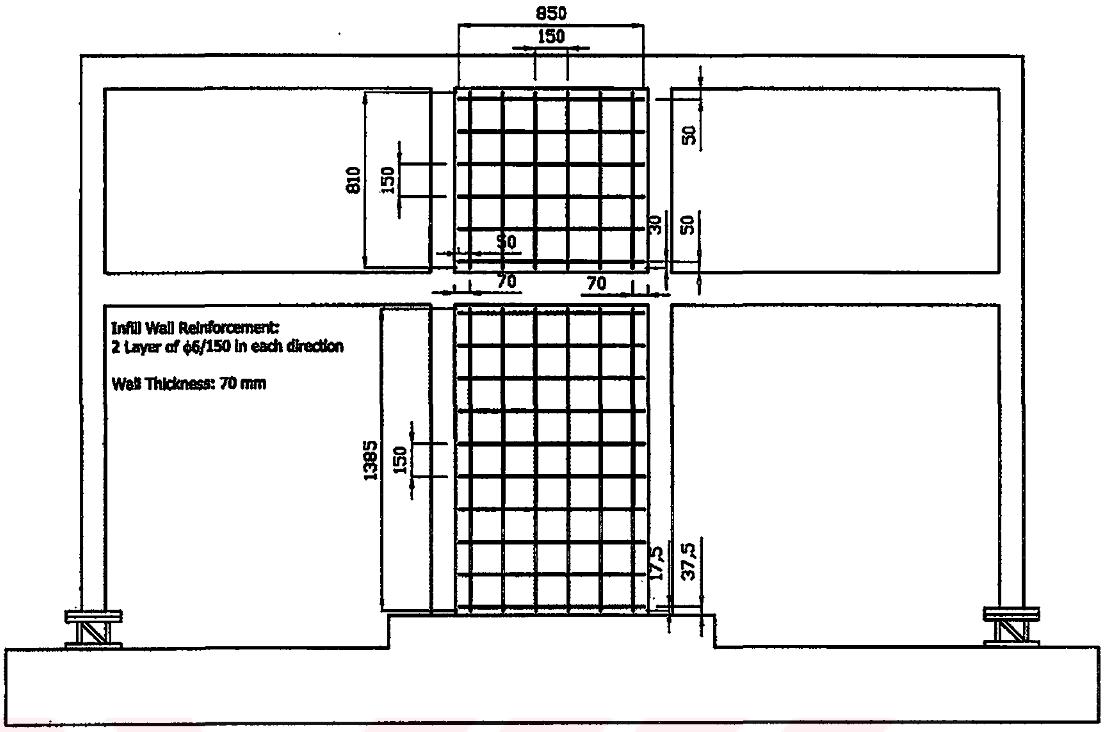

Figure 3.10 Detailed drawing of the wall mesh reinforcement

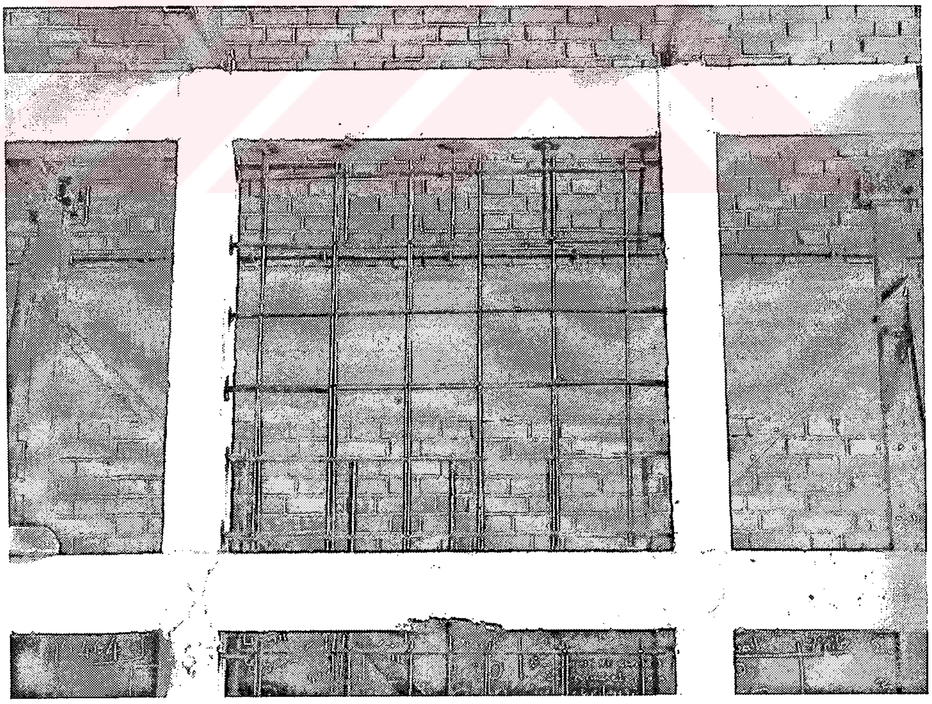

Figure 3.11 A general view of the wall mesh reinforcement of second story

3.3 FOUNDATION OF THE TEST SPECIMEN

The large distance between the holes on the strong floor led to a design of a heavy foundation that required a considerable amount of concrete during the production. Moreover, this design enabled to place two frames on the same foundation.

The foundation has a length of 5 m and a width of 1.5 m. The foundation has a stepped shape at the middle portion to keep column lengths the same. This step had the same height as the transducer, 150 mm. The foundation was fixed to the strong floor at ten points by means of steel bolts (ϕ = 50 mm). To transmit the column load to the footing, 4ϕ8 dowels were placed at locations of the interior columns. These dowels extend into the footing to provide adequate development length. They also extend into the column 40 bar diameters. Additionally, eight 5/8" bolts were placed in the foundation for each force transducer. Force transducers were bolted and fixed to the foundation by means of these bolts. Detailed drawings of the foundation are given below in Figure 3.12, Figure 3.13 and Figure 3.14.

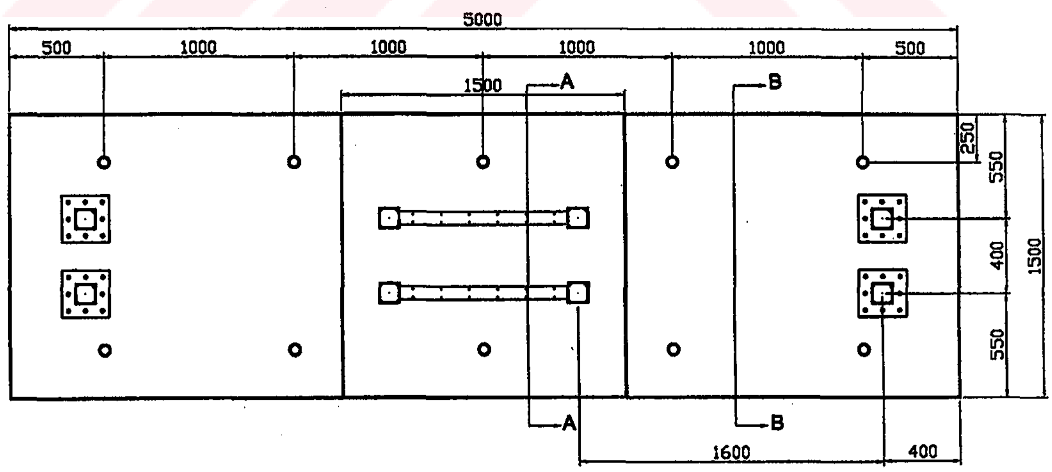

Figure 3.12 Plan view of the Foundation (All dimensions are in mm)

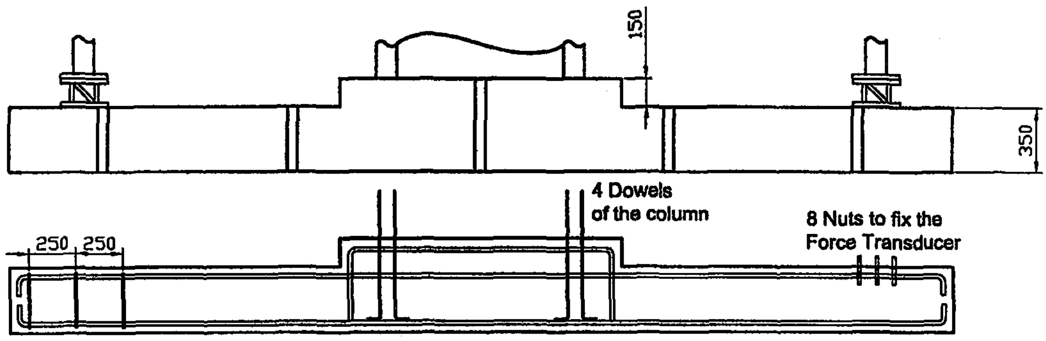

Figure 3.13 Front view and reinforcement of the Foundation

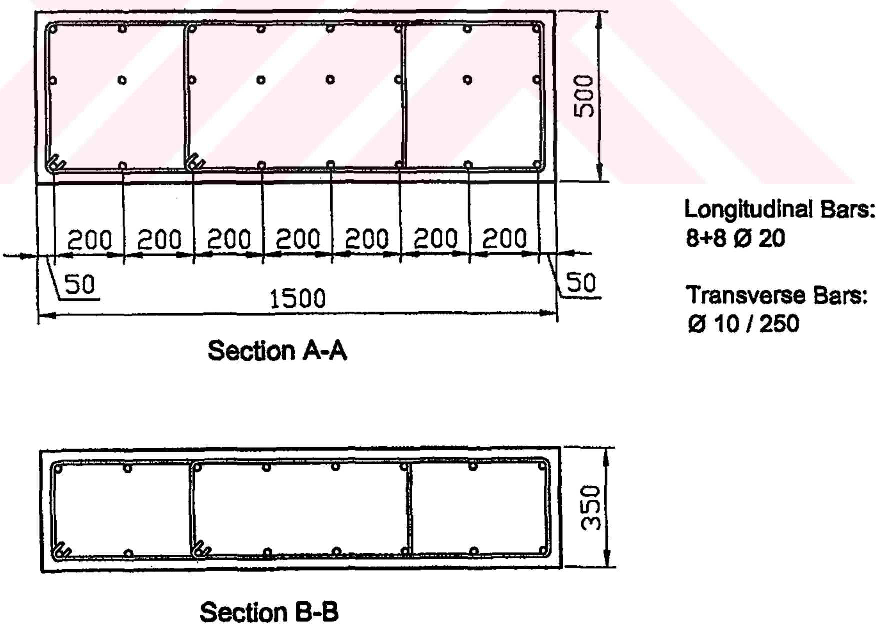

Figure 3.14 Section A-A and B-B of the Foundation (All dimensions are in mm)

Steel forms were made for molding of the foundation concrete. Approximately 2m^3 of concrete was required for the production of this foundation. It was impossible to produce this amount of concrete, in the laboratory, at one or two batches. Therefore, ready mixed concrete was ordered from a ready mixed concrete company. Before placing the concrete, the inside of the forms were cleaned and greased to facilitate their removal when concrete was set. Figure 3.15 shows a photograph of the molding process of ready mixed concrete. Mechanical vibration was used for the compaction of the concrete. This mechanical vibration was imparted by means of a vibrator, which was operated with the help of an electric motor. Some cylinder specimens were taken for the quality control of concrete.

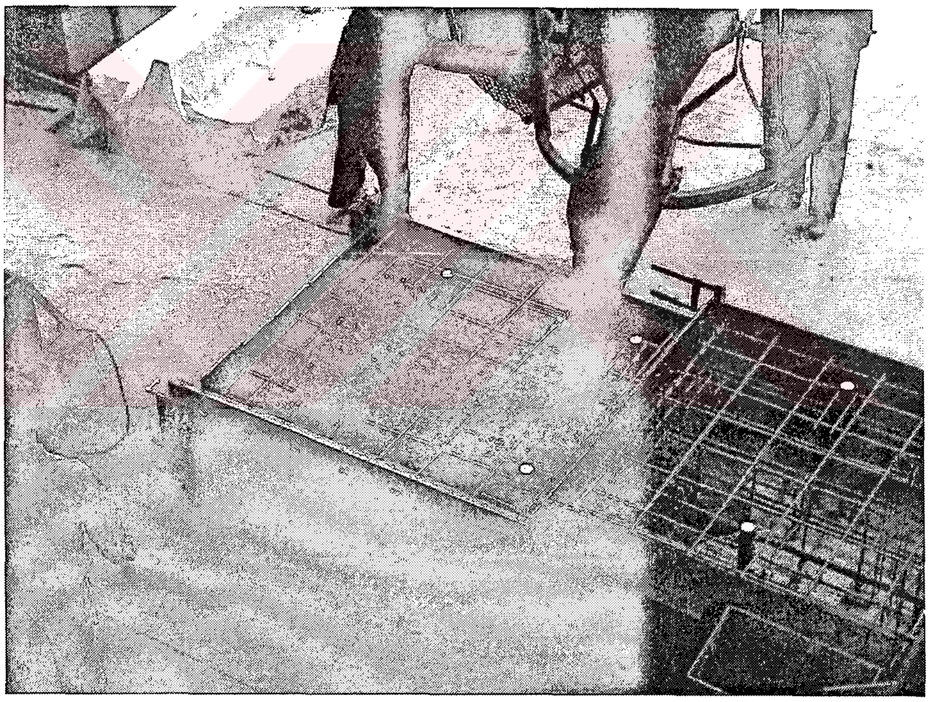

Figure 3.15 A general view of molding the ready mixed concrete of the Foundation

The grade of the ordered ready mixed concrete was C25, which should have a compressive strength of 25 MPa at 28 days. According to the standard cylinder tests, the concrete of the foundation has a final strength of 44 MPa.

3.4 MATERIALS

Concrete of the frames and the infill walls was produced at the Structural Mechanics Laboratory of METU. The target compressive cylinder strength of the frames and the infill wall were 10 MPa and 22 MPa respectively. Table 3.1 and Table 3.2 give the mix proportions of concrete for frames and infill walls. Materials used in the mix are given by weight for 1 m^3 concrete.

At the test day of bare frame test, the strength of concrete was 13.2 MPa. During the infilled frame test, the compressive strength of concrete was 13.8 MPa for the first story, 16.7 MPa for the second story and 30.8 MPa for the infilled wall.

Special attention was given to curing. Curing was done by covering the specimens with wet burlap which kept the concrete moist and as near as possible to the ideal temperature for chemical hydration.

In order to determine the concrete strength, nine standard cylinder test specimens were taken from each batch. The test cylinders were 150 mm in diameter and 300 mm in height. The test cylinders were kept under the same moist curing conditions as the test specimens. Each time, three cylinders were tested to obtain the average strength of concrete.

Table 3.1 Mix Design of the frames (weight for 1 m^3 of concrete)

	Weight (kg)	Proportions by weight (%)
Cement	240	10.53
0-3 mm Aggregate	1060	46.49
3-7 mm Aggregate	750	32.89
Water	230	10.09
Total	2280	100.00

Table 3.2 Mix Design of the infill wall (weight for 1 m^3 of concrete)

	Weight (kg)	**Proportions by weight (%)**
Cement	436	19.05
0-3 mm Aggregate	864	37.75
3-7 mm Aggregate	745	32.55
Water	240	10.48
Sikament 300	4	0.17
Total	2289	100.00

In each column and beam of the frames, four longitudinal plain bars were used. Longitudinal steel was 8 mm in diameter. The longitudinal reinforcement of all specimens was prepared from the same batch of steel. Three test coupons were randomly taken to determine stress-strain relationship of steel used. The coupons were tested in tension. In both columns and beams of the frames, 4 mm plain bars were used as lateral reinforcement. The anchorage of ties was provided by 90° hooks.

Infilled walls were applied to the frames for strengthening purpose. Force transfer between the wall and frame was achieved by steel dowels. For the application of these dowels, first holes were drilled on the inner faces of the middle bay of the frame. Next, these holes were cleaned by means of water. Then, dowels were inserted into the holes and fixed with epoxy based grout, namely Sikadur-42. Sikadur–42 is a three-component epoxy grouting system, which is solvent free, moisture insensitive and non-shrink. The epoxy is chemical resistant, corrosion and impact resistant and is suitable for applications requiring vibration resistance. Dowels were selected from deformed 10 mm bars. For the infill wall, the reinforcement pattern was selected as 2-ϕ6/150 mm in each direction on each face. The bars used as mesh reinforcement were plain bars. Typical properties of bars used in this study are given in Table 3.3.

Table 3.3 Properties of Reinforcing Bars Used

Steel No	f_y (MPa)	f_{ult} (MPa)	Properties
ϕ4	322	422	plain
ϕ6	378	484	plain
ϕ8	400	532	plain
ϕ10	757	940	deformed

3.5 INSTRUMENTATION

In the instrumentation of the specimens, LVDTs (Linear Variable Displacement Transducer) and electrical dial gages were used for displacement measurements and load cell was used for load measurement. Load measurements were made using a 110 kN compression-tension load cell. Deformations were measured by LVDTs with 200, 100 and 50 mm strokes and dial gages with 20 mm strokes. The details of the instrumentation are given in Figure 3.16.

Internal forces at the column ends were measured by means of force transducers designed and manufactured for this study. Each force transducer consisted of six small load cells. The six axial strain readings were used to calculate the axial force, shear force and the moment. Since a lot of time and effort were spent for the design and construction of these transducers and since the distribution of lateral forces to the columns and the wall was the main concern in this study, these transducers are discussed in detail in Chapter 4.

Voltage outputs from the instrumentation were fed into a data acquisition system, from which all signals were directed to a personal computer. A computer program written at METU stored the data as force and displacement. This program also monitored the data as numbers and graphics on the screen.

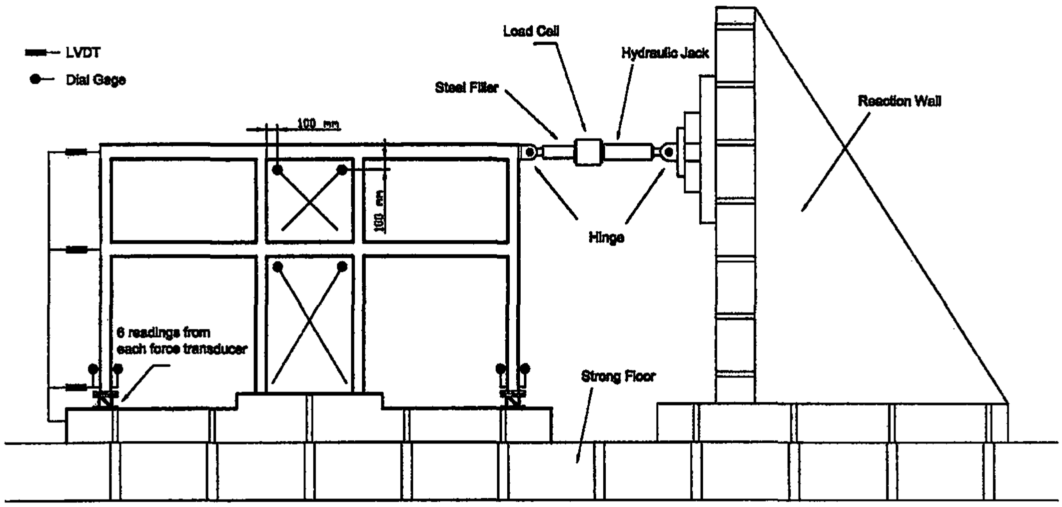

Figure 3.16 Details of the test setup, loading system and instrumentation

As can be seen in Figure 3.16, displacement of each story was measured with respect to the foundation. These readings would be used to construct load-displacement and load-inter-story drift curves. Shear deformations were measured on both first and second story walls. Strains were measured on both faces of the external columns at the base, which would enable the calculation of the curvature.

The rigid body rotations and displacement of the foundation and reaction wall were measured by means of mechanical dial gages. Two gages in horizontal direction and one gage in vertical direction were mounted on the foundation and reaction wall. These gages were monitored manually. The readings were acquired at the end of each cycle. No appreciable movement was observed in these dial gages ($\Delta \approx 1/50$mm), which meant that in the load range applied during the test, no appreciable movement occurred either at the foundation or at the reaction wall. These mechanical gages are not shown in Figure 3.16. Moreover, all the measurements on the test specimens were taken relative to the foundation. Therefore, rigid body movements would not affect the readings of the test specimens.

The lateral displacements of the test specimens at each floor level were measured by means of displacement transducers. Two 200 mm capacity LVDTs were mounted at the second story floor level in order to measure the horizontal top displacement. Due to the importance of this measurement, two LVDTs were placed at this location where one of them reserves the other. At the first story level, one 100 mm capacity LVDT was placed to measure the displacement. Additionally, one 50 mm LVDT was set at the almost bottom of the first story column. As expected, this transducer yielded zero displacement.

In the infilled specimen, average shear deformations of the wall panels were measured by means of diagonally placed displacement transducers. Transducers were located 100 mm away from the corner of the infills. The reason for choosing this location was to avoid localized effects like crushing of concrete during the experiment.

Furthermore, strains on both faces of the external columns were measured at the base. It would be possible to calculate curvatures, from these strain measurements. For this purpose, two dial gages were mounted at the opposite faces of the columns at the base. The plastic hinge length was decided to be equal to the width of the column. Therefore, measurements were made between 50 mm and 160 mm above the base of the columns. The first gage point was at 50 mm level. The reason was that, the first 50 mm was the welded splice region and therefore, no hinging was expected in this area due to increased reinforcement. Figure 3.17 shows a general view of the curvature measurement at the base of external columns.

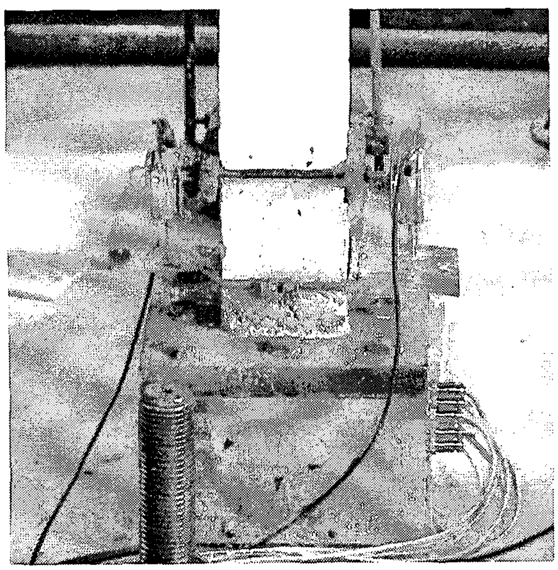

Figure 3.17 A general view of the curvature measurement at exterior columns

3.6 TEST SETUP AND LOADING SYSTEM

The testing system consisted of the strong floor, reaction wall, loading equipment, instrumentation and the data acquisition system.

The Structural Mechanic Laboratory of METU has a strong floor for fixing the test specimens to the test floor. This floor has a thickness of 600 mm. Additionally; a working drift (gallery) lies under the strong floor that enables easily to work under the floor. Holes are left on the floor which allow fixing of the specimens to the floor. Totally, 48 holes are lined up as two rows with 1-meter spacing. The distance between the two rows is also 1 meter. The diameter of these holes is 150 mm.

The foundation of the test specimen was fixed to the strong floor by means of specially produced high strength steel bolts (Dywidag). These bolts had a diameter of 50 mm. 10 holes were used for fasten the footing to the strong floor. The footing had to be anchored with a uniform force to the floor. To accomplish this, a pre-tensioning system was built from steel sections. First, all dywidags were tensioned with this system up to 100 kN. Then, the bolts were tightened at their stretched position. After bolting, the tensioning force was released from the dywidags. All the dywidags had been tightened almost by the same amount of force in this way.

To make possible vertical testing of specimens, there was a need for a reaction wall that provides lateral loading. In the laboratory, a reaction wall was fixed to the strong floor by means of totally 8 dywidags. The total height of the reaction wall was 4.5 m. There are totally 14 holes on the wall that are spaced at two columns and seven rows. These holes matches correctly the holes on the floor; in other words, the distance between the two columns is 1 m. Also, the length between the rows is 700 mm.

The system of lateral loading had to be fixed perpendicularly to the reaction wall and top beam of the test specimen. This loading system consisted of hinges at both ends, a load cell and a hydraulic jack (cylinder). This loading system had to enable the loading jack to come exactly to the center-point of the top beam. Therefore, this system had to be freely moveable on the reaction wall allowing accurate positioning. For this reason, a rail system was designed using heavy steel sections. A photograph of this system is given in Figure 3.18. The top and bottom part of the system consisted of built-up box sections welded to two U200 steel sections. To provide sliding, two U140 steel sections were put together with a space in between. The width of this space was 40 mm. U140 steel sections were strengthened by welding 6×1 mm steel plates to the flanges. The sliding system was welded to the top and bottom head to form the left and right columns. These columns enable sliding in up and down directions. In order to allow movement in horizontal direction, the same sliding mechanism was placed on the steel columns. A 400×400 mm steel plate with a thickness of 30 mm was attached on this mechanism. This plate allowed fixing the hinge of the lateral loading system.

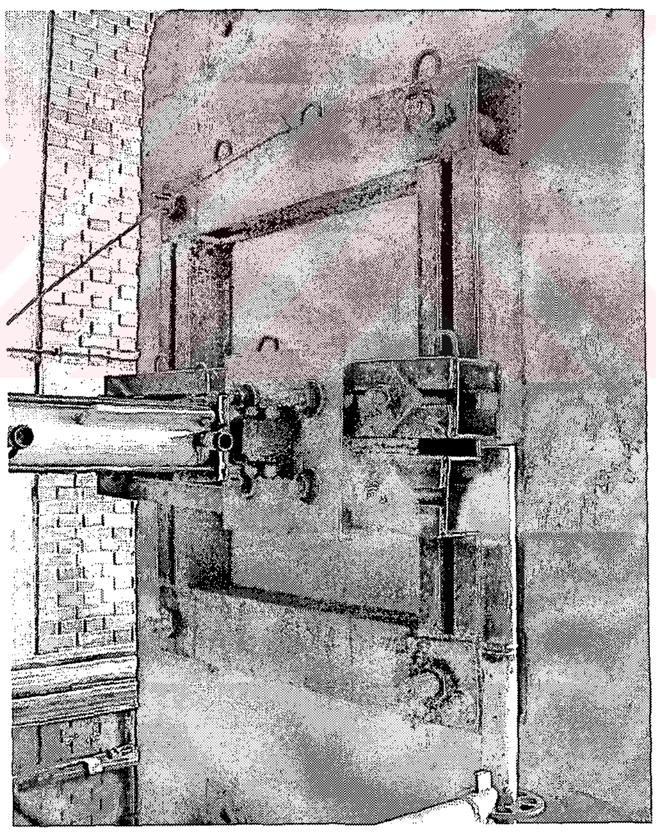

Figure 3.18 A general view of the interface system between the reaction wall and lateral loading.

The lateral load was applied at the second story floor level through a hydraulic jacks. Before molding of concrete of the second story, a steel plate was placed at the face of the exterior joint. This plate was welded both to the longitudinal reinforcement of the beam and column to transmit the lateral load from the hydraulic jack safely during the cyclic loading. A load cell was connected infront of the hydraulic jack in order to measure the magnitude of the applied lateral load. A steel stiffened pipe was put between the load cell and test frame to fill the gap between the reaction wall and test frame. This pipe was welded to the steel plate at the joint. At both ends of this loading system, hinges were placed to ensure axial load application. Figure 3.16 shows the details of the test setup and the loading system. Additionally, a general view of the loading system is given in Figure 3.19.

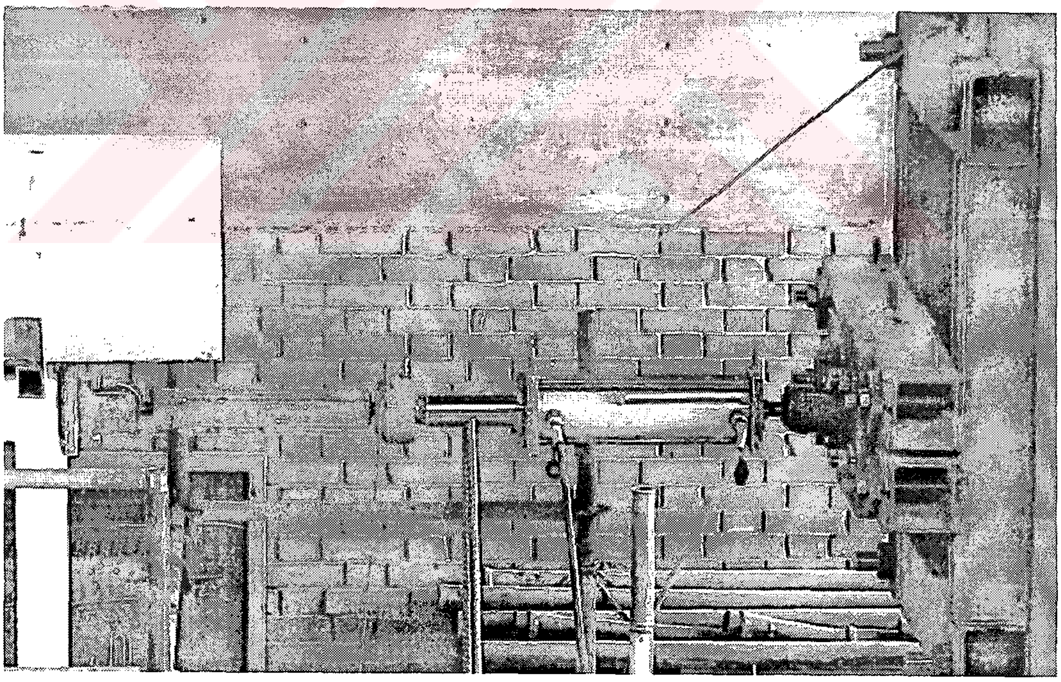

Figure 3.19 A general view of the loading system

The axial load on the columns was provided by two concrete blocks placed on the top of the second story. These concrete blocks were 580 mm wide, 2400 mm long and 400 mm deep. The weight of these blocks was 14 kN. To increase the weight of these blocks, 4 kN steel plates were added on the concrete blocks. The longitudinal reinforcement of the second story columns at the top was not bent 90°, but were left straight sticking out from the column. A square steel section was placed perpendicular to the frame direction and welded to these longitudinal bars. These square steel sections were used as supports for the concrete blocks. Steel angles were welded at the ends of these steel sections to position the concrete blocks accurately. Figure 3.20 shows a general view of the concrete weights and their steel supports. With this arrangement 9 kN axial load to exterior and interior columns were applied prior to the application of the lateral load.

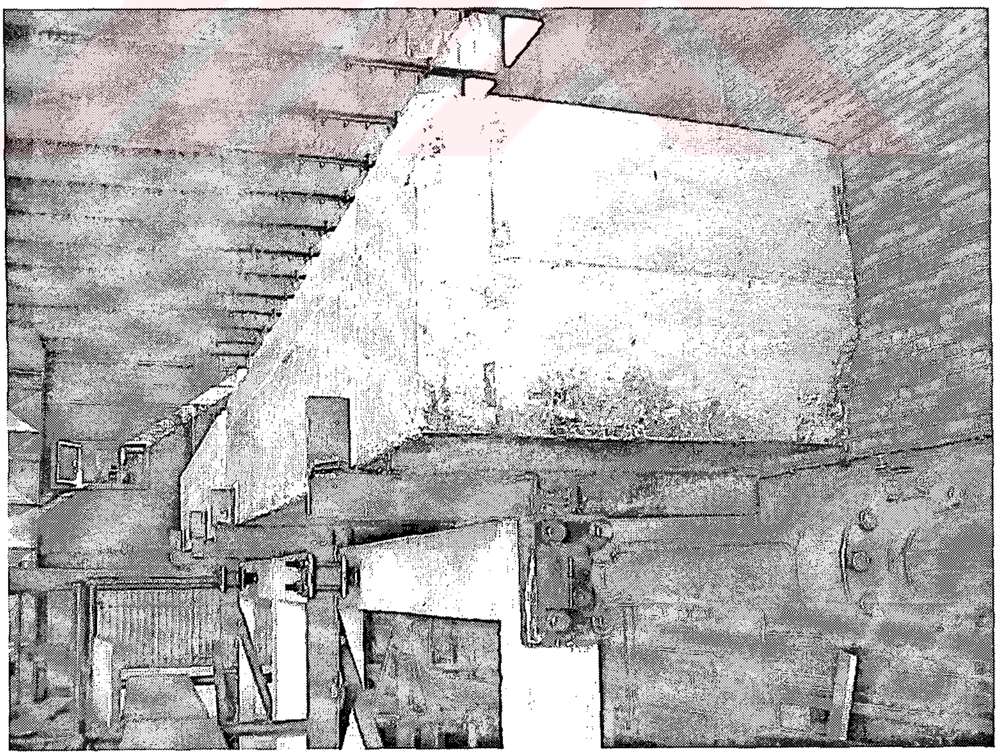

Figure 3.20 A general view of the concrete weights and their supports

The in plane stability of the test specimen with these extra weights raised some concern. Therefore, out of plane movement of the frame had to be prevented. A steel stability frame was constructed around the test specimen to prevent out of plane movement. This stability frame consisted of four steel columns fixed to the foundation, using the dywidag bolts. These columns were strengthened by means of steel bracings in each direction. This stability frame touched the test specimen only at second story beam level with four supports. These supports were roller supports in order to permit in-plane movement of the specimen. First, it was thought to place bearings in horizontal direction as supports; but the specimen had to make vertical displacements as well. Therefore, a bearing that can rotate in each direction had to be placed as support. A ball transfer unit was found to be satisfactory for this purpose. The ball transfer units used in this experiment had an axial load capacity of 2.5 kN. A detailed view of the supports made of ball transfer unit is given in Figure 3.21.

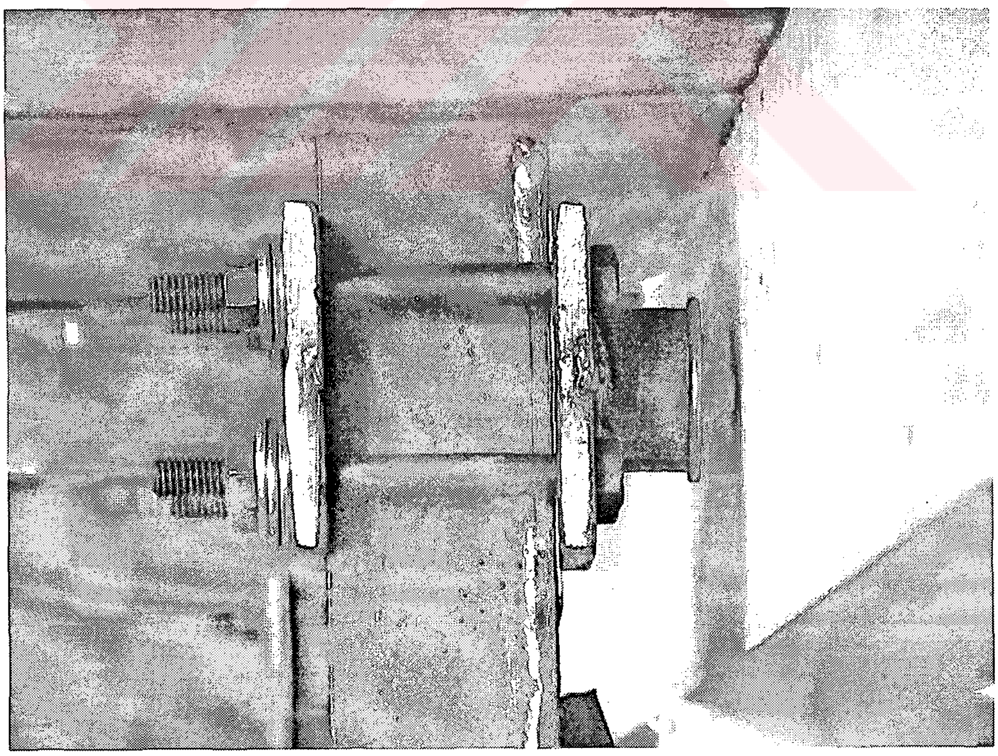

Figure 3.21 A general view of the ball transfer unit

A general view of the test setup, loading system, instrumentation, reaction wall and data acquisition system for specimen B1 is shown in Figure 3.22. The same set-up for specimen R1 is shown in Figure 3.23.

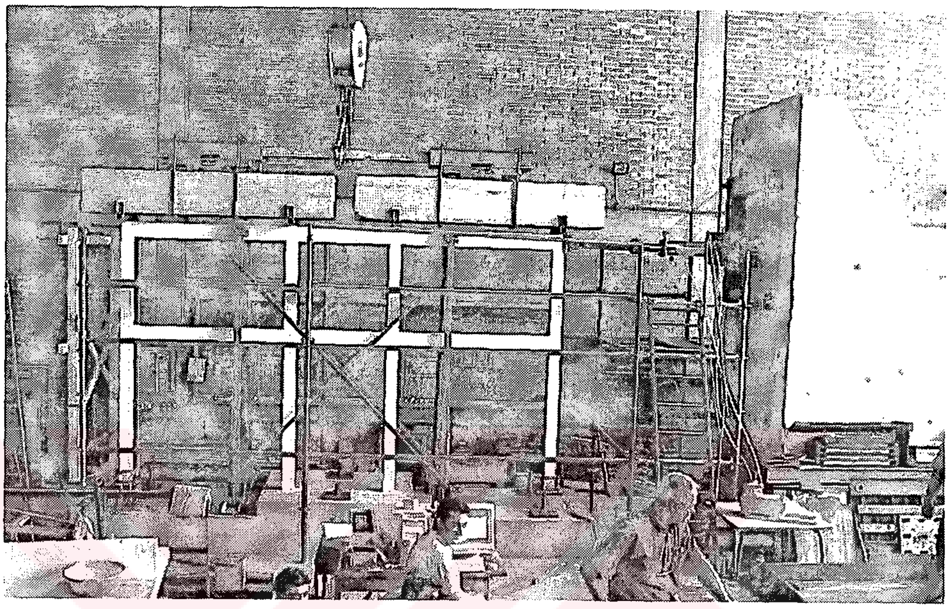

Figure 3.22 A general view of the test setup for the bare frame test

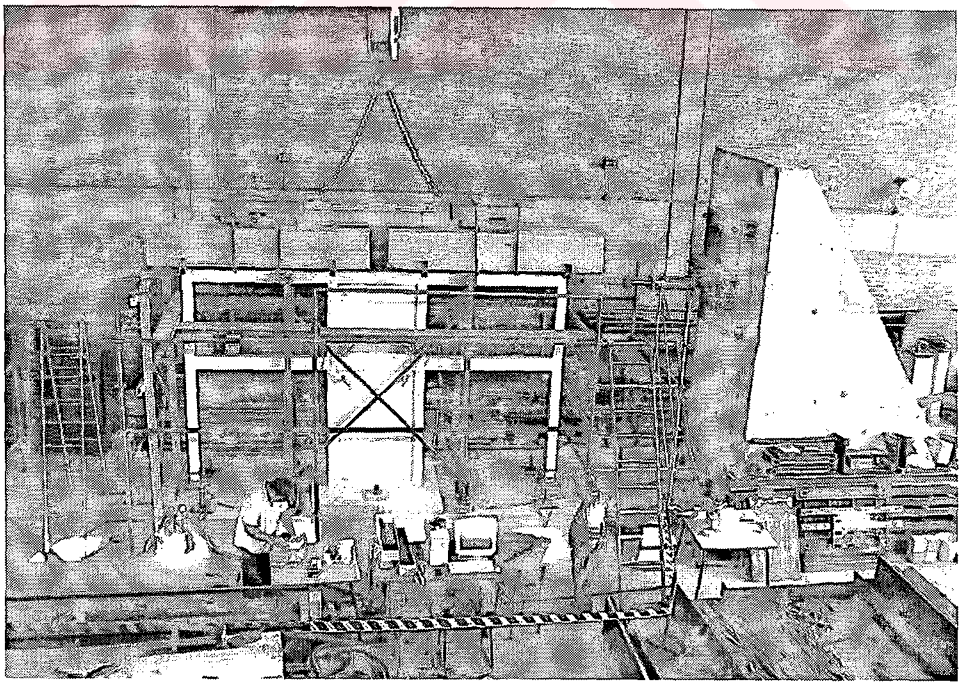

Figure 3.23 A general view of the test setup for the infilled frame test

3.7 TEST PROCEDURE

Following the curing period, the specimens were carried to the front of reaction wall where they would be tested. They were positioned carefully so that they were exactly perpendicular to the reaction wall. Afterwards, they were fixed to the strong floor by means of dywidags. Specimens were whitewashed in order to be able to monitor the cracks more clearly during the test. Then, dial gages, LVDTs and the load cell were mounted to the test specimen and their connections to the data acquisition system were made. The calibration of the transducers was re-checked. Eventually, the concrete weights were placed at predetermined locations and suspended to the crane in order to avoid any accident. Moreover, concrete cylinders were tested in order to get the compressive strength of the specimens.

Loading a specimen to a predetermined level and then unloading to zero level constitutes a half cycle loading. Addition of a reversed half cycle to a half cycle represents a full cycle. All specimens were tested under lateral cyclic loading. During the test, top displacement versus lateral load diagram was monitored. The load level was kept in elastic range for the first few cycles. In the following cycles, the load was increased beyond the yield level. At each maximum load level of half cycles, cracks were marked on the specimens and notes were taken describing the observations.

CHAPTER 4

FORCE TRANSDUCERS

4.1 GENERAL

The technical information about the force transducers, strain gages and application techniques were mainly taken from the booklet "Strain Gage Based Transducers" [37] and technical notes [45, 46, 47, 48, 49] published by the staff of the Measurements Group. Although, the information given in this thesis were briefly summarized from the above documents, in some cases the sentences were exactly repeated.

In rehabilitated structures, in which reinforced concrete infills are introduced to certain bays of the frame, it is very important to know the distribution of lateral forces between the bare frames and infilled frames at all stages up to the limit state. The main objective of this research was to observe the distribution of the lateral force in the test structure, in which one bay had reinforced concrete infills. However, in statically indeterminate reinforced concrete structures, measuring force distribution of this type is extremely difficult. It would be possible to apply strain gages and displacement transducers (such as dial gages and LVDT's) to the columns and infilled wall to determine the internal forces. However, such a measuring technique will not yield reliable results in the inelastic range. For instance, strain gages mounted on concrete surface, give unreliable readings after some reversals of inelastic straining, with spalling off the cover concrete.

Force transducers, capable of directly measuring the internal forces of the columns, would be more reliable for measuring the force distribution. The column internal force transducer could measure the shear carried by the two columns. The remaining shear force must be carried by the infill wall. Therefore, the distribution of base shear between the columns and the infill wall can be determined.

$$SHEAR\_FORCE_{infill\ wall} = LATERAL\_LOAD_{applied} - SHEAR\_FORCE_{columns}$$

It was intended to calculate the overturning moment. The overturning moment is carried by the structure through flexure of the infill wall and columns, and axial force in the columns. The axial force and moment in the columns have to be measured by the internal force transducer. As a result, the overturning moment carried by the columns can be calculated. The remaining moment must be carried by flexural action of the infill walls. Therefore, the distribution of overturning moment can be determined.

The characteristics of the force transducer described above should be:

- Materials used for the force transducers should have reliable force-deformation relations,
- Force transducers should be instrumented to give reliable results,
- Force transducers should be properly calibrated so that it would be possible to measure the internal forces directly.

The disadvantage of such a force transducer is the interference of the measuring device with the continuity of the structural member, in which the internal forces are being measured, i.e., the disturbance of the structural response that can be caused by the introduction of the internal force transducer. To eliminate or minimize discontinuity in the structural members, the internal force transducer design criteria should include careful selection of its different stiffnesses, and of the type of connection to the structural elements. Furthermore, according to the expected response of the element to which it will be connected, internal force transducer design criteria should include careful consideration of the required sensitivity and range (capacity).

Stiffness properties of the internal force transducer must be designed to match those of the element into which it is placed to minimize the disturbance of the response of that element. The transducer must be designed to withstand forces somewhat larger than the expected in the structural element without affecting its calibration. Thus, the transducer must be designed so that the forces to which it is subjected (load range) will strain the transducer material within its elastic range only. Since the internal force transducer instrumentation will measure strains on the transducer material, the sensitivity of the transducer output is directly affected by transducer stiffness. Therefore, this instrumentation should be chosen and located on the transducer so that its resolution corresponds (through a stiffness relationship) to small values of internal force.

The internal force transducer material should be chosen so that stress-strain relationship is linear within the load range. Linearity greatly simplifies the calibration procedures. The installation procedure should be simple and should minimize disturbance of the structure. Finally, if several force quantities (bending moments, shear and axial forces) are to be measured, each should be independent of the others.

4.1.1 The Bonded Strain Gage as a Transducer Element

Broadly speaking, a transducer is a device, which transforms one type of energy into another. In this study, a specific class of transducer devices have to be used, which should translate an input of mechanical energy into equivalent electrical signals for measuring the input phenomena [37].

Transducers can be, and are, manufactured on many different operating principles – resistive, inductive, capacitive and piezoelectric. However, the bonded metallic resistance strain gages, because of their unique set of operational characteristics, have dominated the transducer field in the past twenty years. The most significant operational characteristics of the bonded metallic resistance strain gages for transducer application are summarized below.

- *Small size and very low mass:* Important in minimizing inertial (shock) effects. Allows operation over a very wide frequency range – from d.c. (static) to over 50 kilohertz. The upper frequency limitation is set primarily by the strain gage grid size (gage length).
- *Fully bonded to basic spring structure*(*): Together with above statement, this freedom from critical mechanical connections – or "loose parts" – results in rugged, shock-resistant construction.
- *Excellent linearity over wide range of strains:* In most cases, overall linearity will be limited by characteristics of the spring element rather than the strain gage.
- *Low and predictable thermal effects:* Simple compensation and correction methods allow accurate operation over a wide temperature range.
- *Highly stable with time:* When suitably protected from overloads and destructive environments, strain gage transducers retain calibration very well over extended periods of time.
- *Relatively low in cost:* Overall transducer cost is a complex and important aspect of the design process. Gage cost is seldom an important factor.
- *Circuit output is a resistance change:* The resistance strain gage is a passive (as opposed to self-generating) sensor. Because it is essentially insensitive to supply-voltage frequency, it can be used with a.c. (carrier) or d.c. excitation systems. Gages normally operate in some form of bridge circuit, and these circuits can be easily arranged for altering transducer response through the addition or subtraction of moments and forces. This permits relatively straightforward design of complex transducers, which respond to (or reject) multiple components of input force as required.

(*) Spring structure is the steel body on which strain gages are mounted.

4.1.2 Column Load Cells

The column load cell has a history, which dates back to the earliest strain gage transducers. The column spring element consists of generally cylindrical members. The spring element is intended for axial loading; and typically has a minimum of four strain gages, two in the longitudinal direction, and two oriented transversely to sense the Poisson strain. The gages are connected to form a full-bridge circuit; but not a fully active bridge circuit because the transverse Poisson strain is much smaller than the axial strain.

The column is preferably made long enough with respect to its cross section so that a uniform strain field, unaffected by end conditions, is established at the strain gage locations. The column spring element can also be made hollow. For the same net cross-sectional area (and therefore the same compliance with respect to purely axial loads), the hollow cylinder is more resistant to bending because of its greater moment of inertia.

In this research, totally six load cells are combined to construct the internal force transducer. Detailed information about the load cells is given in the following parts of this chapter.

4.1.3 Selecting the Strain Gage Characteristics

The strain gage resistance is an important factor in transducer design, primarily because of its combined effects on output-signal amplitude and power dissipation. Transducers are commonly classified for sensitivity according to their full-scale output in mV/V (millivolts of output signal per volt of circuit excitation). Obviously, the signal-to-noise ratio can be noticeably improved by increasing the excitation voltage.

However, the improvement in signal quality is not "free", since the power dissipated in a strain gage increases with the square of the excitation voltage. Of broader significance, it may also cause problems in transducer stability and accuracy due to the thermal effects. All of the power consumed by the gages in a transducer must be dissipated as heat, flowing through the spring element, and its geometric configuration, along with the size and disposition of the gages, the maximum allowable power dissipation is ordinarily limited by the accuracy requirements.

In practice, many of the mechanical design parameters for a transducer are often largely fixed by the nature of the application. An attractive alternative for increasing the output signal without adding to the power dissipation is to use a higher resistance gage in conjunction with increased excitation voltage. Since most gage types are available in both 120- and 350-ohm versions, the latter is then preferred for transducers. Therefore, in this internal force transducer design, it is decided to use 350-ohm gages (J2A-06-S109M-350, Micro-Measurements) [38].

J2A series strain gages are encapsulated constantan-alloy patterns. Both the encapsulation and backing are thin, laminated polymide film. Gage soldering tabs are exposed for simplified lead connections. This series is capable of low and repeatable creep performance. J2A series strain gages are primarily recommended for use in precision transducers. Some specifications about J2A series strain gages are given in Table 4.1 [47].

Table 4.1 Specifications of J2A Series Strain Gages

Gage Series	Temperature Range		Strain Range	Gage Factor	Fatigue Life	
	Static	Dynamic			Strain Level in $\mu\varepsilon$	Number of Cycles
J2A	-75° to +95°C	-75° to +95°C	±3%	2.05 nom.	±1700 1700	10^6 10^7*

* Unidirectional Strain

4.2 Determination of the Capacity of the Internal Force Transducer

The main objective of this study was to test a structure that models a three-bay, four-story frame. This sub-assemblage will be constructed with three bays and two stories, of which the middle span will be infilled. For simplicity, the frame is chosen to be symmetrical about its center. For this structure, the distribution of the forces between the frame columns and infill wall will be investigated both experimentally and analytically at different load stages.

It was decided to take 1/3 for the scale factor of the model. In this case, length of the foundation will be approximately 5 meters and the story height including foundation will be 3 meters. The effect of upper two stories of the prototype structure should be incorporated to the model structure. It is very difficult to apply external moment and shear to the top of the columns of the model. Therefore, only axial force is taken in the account for model structure.

The prototype structure was modeled by the computer program SAP90 [39]. Axial forces to be applied on the model structure were calculated according to the result of the analysis of the prototype structure. Afterward, the model was analyzed by computer program DRAIN-2DX [40]. This computer program is a well-known nonlinear structural analysis program. Pushover analysis was performed both on the bare and infilled frames. Accordingly, the maximum internal forces were determined at the column end where the internal force transducer will be replaced. Table 4.2 shows the maximum internal forces at the level of transducers.

Table 4.2 Internal Force Transducer Load Range (At the base of the column).

Axial Load (kN)	Shear Force (kN)	Moment (kNm)
35	4	3

4.3 SHAPE OF THE INTERNAL FORCE TRANSDUCER

After deciding to manufacture a transducer for precisely measuring the internal forces at the bases of the two columns, an extensive literature survey was made to see what was done in the past. In the light of the observation of the past researches, it was decided to design the force transducer as a space truss. Some pre-design studies were carried out. Then, it was decided to use four bars placed vertically and two bars diagonally. It was assumed that four vertical bars would measure the axial force and the moment, and two diagonal bars would measure the shear force. It was recognized that hinge type of connections could not be used due to the difficulties in the manufacturing process. It is very difficult to obtain a perfect hinge behavior in the joints of truss members. Therefore, hinged connections were replaced with welded connections. Although, there are some examples of welded connections in the literature, experts on the transducer design, definitely prohibit the use of the welding in the manufacturing process. Reasons for this can be summarized as the following:

- The use of welding causes stress concentrations on the applied surface. These unknown stresses alter the linear behavior of the metal. A nonlinear metal could not be used as a transducer material.
- In the welding process, temperature rises significantly in the metal. This high temperature changes the characteristics of the metal. Nevertheless, the characteristics of the metal used in the transducer manufacturing must be known exactly.
- After the construction of the transducer, it is almost impossible to bond strain gauges on the bars. Consequently, strain gauges should be bonded on the bars, before they are assembled to a transducer. Therefore, there is always a risk to damage the strain gauges during the welding process.

As a result of above considerations, all links are changed to bolted type of connections. It was decided to have all bars of the transducer with hollow circular sections with 5 mm thickness. Their outer diameters would be 20 mm and the inner diameter would be 10 mm. Thickness of the bar is decreased to 3 mm in the middle region of the bars. It causes higher strains and sensitivity in this 30 mm region. These bars are fixed to the top and bottom plates with bolts. These plates have a dimension of 250×250×27 mm. The members were fabricated according to the drawings given in Figures 4.1, 4.2, 4.3, 4.4 and 4.5.

During the tests, there could be unexpected loadings on the column. Therefore, the safety factor was decided as two. Internal force transducer could be overloaded 100% of its strain capacity and still remaining on the safe side. Steel was selected as transducer material. Material characteristics of the steel are given in Table 4.3.

Table 4.3 Material Characteristics of Steel for Internal Force Transducer.

Yield Stress, f_y (MPa)	**Yield Strain ($\mu\varepsilon_y$)**	**Modulus of Elasticity (MPa)**
401	1759	227970

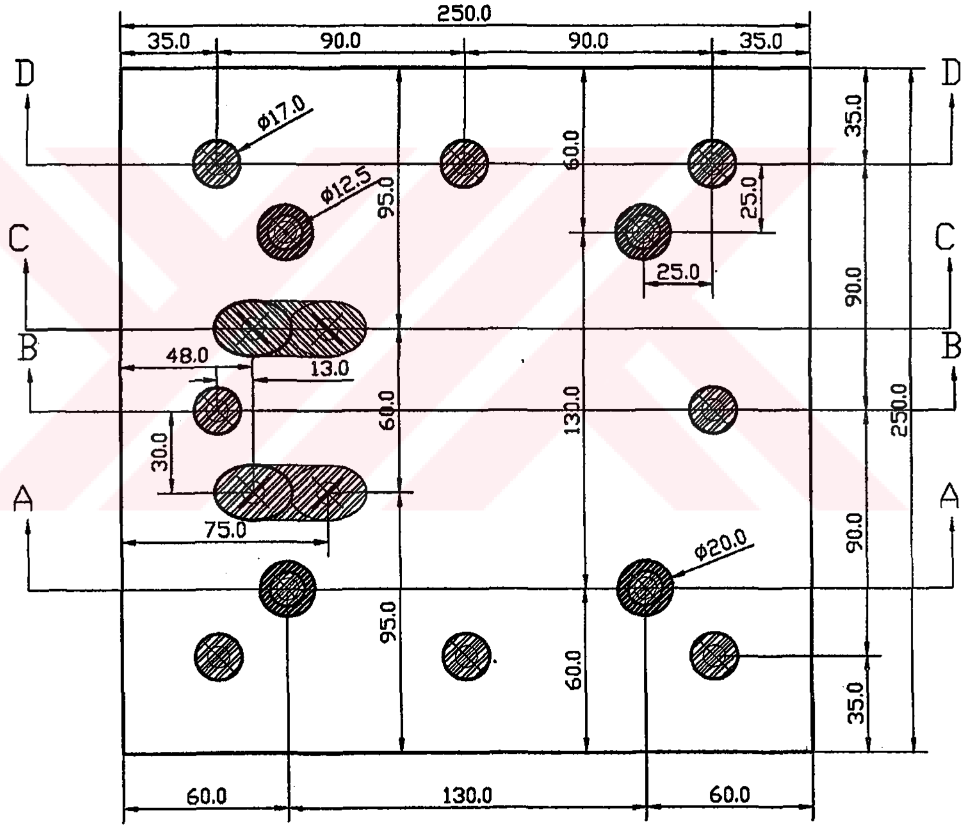

Figure 4.1 Plan of the Transducer

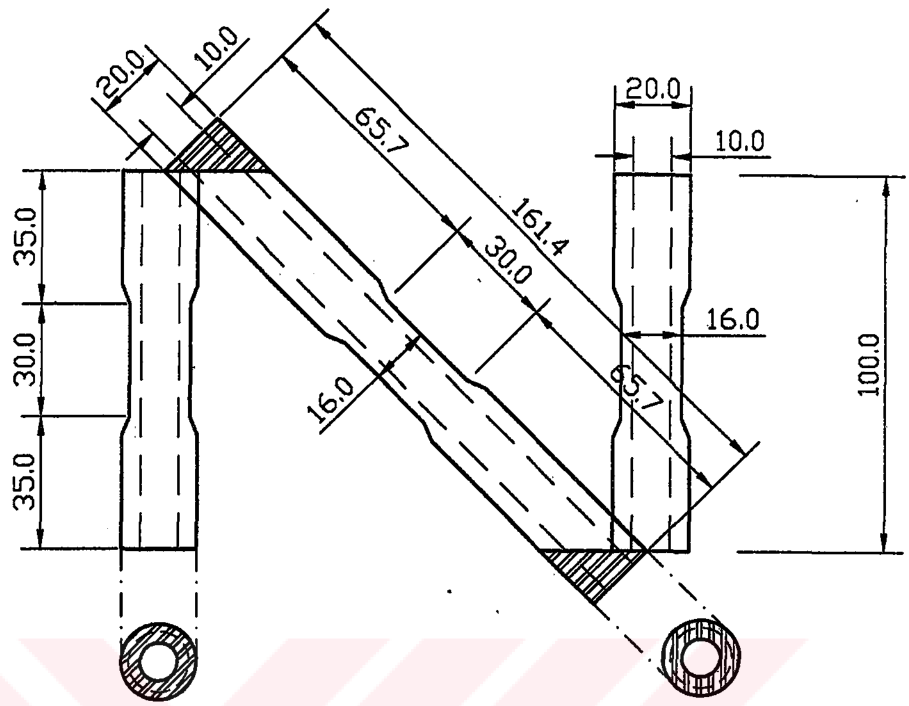

Figure 4.2 Bar Details of the Transducer

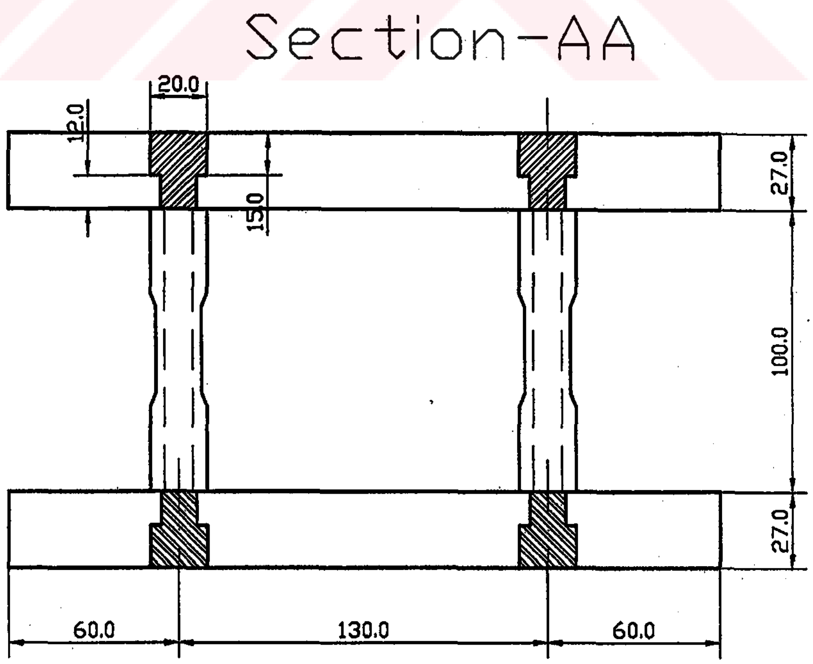

Figure 4.3 Details of the Section A-A

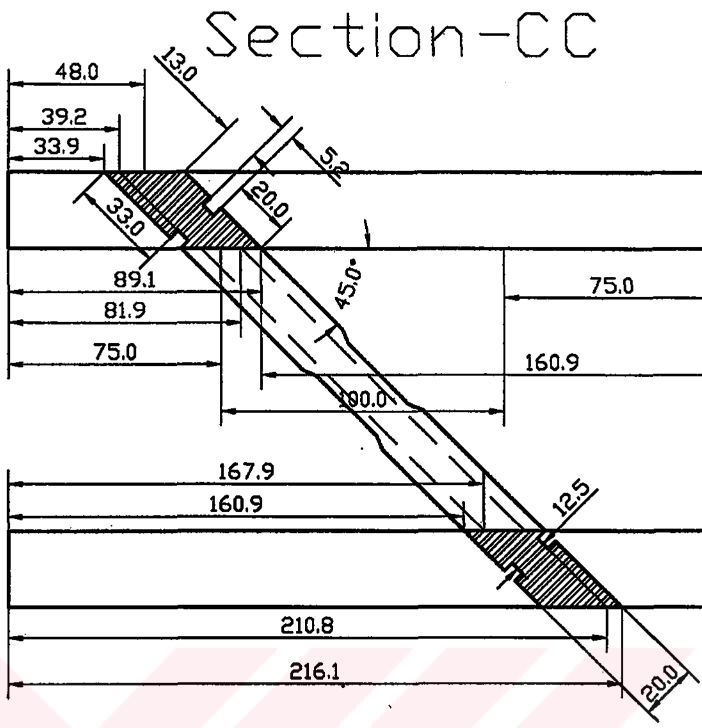

Figure 4.4 Details of the Section C-C

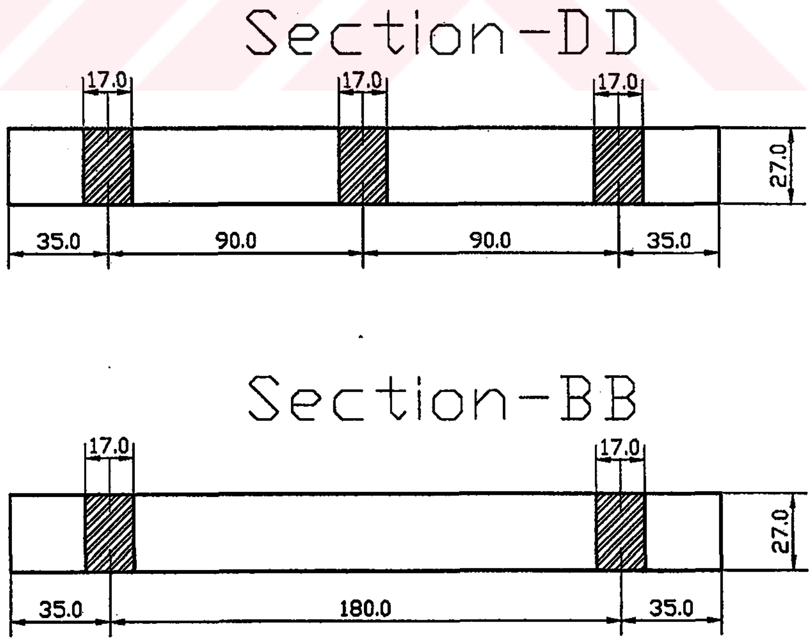

Figure 4.5 Details of the Section B-B and D-D

4.4 SELECTION OF THE LOCATION OF THE INTERNAL FORCE TRANSDUCER

In the literature, all force transducers are located slightly above mid-height of the columns. The most important consideration for this location is to avoid significant interference with the flexural stiffness of the column. The ideal location would be the inflection point of the column, which typically has the lowest flexural demand. However, locating the transducer at the mid-height would significantly influence the continuity of the member. The ideal internal force transducer had to be designed to have the same local stiffness properties as that region of the structural member which it replaces. However, this is impossible in practice, since reinforced concrete will have load dependent stiffness characteristics, while the structural metal used in the transducer will not exhibit these characteristics in the load range that it will be designed for. Besides, it is difficult to match flexural, shear, and axial stiffness simultaneously. Furthermore, during the experiments, at high load levels, as the structure goes to the inelastic range, inflection point of the columns will change its location. In addition, cyclic type of loading will move the location of the inflection point continuously.

Because of these uncertainties mentioned above, it is believed that selection of the mid-story height of the column, as the location of the internal force transducer has no advantage. Therefore, bottom of the column, connection to the base, was selected as the location of the internal force transducer. In this case, the disturbance of the continuity of the column could be minimized.

Placing of the transducer to the column base will change column properties slightly. The internal force transducer, in this case, could be seen both as a part of the column or as a part of the foundation. Some analytical studies were conducted to observe the influence of the transducer on the column internal forces.

Initially, the transducer was considered as a part of the column. Therefore, the total length of the column was reduced according to the transducer length. Since the flexural stiffness of the transducer is higher than that of the column, moment carried by this column will increase accordingly. Increased moment also results in increased shear at the foundation. Due to this drawback, the transducer should be calibrated to its top level to minimize the error. Secondly, the transducer was thought as a part of the foundation. In this case, the original column length had to be kept the same and the transducer had to be connected to the end of the column. In this situation, the transducer can be seen as a flexible foundation, instead of a fixed foundation. This results some moment release at the column end and accordingly, a shear force decrease. To minimize the error in shear force compared the original column and application of the transducer in the column, calibration of the transducer should be done according to its bottom level.

The structure was modeled and analyzed with computer program DRAIN-2DX, which is a non-linear structural analysis program. Two cases mentioned above and the original case without any transducer application, were studied to find out the change of the internal forces at the column base. Figure 4.6 shows the computer models of the structure.

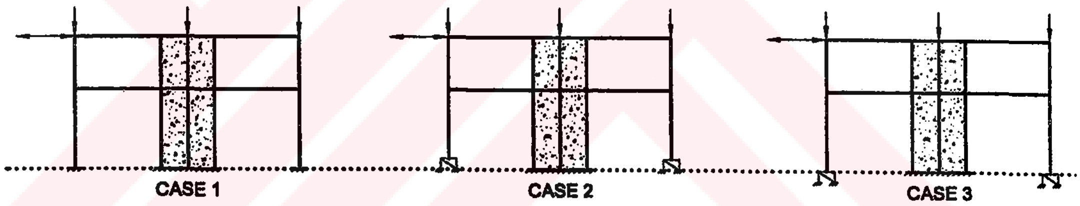

Figure 4.6 Computer models of the structure

In this figure, case 1 shows the original experimental model. Case 2 simulates the situation in which the transducer is a part of the column. Finally, case 3 models the transducer as a part of the foundation. On these structures, a cyclic pushover analysis was performed and changes in the internal forces were monitored at the column base. Figure 4.7, Figure 4.8 and Figure 4.9 show the axial force, shear force, and moment respectively at the bottom of the right column.

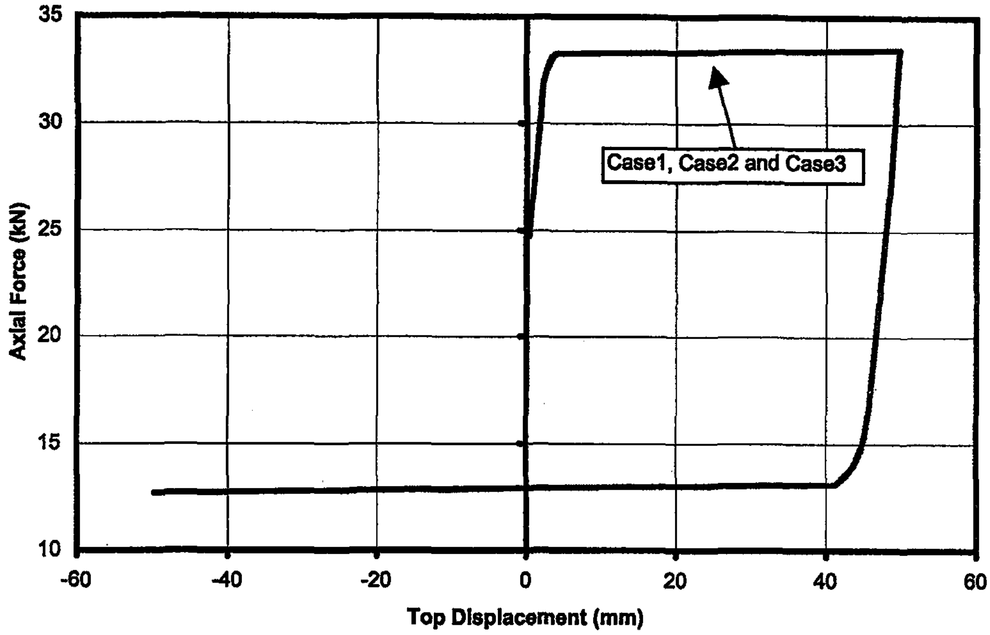

Figure 4.7 Axial force at the base of the right column

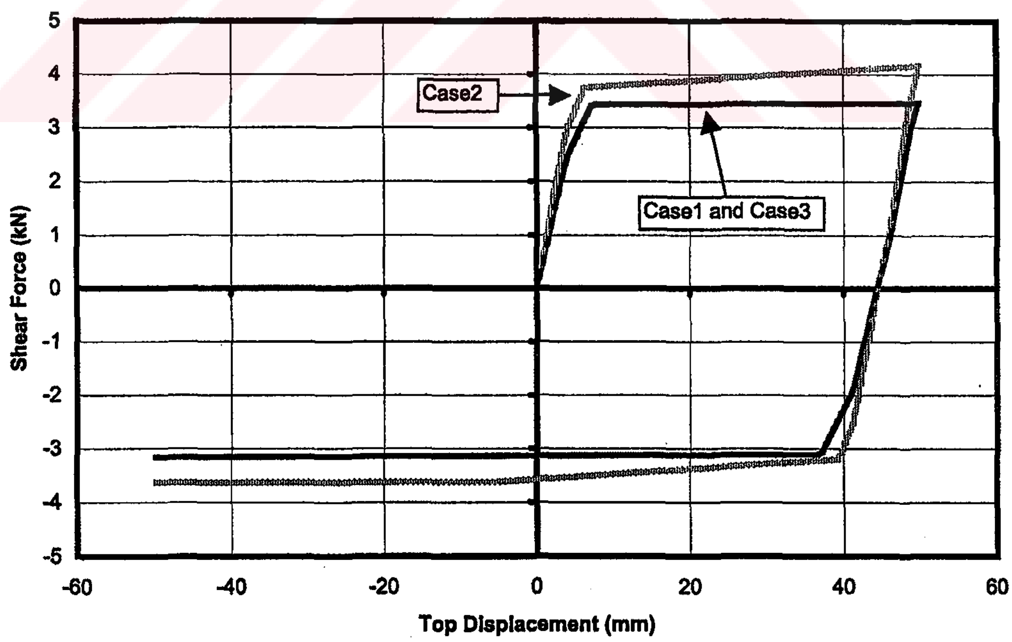

Figure 4.8 Shear force at the base of the right column

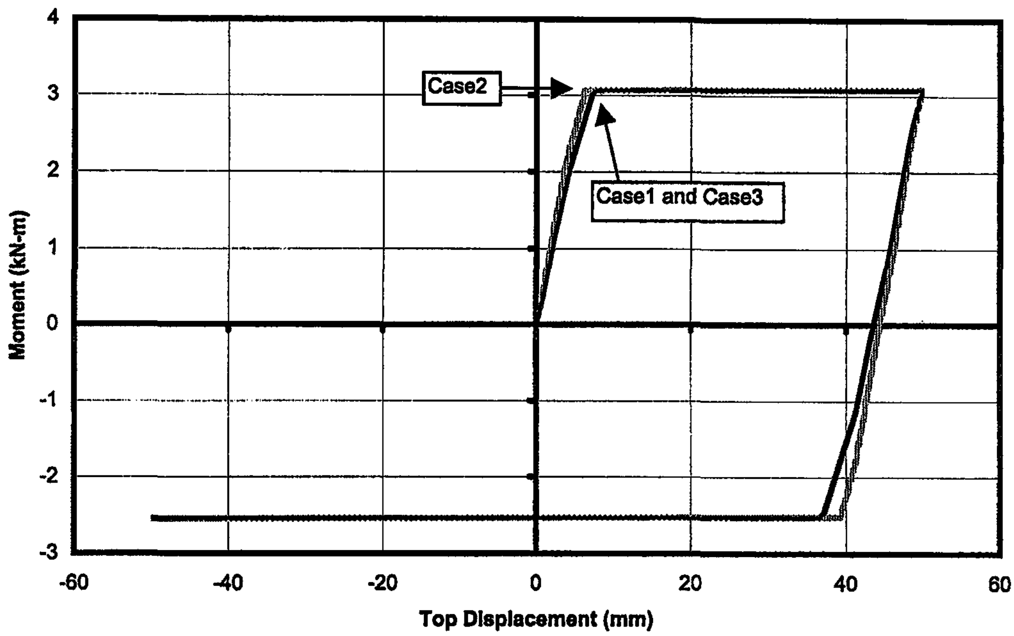

Figure 4.9 Moment at the base of the right column

These figures clearly show that case 3 matches the original structure better than case 2. In the comparison of axial forces, all three curves are almost identical. Error in the moment is also small for engineering purposes. However, shear force is over-estimated approximately 20%, if case 2 is used. A similar study was performed on the bare frame. In the bare frame, almost the same trends were observed in the internal forces.

In the light of the above analytical studies and past reports, the bottom end of the column was selected for the location of the internal force transducer. It should be noted that, in this case the column length will be kept unchanged.

4.5 Instrumentation of the Internal Force Transducer

The strains developed in the members of the transducer during loading are measured using polyimide backed foil strain gauges. Each bar is comprised of an independent full Wheatstone Poisson's arrangement bridge of four strain gages [41,42,43,44]. The Wheatstone bridge is a circuit that can be employed to determine the change in resistance, which a gage undergoes when it is subjected to a strain. Figure 4.10 shows the principle of operation of the Wheatstone bridge as a direct-readout device where ΔE is measured to determine the strain.

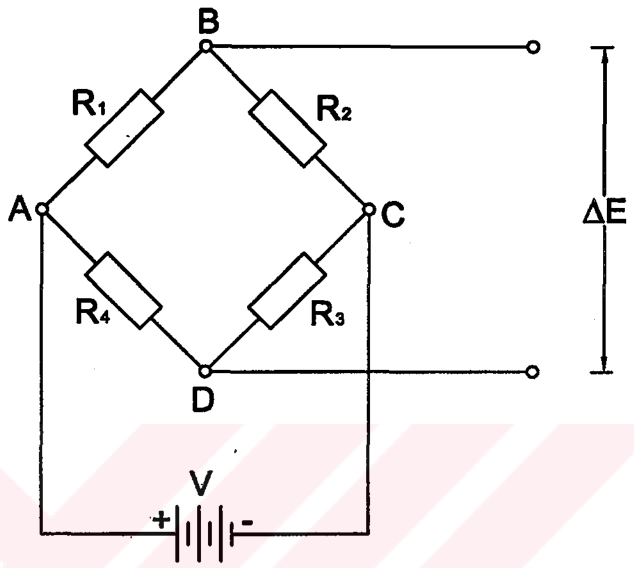

Figure 4.10 Wheatstone Bridge Configuration

Four strain gages were mounted on the central region of the bar with two opposite gages in the axial direction and two opposite gages in the transverse direction, which converts each bar into a load cell, Figure 4.11.

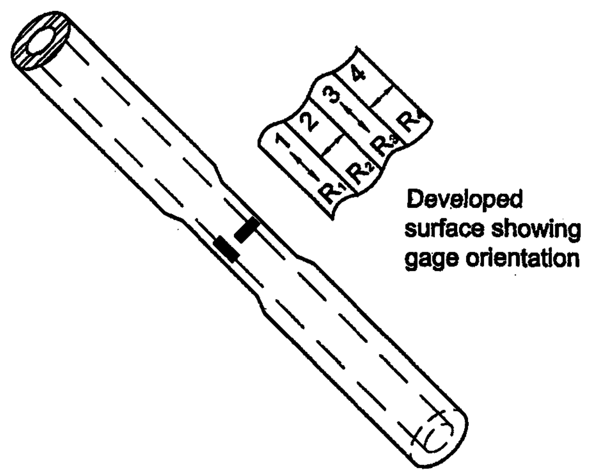

Figure 4.11 Strain gages mounted on a bar to make a load cell

If the four gages are positioned in the Wheatstone bridge as shown in Figure 4.11, the ratio of output voltage to supply voltage $\Delta E/V$ will be as given by Eq. (4.1).

$$\frac{\Delta E}{V} = \frac{1}{4}\left(\frac{\Delta R_1}{R_1} - \frac{\Delta R_2}{R_2} + \frac{\Delta R_3}{R_3} - \frac{\Delta R_4}{R_4}\right) \tag{4.1}$$

Placement of the strain gages on the four sides of the bar as shown above, provides a load cell, which is essentially independent of either flexural or torsional loads. Consider a bending moment M applied to the bar. The moment M may have any direction relative to the axes of symmetry of the cross section, as shown in Figure 4.12. The components M_1 and M_2 of the moment M will produce resistance changes in the gages as follows:

$$\left.\frac{\Delta R_2}{R_2}\right|_{M1} = -\left.\frac{\Delta R_4}{R_4}\right|_{M1} \quad \text{and} \quad \left.\frac{\Delta R_1}{R_1}\right|_{M1} = \left.\frac{\Delta R_3}{R_3}\right|_{M1} = 0$$

$$\left.\frac{\Delta R_3}{R_3}\right|_{M2} = -\left.\frac{\Delta R_1}{R_1}\right|_{M2} \quad \text{and} \quad \left.\frac{\Delta R_2}{R_2}\right|_{M2} = \left.\frac{\Delta R_4}{R_4}\right|_{M2} = 0$$

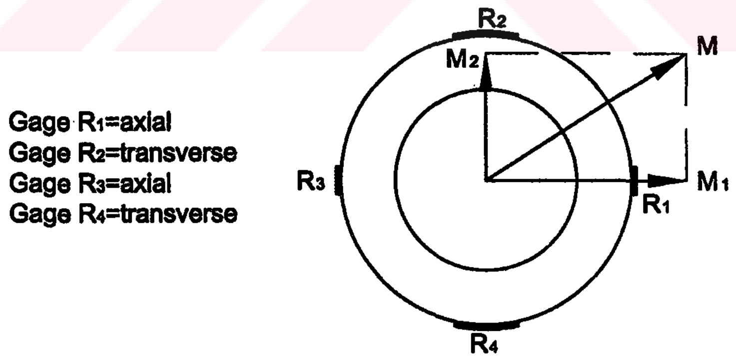

Figure 4.12 Resolution of the moment M into components M_1 and M_2

It could be also proved that if the bar is subjected to a torque T, the output $\Delta E/V$ will be equal to zero. Temperature compensation is also achieved with the four active strain gages in the bridge.

Eq. (4.2) shows the relationship between output voltage of the bridge and axial strain in the bar. The axial strain is also related directly to the excitation voltage V and gage factor K of the strain gages bonded on the bar.

$$\varepsilon = \frac{2\left[\left(\frac{\Delta E}{V}\right)_{strained} - \left(\frac{\Delta E}{V}\right)_{unstrained}\right]\times 10^{6}}{K\left[(\nu+1)+(1-\nu)\left\{\left(\frac{\Delta E}{V}\right)_{strained} - \left(\frac{\Delta E}{V}\right)_{unstrained}\right\}\right]} \tag{4.2}$$

A common requirement in strain gage work is to obtain the recommended value of bridge excitation voltage for a particular size and type of gage. Unfortunately, a simple, definitive answer to this question is not possible, because factors other than gage type are involved. It is important to realize that strain gages are seldomly damaged by excitation voltages considerably in excess of maximum predicted values. The usual result is performance degradation, rather than gage failure.

When the temperature rise is excessive, hysteresis and creep effects are magnified, since these are dependent on backing and glueline temperatures. In addition, zero (no-load) stability is strongly affected by excessive excitation.

Following are factors of primary importance in determining the optimum excitation level for any strain gage application [45]:

- *Strain gage grid area* (active gage length × active grid width).
- *Gage resistance.*
- *Heat-sink properties of the mounting surface.*
- *Environmental operating temperature range of the gage installation.* Creep in the gage backing and adhesive will occur at lower ambient temperatures when grid and substrate temperatures are raised by self-heating effects.
- *Required operational specifications.* Gages for normal stress analysis can be excited at a higher level than under transducer conditions, where the utmost in

stability, accuracy, and repeatability is needed. A significant distinction exists between gages used in dynamic strain measurement and those used in static measurement applications.

- *Installation and wiring technique.* If the gage is damaged during installation, if solder tabs are partially unbonded due to soldering heat, or if any discontinuities are formed in the glueline, high levels of excitation will create serious problems.

When grid area (A_G), gage resistance (R_G), and grid power density (P'_G) are known, bridge excitation (V) can be calculated in volts as given in Eq. (4.3):

$$V = 2 \cdot \sqrt{R_G \times P'_G \times A_G} \tag{4.3}$$

For static experiments with moderate accuracy requirements, power density remains between 1 and 2 watts/in^2 for fair heat-sink conditions (thin stainless steel). The selected strain gage (J2A-06-S113M-350) has a gage length and grid width of 0.110 × 0.080 in^2. These numbers give a bridge excitation between 3.5 and 5 volts. For higher output voltage, 4 volts is selected as bridge excitation voltage.

The full-bridge circuits commonly used in transducers tend to provide inherent compensation for thermal output (apparent strain) if all gages have identical characteristics and sense identical temperatures. Since these conditions can never be precisely satisfied, best transducer accuracy will be achieved by selecting the self-temperature-compensation number of the gages to match the thermal expansion coefficient of the spring material.

On the bars of the transducer, two gages were aligned transversely to the longitudinal axis to sense the Poisson strain. The result is the compensation of the thermal output, accompanied by an augmented output signal (by the factor (1+ν)). A further caution is necessary when strain gages are mounted transversely on small-diameter rods. Under this condition, the thermal output characteristics of a strain gage are different than the case when the gage is mounted on a flat surface of the same material [46].

Strain gages used in the internal force transducer have the self-temperature-compensation number of 6, which means that strain gages have a nominal value at or near room temperature of 6 ppm/F° (10.84×10^{-6} per C°) as coefficient of thermal expansion. This value approximately corresponds to the thermal expansion coefficient of the steel.

Strain gages can be satisfactorily bonded to almost any solid material if the material surface is prepared properly. While a properly prepared surface can be achieved in more than one way, the micro-measurements system of surface preparation is followed in this study [48]. It includes five basic operations. In the usual order of execution, these are:

- *Solvent degreasing*
- *Abrading*
- *Application of gage layout lines*
- *Conditioning*
- *Neutralizing*

Micro-Measurements Certified M-Bond 200 Adhesive is used for the strain gage installation. It is an excellent general-purpose laboratory adhesive because of its fast room-temperature cure and ease of application. M-Bond 200 is a modified alkali cyanoacrylate compound. M-Bond 200 can be used in tests where the elongations are very big in excess of 60 000 microstrain, for fatigue studies, and for one-cycle proof tests to over +95°C or below -185°C. The normal operating temperature range is –30°C to +65°C [49].

Because of normal gage resistance tolerance (0.3%), and additional resistance changes produced during gage installation, the bridge circuit is usually in a resistively unbalanced state when first connected. With stand-alone transducers, for purposes of general applicability with differing instrument systems, it is advantageous to have the bridge circuit initially balanced, or approximately so. A typical transducer of this type would commonly be balanced when its electrical output at no-load deviates from zero by not more than ±1% of full-scale output. After carefully measuring the initial unbalance, the nominal value of the compensating resistor can be calculated directly. The corresponding resistance change can be expressed as given in Eq. (4.4):

$$\Delta R = K \times \varepsilon \times R_B \tag{4.4}$$

where: ΔR = resistance change, ohms

K = gage factor of gages

ε = equivalent output strain

R_B = bridge resistance

137-HWN/Manganin Resistance Wire (diameter = 0.114 mm) was used for compensating the no-load deviation. Since this wire has a resistance of 50 ohm per meter, it was easy to calculate the required length of wire. Depending on the direction of the initial unbalance, the small wire could be inserted in series with the gage in one arm of the bridge for approximate zero balance.

Sensitive strain gage circuits require protection against the environments. Even under indoor conditions, airborne moisture and low-level contaminants can adversely affect long-term stability. Measurements Group M-Coat A was used as protective coating. This coating was suitable for a typical laboratory environment. This coating is a transparent, air-drying solvent-thinned (xylene) polyurethane. It has a moderate hardness and good flexibility.

During the calibration process, transducers were bolted and unbolted many times. Unfortunately, two of the strain gages were damaged by an accidentally strike of a wrench during fixing the transducers. These strain gages were replaced with new ones, re-wired and re-coated. However, strain gages were still unprotected against strikes. Therefore, all bars were covered with transparent hoses by gluing them with silicone at top ends. After this protection, no gages were damaged during the calibration process. Figure 4.13 shows a photo of the protection of the strain gages with hoses.

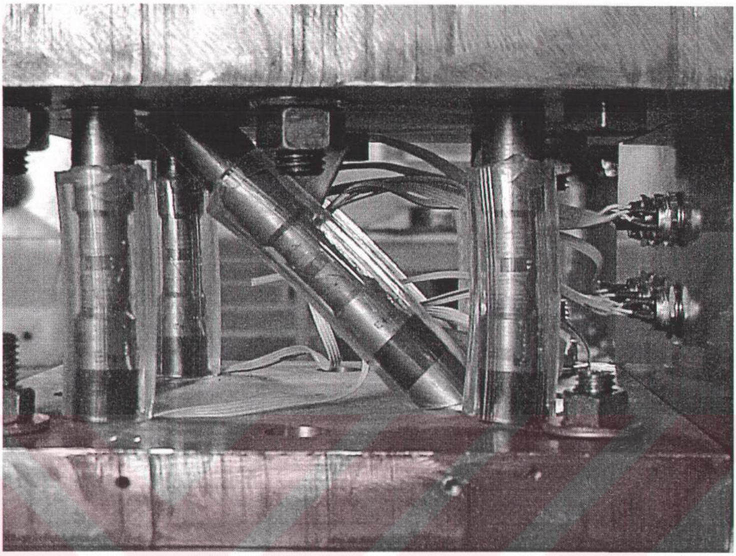

Figure 4.13 Protection of the strain gages with transparent hoses

4.6 Calibration Procedure of the Internal Force Transducer

4.6.1 General

The formulation of the calibration was achieved by the aid of lecture notes of Prof. Tankut [50]. Section 4.6.2 of this thesis is directly taken from these lecture notes.

Internal forces cannot be measured directly, but instead transducer measures a related quantity which can be measured easily. In the internal force transducer, forces are related to strain measurements. Even the measurement of strain is indirect; e.g., the change of electrical resistance is measured. In this case, a reliable formulation of the relationship between the quantity actually measured and the quantity to be determined is needed. This formulation is known as the calibration of the system used [50].

4.6.2 Mathematical Formulation for the Calibration

In the simplest case of one quantity to be determined in terms of the other, which is measured, the calibration can be expressed by the following function,

$$y = f(x)$$

where x is the quantity actually measured

y is the quantity to be determined

The basic requirement of such a formulation is obviously the capability of the system to repeat the same response to the same effect every time.

In the force transducer, there are totally six measured quantities (four vertical bars and two diagonal bars) to determine the three internal forces (axial force, shear force and moment). Since the system used is linearly elastic, the relationship can be expressed in form of a calibration matrix.

$$\begin{aligned} y_1 &= s_{11}x_1 + s_{12}x_2 + \ldots + s_{16}x_6 \\ y_2 &= s_{21}x_1 + s_{22}x_2 + \ldots + s_{26}x_6 \\ y_3 &= s_{31}x_1 + s_{32}x_2 + \ldots + s_{36}x_6 \end{aligned}$$

where y_1, y_2 and y_3 are the axial force, shear force and the moment.

The system can be expressed in the matrix form as given in Eq. (4.5)

$$\begin{Bmatrix} y_1 \\ y_2 \\ y_3 \end{Bmatrix} = \begin{bmatrix} s_{11} & s_{12} & s_{13} & s_{14} & s_{15} & s_{16} \\ s_{21} & s_{22} & s_{23} & s_{24} & s_{25} & s_{26} \\ s_{31} & s_{32} & s_{33} & s_{34} & s_{35} & s_{36} \end{bmatrix} \begin{Bmatrix} x_1 \\ x_2 \\ x_3 \\ x_4 \\ x_5 \\ x_6 \end{Bmatrix} \tag{4.5}$$

or $$\{Y\} = [S]\{X\} \tag{4.6}$$

Since the calibration matrix [S] is somehow constructed, then the above fundamental relationship serves as a transformer. The calibration matrix [S] can be constructed by applying a sufficient number of known {Y} sets and measuring the corresponding {X} sets as explained below.

Stage	Applied	Measured
1	$y_{11}\ y_{21}\ y_{31}$	$x_{11}\ x_{21}\ x_{31}\ x_{41}\ x_{51}\ x_{61}$
2	$y_{12}\ y_{22}\ y_{32}$	$x_{12}\ x_{22}\ x_{32}\ x_{42}\ x_{52}\ x_{62}$
$\vdots$	$\vdots$	$\vdots$
P	$y_{1p}\ y_{2p}\ y_{3p}$	$x_{1p}\ x_{2p}\ x_{3p}\ x_{4p}\ x_{5p}\ x_{6p}$
	$\Downarrow$	$\Downarrow$
	$[\overline{Y}]$	$[\overline{X}]$
	(px3)	(px6)

p is the number of calibration stages ($p \geq 6$). If these values are placed in the fundamental relationship,

$$\begin{bmatrix} y_{11} & y_{12} & \cdots & y_{1p} \\ y_{21} & y_{22} & \cdots & y_{2p} \\ y_{31} & y_{32} & \cdots & y_{3p} \end{bmatrix} = \begin{bmatrix} s_{11} & s_{12} & \cdots & s_{16} \\ s_{21} & s_{22} & \cdots & s_{26} \\ s_{31} & s_{32} & \cdots & s_{36} \end{bmatrix} \begin{bmatrix} x_{11} & x_{12} & \cdots & x_{1p} \\ x_{21} & x_{22} & \cdots & x_{2p} \\ \vdots & & & \\ x_{61} & x_{62} & \cdots & x_{6p} \end{bmatrix}$$

or

$$[\overline{Y}]^T = [S] \times [\overline{X}]^T$$

or

$$[\overline{Y}] = [\overline{X}] \times [S]^T$$

pre-multiplying both sides by $[\overline{X}]^T$,

$$[\overline{X}]^T \times [\overline{X}] \times [S]^T = [\overline{X}]^T \times [\overline{Y}]$$

solving for [S],

$$[S] = \left[\left([\overline{X}]^T [\overline{X}] \right)^{-1} [\overline{X}]^T [\overline{Y}] \right]^T \tag{4.7}$$

The above expression represents the best solution using the method of least squares. There are 6x3 unknowns from px3 equations (more than minimum required, since $p \geq 6$).

All calculations on the calibration matrix are performed by the aid of computer program MathCAD2000 Professional(*). "x" and "y" matrices are prepared as an Excel file. Then, the calibration matrix "s" is computed according to Eq. (3.7). Applied force is recalculated by multiplying calibration matrix "s" with the transpose of the "x" matrix, which contains six voltage readings during the calibration process and given as matrix "ReCalc". Figure 4.14 shows the code of the MathCAD program.

ORIGIN := 1

x := C:\..\x.xls

y := C:\..\y.xls

$$s := \left[\left(x^{T} \cdot x\right)^{-1} \cdot x^{T} \cdot y\right]^{T}$$

C:\..\s.xls

s

$$ReCalc := s \cdot x^{T}$$

C:\..\kalib.xls

$ReCalc^{T}$

Figure 4.14 The Code of the MathCAD Program for Calculating the Calibration Matrix

4.6.3 Mechanics of Calibration

A certain test set-up is developed for the calibration of the internal force transducer considering the requirements set for the system. In arranging this set-up, the following important points should be taken into account:

- The input (i.e. quantities to be determined later) must be very well defined and provided by a reliable source (reference of calibration).
- Preferably, the same instruments should be used in the calibration as in the test frame.

(*) Licensed by METU

- Calibration procedure should preferably be repeated many times to ensure that the system repeat the same response to the same effect, and then the data obtained must be processed to obtain the best statistical fit (e.g. by the method of least squares)

It is necessary to load the force transducer above the specified load range before calibration, to insure a stable zero reference. This "overloading" is effective in relieving residual stresses in the strain gages due to their application. For all the calibrations, 4 to 6 cycles of loading were used, until the strain reading corresponding to zero load remained constant for 2 load cycles.

Although the calibration for the axial force is a simple procedure, careful consideration of the boundary conditions is required. Since the transducer has a width to height ratio of almost unity, it is important to distribute the load to the transducer end plates in a uniform manner. To provide uniform bearing, several smooth plates are stacked between the transducer and the load head. In addition, a hinged joint is used in providing the load. Figure 4.15 below shows the set-up used for the axial load calibration for the transducer.

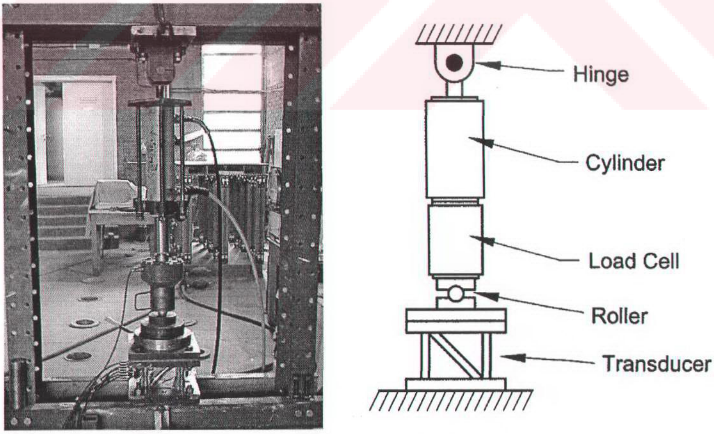

Figure 4.15 The Set-up used for the Axial Calibration of the Transducer

Since, the mid-height of the top plate of the transducer is chosen as reference point, it greatly simplifies the shear calibration set-up. However, in this type of a set-up, some moment is applied to the transducer. However, the magnitude of such moments is low. This moment is also considered during the calculation of the calibration matrices. Figure 4.16 shows the shear calibration set-up for the transducer.

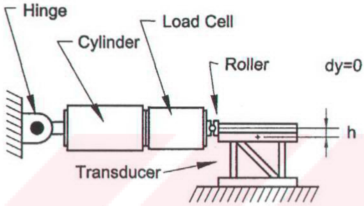

Figure 4.16 The Set-up used for the Shear Calibration of the Transducer

Combined moment, shear and axial force calibration was achieved by applying an inclined force at a given distance. By chancing the angle β and the distance ℓ, it was possible to apply the three forces in many different combinations simultaneously. By adjusting the angle β and the distance ℓ, force combination close to the values reached in the sub-assemblages could be obtained. The set-up used for the combined force application is given in Figure 4.17.

Totally, eight different types of loadings were applied on each transducer during the calibration procedure. The first four sets are for a combined moment, shear and axial load application. The fifth and eighth sets are for axial compression and tension. Finally, sixth set is for positive shear and seventh for negative shear with a little moment applied simultaneously on the transducers. Positive directions of the applied forces and orthogonal x and y-axes are shown in Figure 4.17. The following equations could be written from the figure:

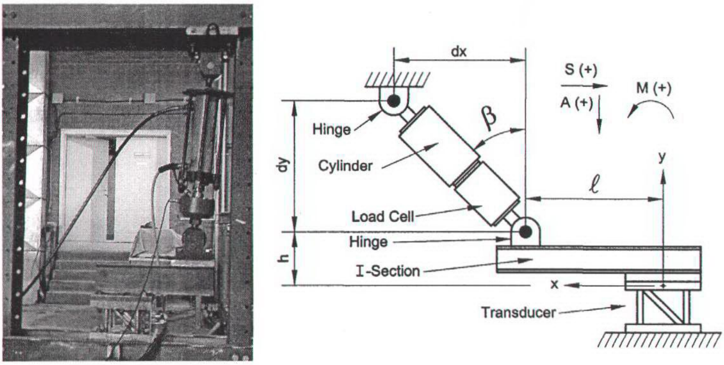

Figure 4.17 The Set-up used for the Combined Moment, Shear and Axial Load Calibration of the Transducer

$$\beta = arc\ tan\left(\frac{dx}{dy}\right)$$
$$A = F \cdot cos\ \beta$$
$$S = F \cdot sin\ \beta$$
$$M = F \cdot cos\ \beta \cdot \ell - F \cdot sin\ \beta \cdot h$$

where,

A : Axial Force applied on the transducer

S : Shear Force applied on the transducer

M : Moment applied on the transducer

F : Applied forces obtained from the load cell

Table 4.4 given below summarizes the values of variables for different types of loading. These variables can be followed from Figure 4.17.

Table 4.4 Variables under different loading

Calib. No	Transducer #1					Transducer #2				
	ℓ (mm)	h (mm)	dx (mm)	dy (mm)	α (degree)	ℓ (mm)	h (mm)	dx (mm)	dy (mm)	α (degree)
1	290	276	54	735	4.202	290	276	55	735	4.279
2	-290	276	-52	735	-4.047	-290	276	-53	735	-4.124
3	290	276	310	735	22.868	290	276	308	735	22.736
4	-290	276	-309	735	-22.868	-290	276	-308	735	-22.736
5	0	-	0	0	0	0	-	0	0	0
6	-	28	-	-	90	-	28	-	-	90
7	-	28	-	-	90	-	28	-	-	90
8	0	-	0	0	0	0	-	0	0	0

4.6.4 Results of the Calibration Procedure

Calibration matrices of the force transducers are calculated using Eq. (4.7). These matrices, S_1 and S_2 of transducer no 1 and no 2, are provided below (In metric units). For showing the success of matching the applied forces with calculated forces, totally six figures were plotted. Figures 4.18, 4.19, 4.20, 4.21, 4.22, 4.23 correspond to axial force, shear force and moment for transducer no 1 and no 2 respectively. These figures show applied forces on the transducer and the forces calculated by multiplying the six voltage outputs of the bars by the calibration matrix.

$$S_1 = \begin{bmatrix} 287.5 & 615.1 & 341.6 & 578.2 & 283.9 & 364.3 \\ -56.3 & 37.7 & -76.5 & 74.1 & 242.1 & 550.5 \\ 2739.4 & 3147.3 & -2745.3 & -3340.6 & 5956.7 & 10.7 \end{bmatrix}$$

$$S_2 = \begin{bmatrix} 535.7 & 318.8 & 572.5 & 288.6 & 209.2 & 367.1 \\ -2.0 & 31.7 & -13.8 & 59.9 & 324.5 & 363.1 \\ 2870.6 & 3081.4 & -1434.7 & -3979.7 & 2735.8 & 2267.4 \end{bmatrix}$$

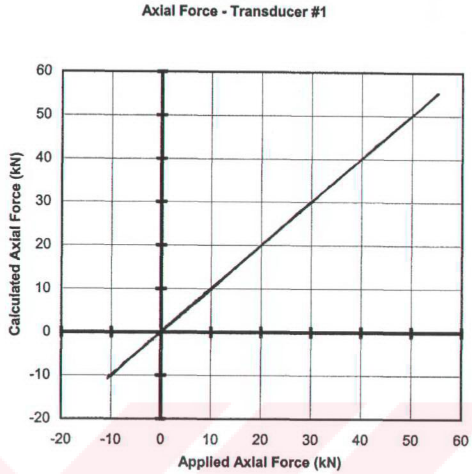

Figure 4.18 Comparison of the Applied and Calculated Axial Forces during the Calibration of Transducer No 1

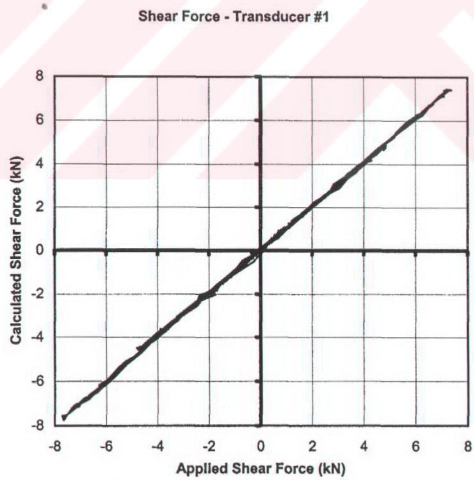

Figure 4.19 Comparison of the Applied and Calculated Shear Forces during the Calibration of Transducer No 1

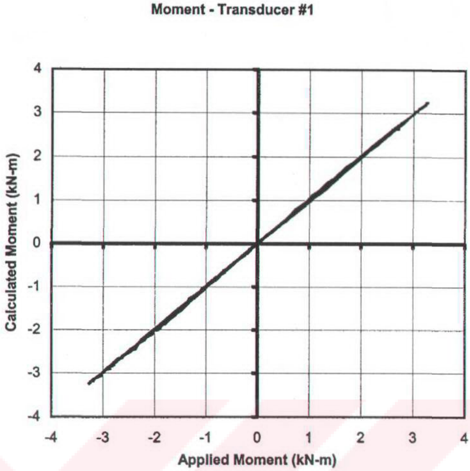

Figure 4.20 Comparison of the Applied and Calculated Moments during the Calibration of Transducer No 1

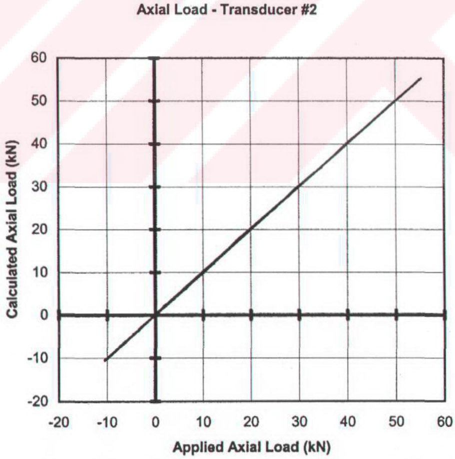

Figure 4.21 Comparison of the Applied and Calculated Axial Forces during the Calibration of Transducer No 2

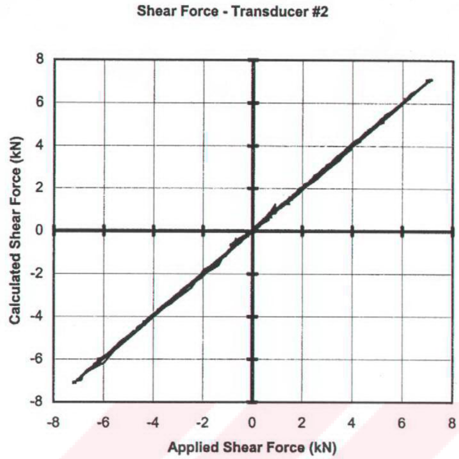

Figure 4.22 Comparison of the Applied and Calculated Shear Forces during the Calibration of Transducer No 2

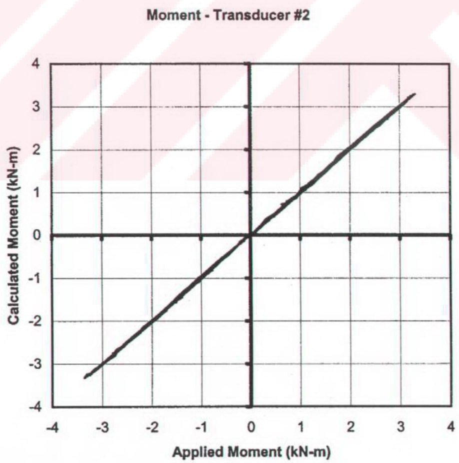

Figure 4.23 Comparison of the Applied and Calculated Moments during the Calibration of Transducer No 2

Finally, a typical example of the calibration output is given in Figure 4.24 (In metric units). This figure shows the strain values of the six bars during the first calibration set of the first transducer. In this calibration set, high moment, moderate axial force and very small shear force was applied on the transducer. Load was applied with a very small inclination aligned with the vertical line (α=4.202°). Therefore, shear force in the transducer remained at very low levels. Additionally, axial load applied to the transducer was almost equal to the load applied through the load cell. In this figure, the maximum axial load applied to the transducer was 1.2 tons, shear force was 0.09 tons and the moment was 0.33 t-m. The figure below reveals that due to high moment, the front vertical bars (CH1, CH2) are in compression, whereas vertical bars behind (CH3, CH4) are in tension. Due to the effect of the axial load, bars in the back and front did not show the same strains. Because of the low level of shear force applied on the transducer, the two diagonal bars (CH5, CH6) showed very small strains. In these high levels of moment and axial forces, the transducer was kept at a maximum strain level of only 600 $\mu\varepsilon$, which provides a linear hysteretic behavior and a minimum safety factor of 2.0 against overloading.

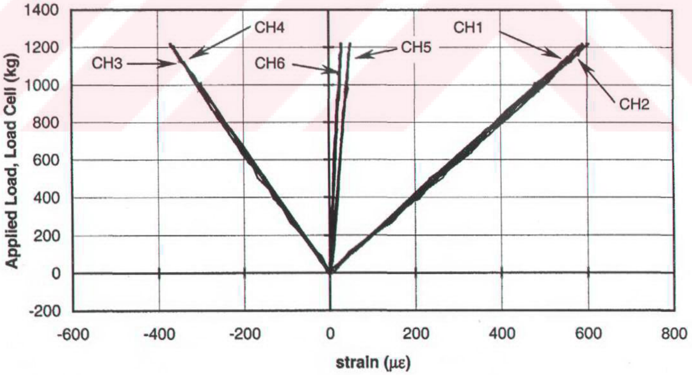

Figure 4.24 A typical strain output of six bars of the transducer #1 during the calibration process #1

CHAPTER 5

TEST RESULTS AND OBSERVED BEHAVIOR

5.1 GENERAL

In this chapter, test results and experimental observations are presented in detail. For each specimen, the loading history, load displacement curves, moment-curvature curves, drift ratio curves and the variation of the forces at the base of the external columns with the lateral load are given.

The load history curves show the loading pattern of the specimens. The absolute maximum values at each half cycle can be observed from these curves.

In this chapter, curves showing the variation of the lateral displacements of the first and second stories with the lateral loading are also given. During the test, the horizontal load was applied only at the second story level. Therefore, lateral load is equal to the total base shear. Hence, the values on the lateral load axis can be taken as the total base shear. In addition to the lateral load-displacement curves, curves showing the variation of drift ratios of the first and second stories are also given. Drift ratio of a story was calculated as the relative displacement of that story divided by the story height. Relative displacement is equal to the difference in displacement between that story and the upper story.

The moment-curvature curves are also given in this chapter. Moments at the base of external columns were calculated using the data obtained from the force transducers. Curvatures were calculated using the readings from the two dial gages mounted near the base of the columns. A sketch of the dial gage locations and dimensions for curvature calculations are given in Figure 5.1.

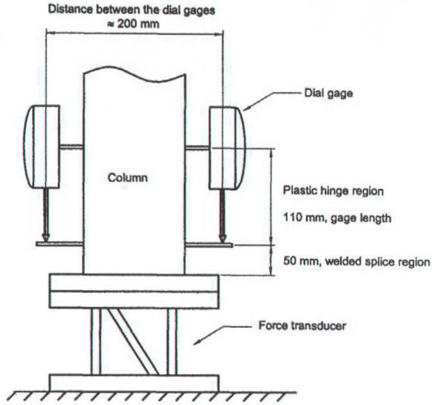

Figure 5.1 A sketch of the dial gage arrangement

Finally, the internal forces measured by the transducers at the base of external columns were plotted against lateral load.

5.2 BARE FRAME, B1

B1 was the bare frame. The aim of this test was to produce a reference specimen and to compare the results with the results of the infilled frame test.

The specimen B1 was damaged under the lateral loading history presented in Figure 5.2. The first two cycles remained in the elastic range. At the first positive loading, there was a problem with the hydraulic jack. Consequently, the load was released and the hydraulic jack was replaced with a new one. During the test, 9 kN constant axial load was applied to each of the four columns. The strength of concrete at the day of the test was 13.2 MPa. Therefore, the applied axial load was about $0.056 f_{ck} A_c$ before the application of the lateral load.

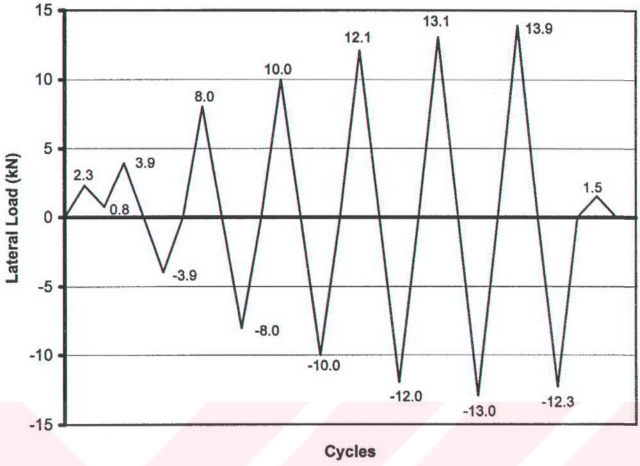

Figure 5.2 Lateral Load History of Specimen B1

The maximum lateral load applied on the bare frame was 13.9 kN. At this load level, the top displacement of the frame was 40 mm. In Figure 5.3 and Figure 5.4, load-displacement curves are presented for each story.

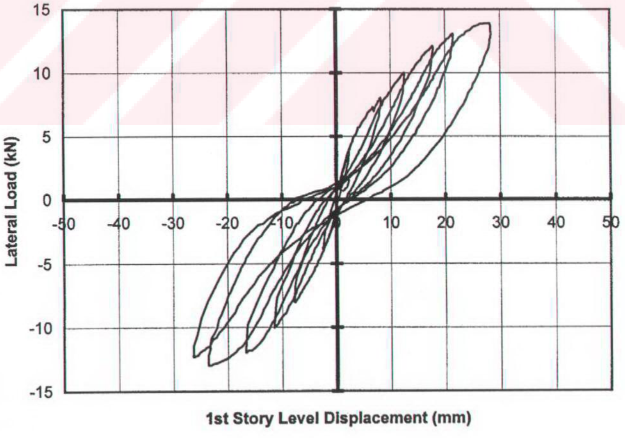

Figure 5.3 Lateral Load-Displacement Curve of the 1st Story, Specimen B1

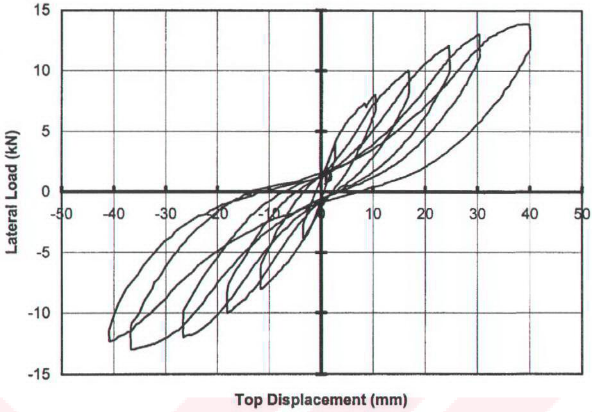

Figure 5.4 Lateral Load-Displacement Curve of the 2nd Story, Specimen B1

At 10 kN level of the third cycle, cracks were observed at the ends of the beams of the first story. Joint cracks were observed in the negative direction of this cycle. New cracks occurred in the following cycles. The maximum measured crack width was 0.8 mm at fourth cycle and 1 mm at the fifth cycle. At the sixth and last cycle, cover separation occurred at the left exterior joint of the first story and the 90° bent portion of the beam longitudinal reinforcement came out due to the poor detailing (no confinement at the joint). Figure 5.5 shows this cover separation at the left exterior beam-column joint. Crack pattern in the 1st story exterior beam-column joint is shown in Figure 5.6. The crack patterns at the second story right interior beam-column joint and at the outer face of the right exterior column are given in Figure 5.7 and Figure 5.8 respectively.

The drift ratio of each story was calculated and plotted against the applied lateral load. Since, the displacements in these curves are relative and normalized with respect to the story height, they are more meaningful. It is obvious from the Figure 5.9 and Figure 5.10 that, drifts of the first and second stories were very high. The ratio was approximately 2% for the first story and 1.5% for the second story. Therefore, the frame could be classified as "Moderately Damaged".

Figure 5.5 Cover separation at the left exterior column-beam joint (1st story), Specimen B1

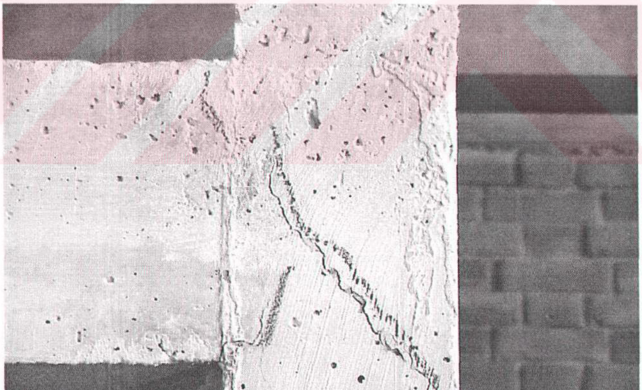

Figure 5.6 Cracks at the 1st story right exterior beam-column joint, Specimen B1

Figure 5.7 Cracks at the second story right interior beam-column joint, Specimen B1

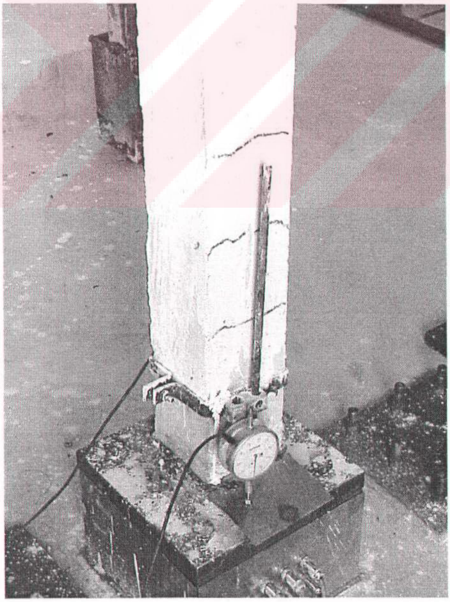

Figure 5.8 Cracks at the outer face of the right exterior column, Specimen B1

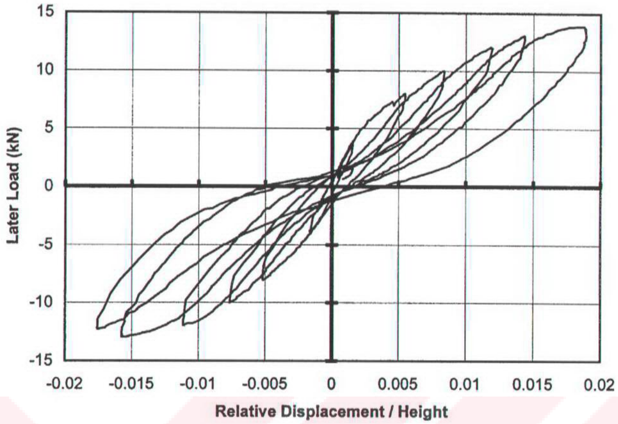

Figure 5.9 Variation of the 1st story drift ratio with the applied load, Specimen B1

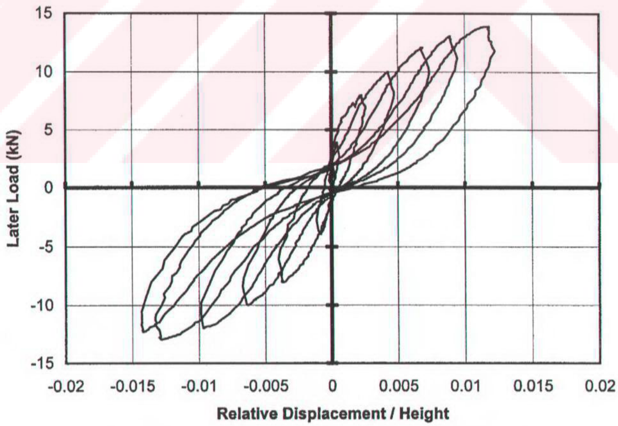

Figure 5.10 Variation of the 2nd story drift ratio with the applied load, Specimen B1

With the instrumentation described in Chapter 3, it was possible to calculate the curvatures from the strain measurements taken at the base of the external columns. The corresponding moments were measured by the force transducers mounted at the bottom of the columns. Figure 5.11 and 5.12 show the moment-curvature curves at the base of the left and right exterior columns respectively. These figures indicated that both columns reached their flexural capacities during the test. Large plastic curvatures were observed in the last positive half cycle of the left exterior column. Yielding of the right column at the base was also obvious from Figure 5.12. Wide flexural cracks at the base of the columns confirmed the yielding of the columns.

Throughout the test, a total of twelve readings were acquired from the two internal force transducers for each load stage. After some mathematical manipulations, the internal forces were calculated at the base of external columns. The details of this calculation were given in Chapter 3. Figures 5.13 through 5.18 show the variation of the internal forces at the base of columns with the applied lateral load.

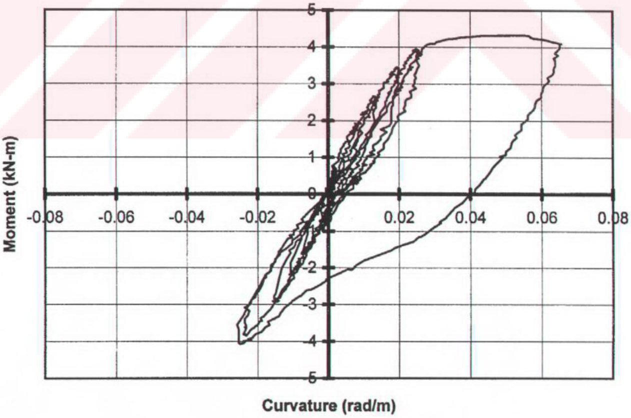

Figure 5.11 Moment Curvature curves at the base of the left exterior column, Specimen B1

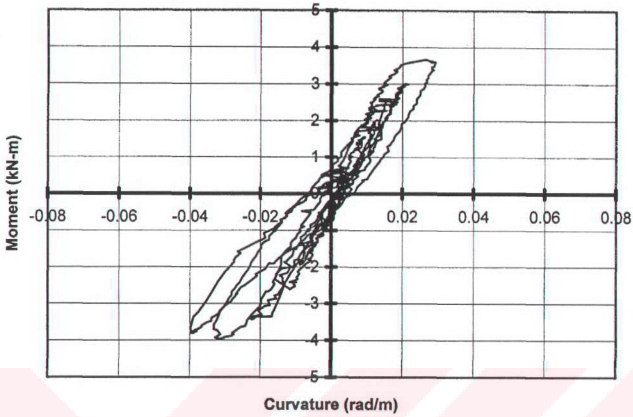

Figure 5.12 Moment Curvature curves at the base of the right exterior column, Specimen B1

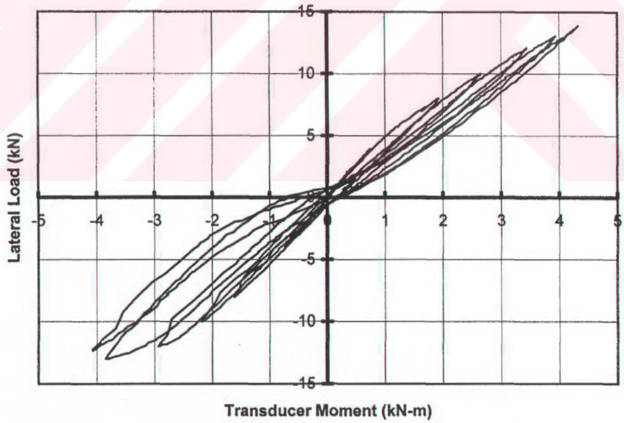

Figure 5.13 The variation of the moment at the base of the left exterior column during the test, Specimen B1

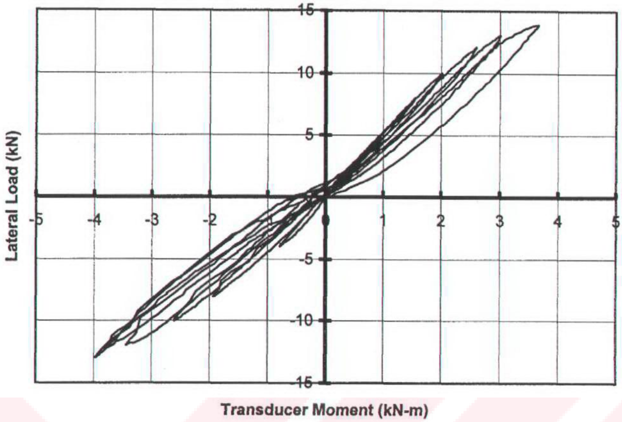

Figure 5.14 The variation of the moment at the base of the right exterior column during the test, Specimen B1

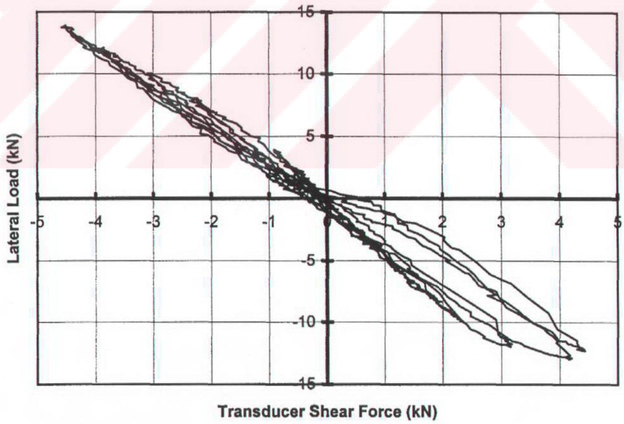

Figure 5.15 The variation of the Shear force at the base of the left exterior column during the test, Specimen B1

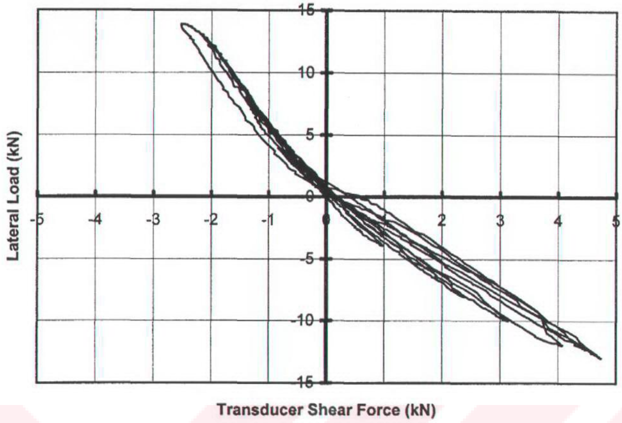

Figure 5.16 The variation of the Shear force at the base of the right exterior column during the test, Specimen B1

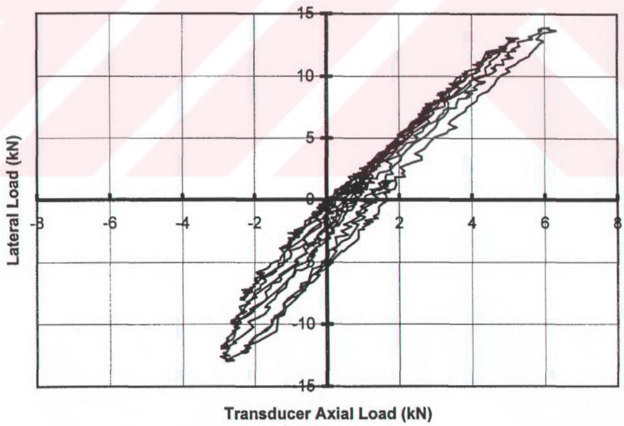

Figure 5.17 The variation of the axial force at the base of the left exterior column during the test, Specimen B1

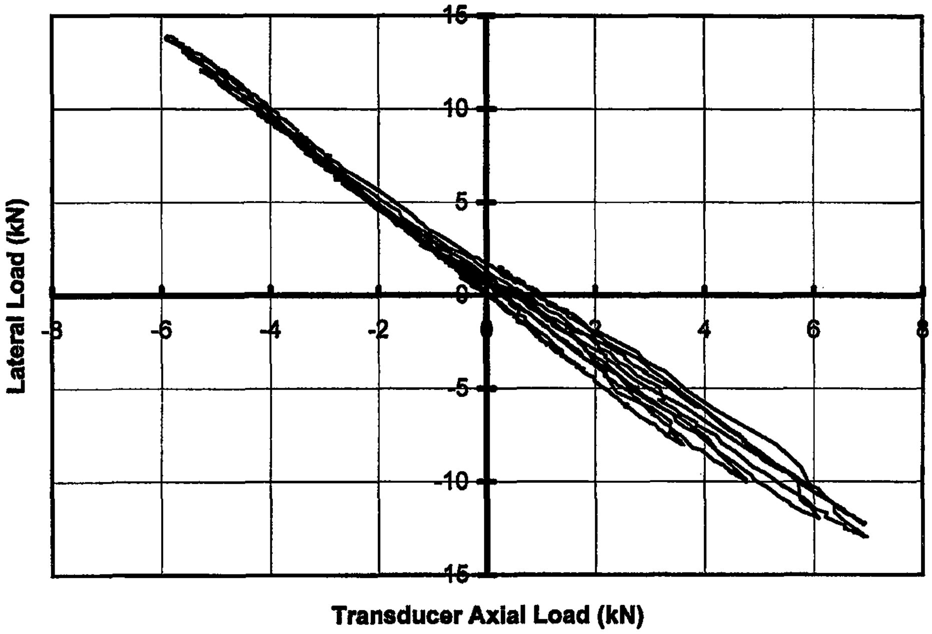

Figure 5.18 The variation of the axial force at the base of the right exterior column during the test, Specimen B1

5.3 REPAIRED FRAME, R1

After the bare frame B1 was tested, it was strengthened by introducing a reinforced concrete infill to the middle bay. This strengthened frame was the second test specimen that was designated as R1. The aim of this experiment was to observe the behavior of the strengthened frame. The results of the strengthened frame were compared with those of the bare frame. In the next chapter, these comparisons will be discussed in detail.

The specimen R1 was tested under the lateral load history given in Figure 5.19. In the first cycle 10kN lateral load was applied to the specimen. Then, the load was increased by 5kN steps up to the yielding of the strengthened structure. The test was load-controlled until lateral load reached 45kN level. At this load level, the test was at 8th cycle and the top displacement was approximately ±7 mm in each direction. After this stage, that yield stage, the test continued by controlling the displacements. At the 9th positive half cycle, almost 50kN lateral load could be applied to the specimen and the top displacement at this load level reached about 11 mm. At the negative direction of this cycle, the lateral load reached was 47kN at the displacement foreseen. At this load level, the top displacement was measured to be 14 mm. In the following cycles, 5mm incremental displacement was aimed. In the last cycle, that is cycle 14, it was intended to increase the lateral top displacement up to 40mm in each direction. But, the displacements remained at 39mm and –34mm in the positive and negative direction respectively. The test was terminated thinking of probable instability due to extensive damage in the infill wall.

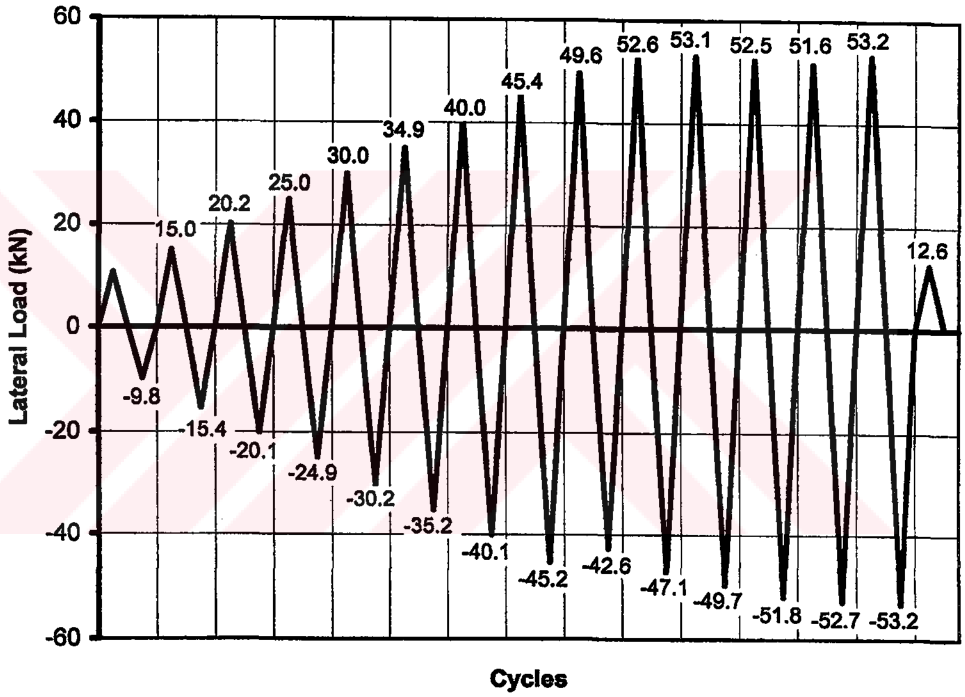

Figure 5.19 Load History of Specimen R1

In testing the strengthened structure, yield point was quite obvious. The yield displacement was determined as 8 mm in positive direction and 7.5 mm in negative direction. The displacement history is given in Figure 5.20. The ordinate of this curve was the ratio of the top displacement to the yield displacement.

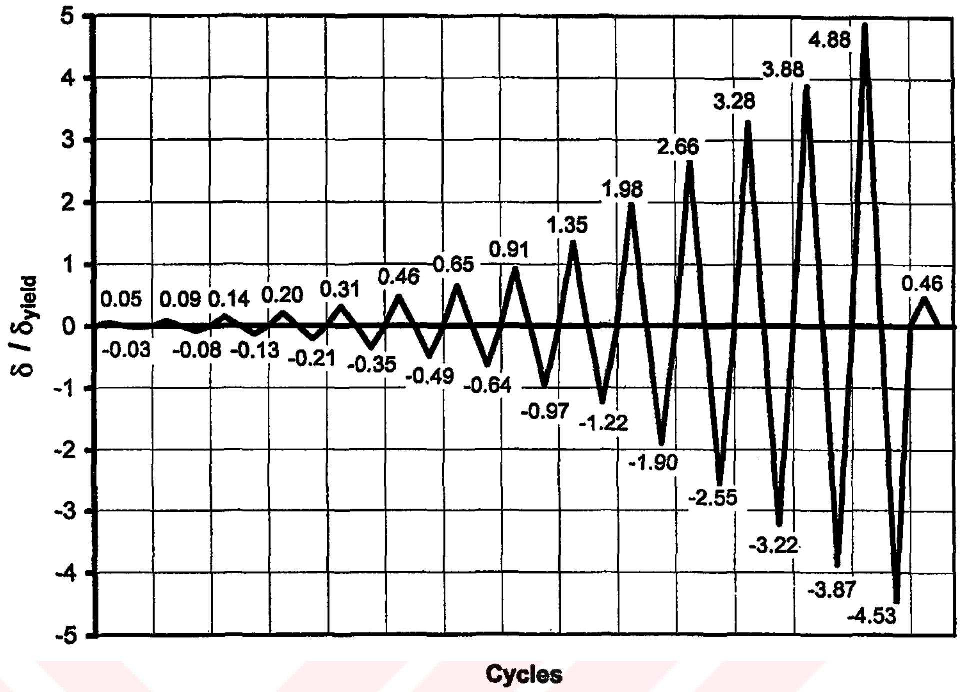

Figure 5.20 Displacement History of Specimen R1

During the test, similar to B1, a 9 kN constant axial load was applied to each of the four columns. Axial load on infill wall was applied on the outer edge columns of the wall. Total applied axial load on the infill wall was 18 kN (9+9). At the day of the test, the strength of concrete in the frame members was 13.8 MPa and 16.7MPa for the first and second story respectively. The strength of concrete in the infill was 30.8 MPa.

The maximum lateral load applied on the strengthened structure was 53.2 kN. At this load level, the top displacement of the frame was 39 mm. In Figure 5.21 and Figure 5.22, lateral load-displacement curves are presented for each story.

The area under the load-displacement curve could be taken as a measure of the energy dissipated during the reversed cyclic loading. These curves indicate that considerable amount of energy was dissipated during the test. The pinching in the curves decreases the energy dissipation per cycle. The reason for the pinching can be attributed to the closing of cracks in the compression zone and bar slip.

At 25 kN level (fourth positive cycle) first cracks were observed at the bottom of the infill wall. The observed cracks were flexural cracks at the foundation level. After the initiation of the cracks, the stiffness dropped noticeably. In the negative direction of the same cycle, the other face of the wall was in tension and new tension cracks were observed on that face of the wall. The stiffness in the negative direction also dropped considerably due to these cracks. This can be observed on the curves given in Figures 5.21 and 5.22.

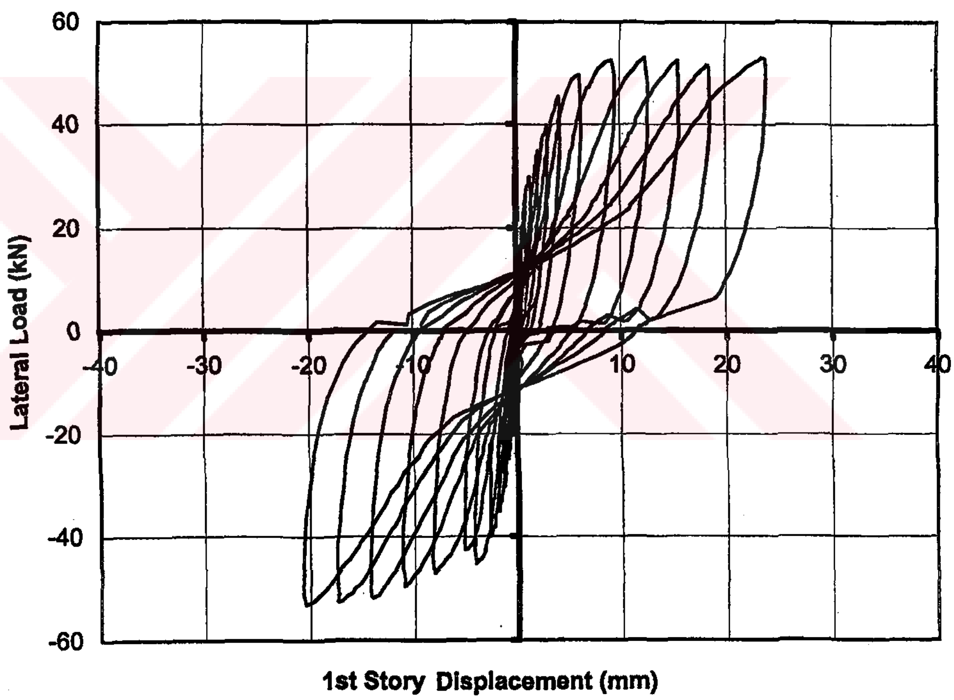

Figure 5.21 Load-Displacement curve of the 1st story, Specimen R1

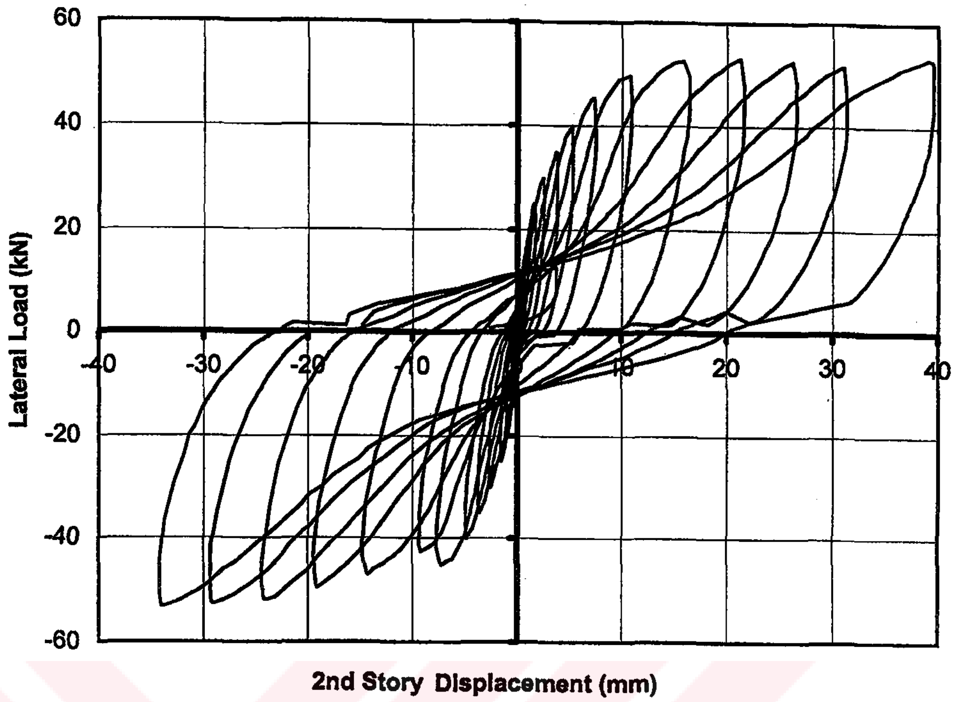

Figure 5.22 Load-Displacement curve of the 2nd story, Specimen R1

The lap splice length of the edge columns of the infill wall was 320 mm and the embedment length of the dowels into the wall was 300 mm. At the fifth cycle, new flexural cracks were observed on the infill panel at approximately 300 mm elevation. These cracks were numbered as 2 and 3 for the positive and negative direction respectively (see Figure 5.23). During the sixth cycle, existing cracks widened and crack widths increased. At this cycle new flexural cracks formed approximately 300-500 mm above the existing cracks on the wall. These cracks were marked as 4 at the positive half cycle and as 5 at the negative half cycle. Figure 5.23 shows the crack pattern of the infill wall during the positive 6^{th} cycle. It is of important that the first crack, marked as 1, lay just on the foundation, not on the infill wall.

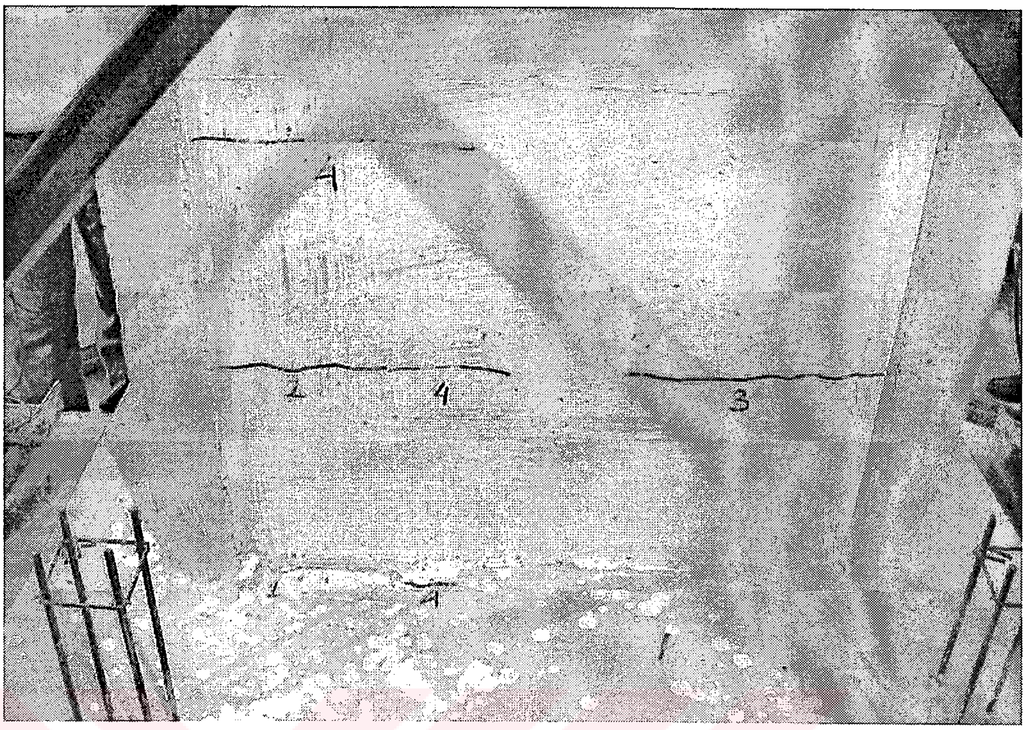

Figure 5.23 Crack pattern on the infill wall during the 6th positive half cycle, R1

At the seventh cycle, existing cracks widened and elongated with a slight inclination. During the negative half cycles of the experiment, second story beams were in tension due to the applied lateral load. Therefore, cracks at beam-column joints were observed at the second story in the negative direction of this cycle (no 7). Figure 5.24 shows the joint crack at the exterior beam-column joint.

During the eighth cycle, new cracks were observed on the wall which were slightly inclined. In the negative direction of this cycle, the applied lateral load was –45.2 kN. Due to high axial tension on the second story beam next to the loading system, several direct tension cracks formed on the beam. The cracks in the negative direction of the eighth half cycle were marked as 9. Figure 5.25 shows these cracks on the beam. Additionally, during this half cycle, the crack marked as 3 was opened considerably.

The infilled wall reached its flexural capacity and yielded at the ninth cycle. In the positive half direction of this cycle, the applied lateral load was 49.6 kN and top displacement was 10.8 mm. New cracks formed during this cycle at the wall-foundation joint which were marked as 10.

Figure 5.24 Crack on the second story left beam-column joint during the 7th negative half cycle, Specimen R1

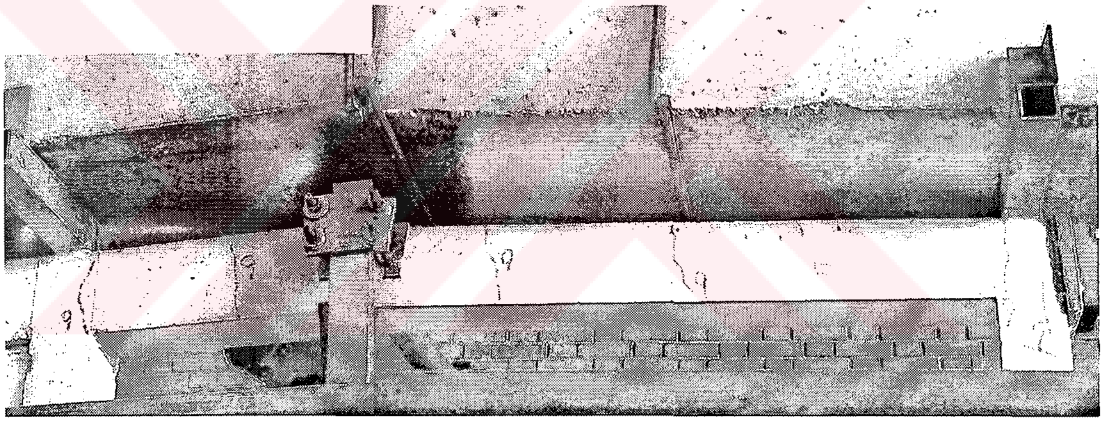

Figure 5.25 Direct tension cracks at the second story right beam during the 8th negative half cycle, Specimen R1

After the yielding of the wall, crack widths increased rapidly. The crack width of no. 3 in the negative direction of the tenth cycle was 3.5mm on the panel and 5.5 mm on the outer face of the boundary column. At the positive eleventh cycle, the width of the crack no. 2 was 3.7 mm, which was measured on the infill wall. The cracks formed at this cycle were marked as number 11. In the twelfth cycle, the width of crack no.2 reached to 6.4 mm.

After yielding of the wall (9th cycle), slip occurred at the foundation level of the wall. At the foundation level, a gap was observed between the wall and the foundation. After the unloading of the lateral force, this gap became smaller, but did not close. But, at the beginning of the load application in opposite direction, the gap closed rapidly. This gap closing was reflected as a horizontal line on the load deflection curve. During the closing of the gap, the displacement transducer at the top level measured approximately 5 mm displacement without any load increase. This problem was also faced in negative direction during the last two cycles. A snapshot of the last negative cycle (14th cycle) is shown in Figure 5.26. In this picture, high lateral displacement of the wall, the crack at the splice level and the gap at the foundation level at the edge of the wall can be seen clearly.

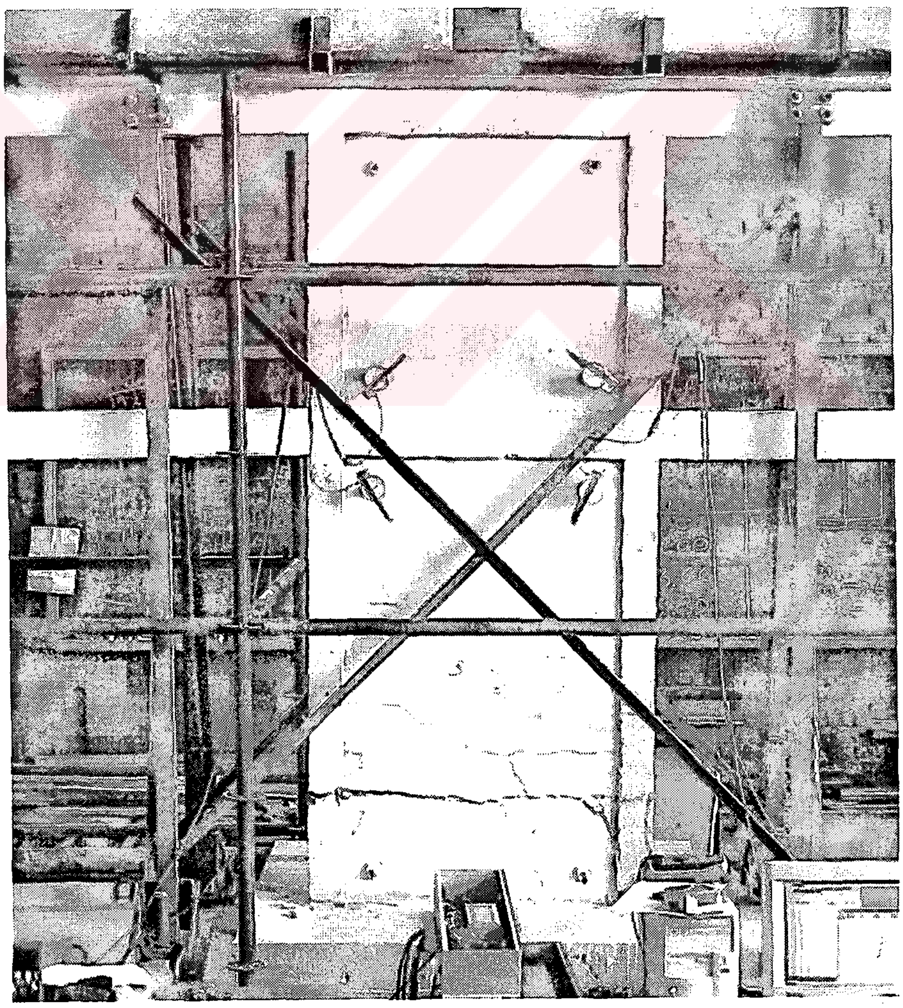

Figure 5.26 Cracks on the wall during the 14th negative half cycle, Specimen R1

During the last five negative cycles, the top beam was exposed to high axial tension. Therefore, second story beam-column joint was damaged at the load application region. Since the longitudinal reinforcement of the column and beam were welded to the interface plate, the applied force could be transferred to the frame. Figure 5.27 shows both faces of the damaged joint. The exterior column-beam top joint at the other end was also damaged due to axial tension applied, Figure 5.28. However, the design of the joints was also very poor. No confinement was supplied at the joints. No ties were continued in horizontal or vertical directions. All joints at the first and second story levels were damaged during the bare frame test. These joints and members were not repaired. Therefore, they remained as damaged in the specimen with the infill. The only rehabilitation on the frame was the application of the reinforced concrete infill wall.

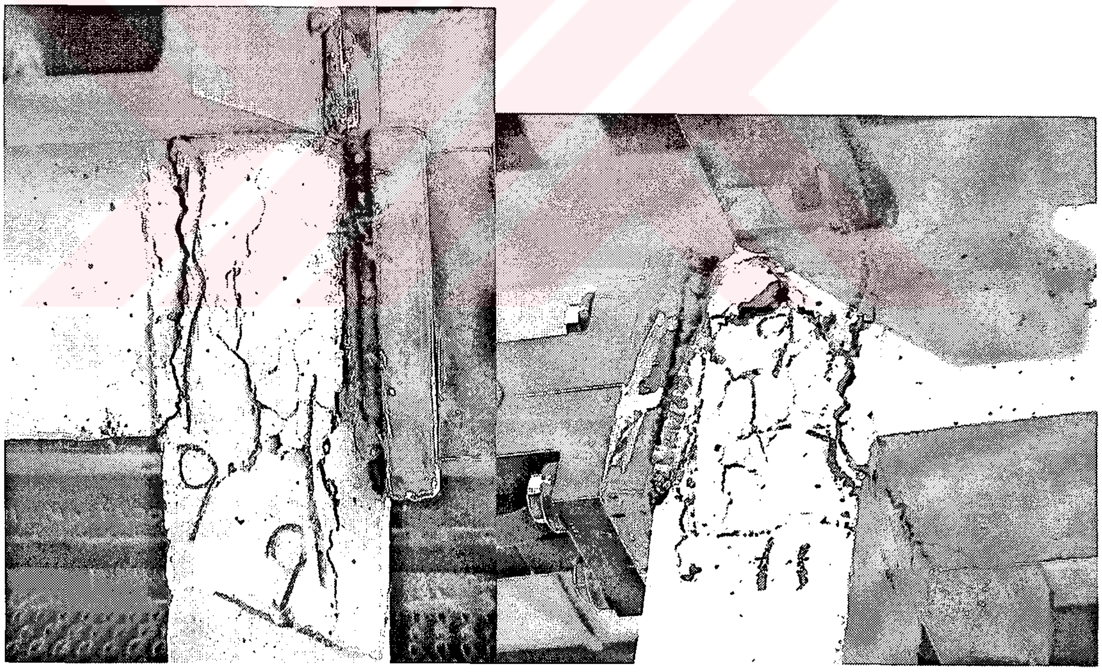

Figure 5.27 Damaged joint due to the high axial tension, Specimen R1

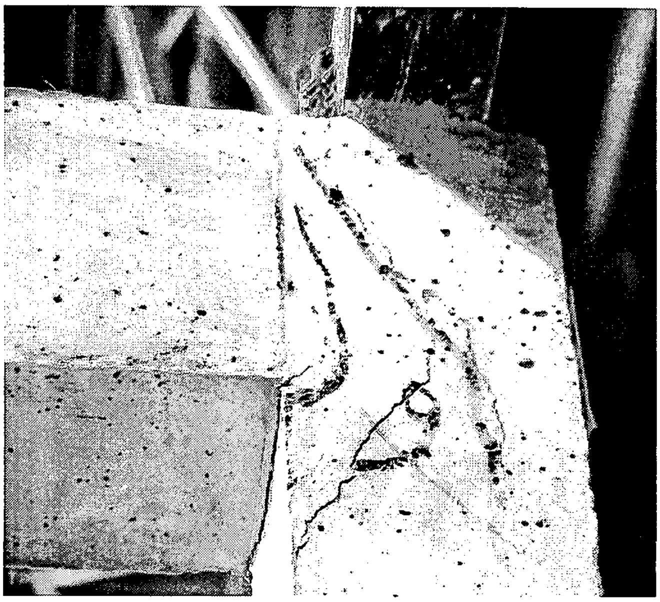

Figure 5.28 Damage at the left top column-beam joint, Specimen R1

During the test, specimen was forced to high lateral displacements. Therefore, the infill wall was severely damaged. The failure of the infill wall was due to flexure. The tension reinforcement yielded and no inclined shear cracks were observed on the infill. The main flexural crack initiated at the end of lapped splice. During the reversed cyclic loading cracks formed on both sides of the infill wall symmetrically. After the yielding of the frame, these cracks joined together and formed a continuous crack along the cross-section of the wall. However, no sliding shear mechanism was observed during the test. The front and back views of the infill wall of the first story after the tests are given in Figure 5.29 and 5.30.

Figure 5.29 Front view of the infill wall after the test, Specimen R1

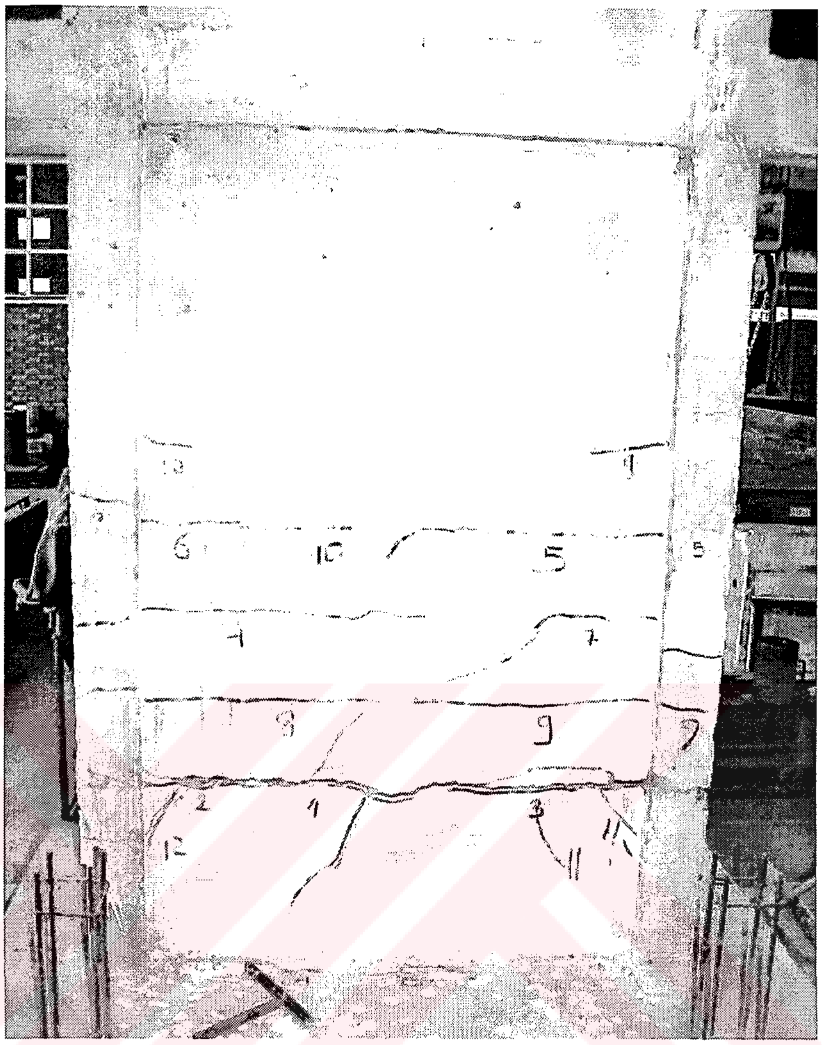

Figure 5.30 Rear view of the infill wall after the test, Specimen R1

As mentioned before, the frame was forced to high lateral displacements. The lateral load vs. lateral displacement curves of the first and second story were given in Figure 5.21 and 5.22. Since the drift ratio is also an important indication for damage level, drift ratios of the stories were calculated and plotted against the lateral load, Figure 5.31 and Figure 5.32. In the last loading cycle, the drift ratio reached 1.5 percent. However, when the wall reached its capacity by yielding of the vertical reinforcement, the drift ratio was less than 0.5 percent. During the experiment no cracks were observed on the second story infill wall. Flexural cracks on the first story infill were in the lower half of the infill. The infill frame behaved as a cantilever beam. Therefore, the drift ratios of the first and second story were almost the same.

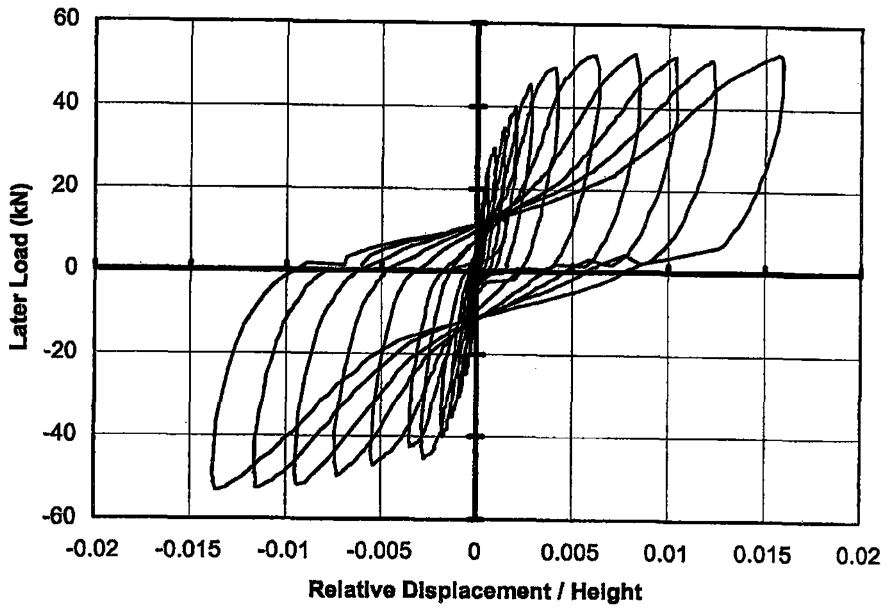

Figure 5.31 Drift ratios for the 1st story, Specimen R1

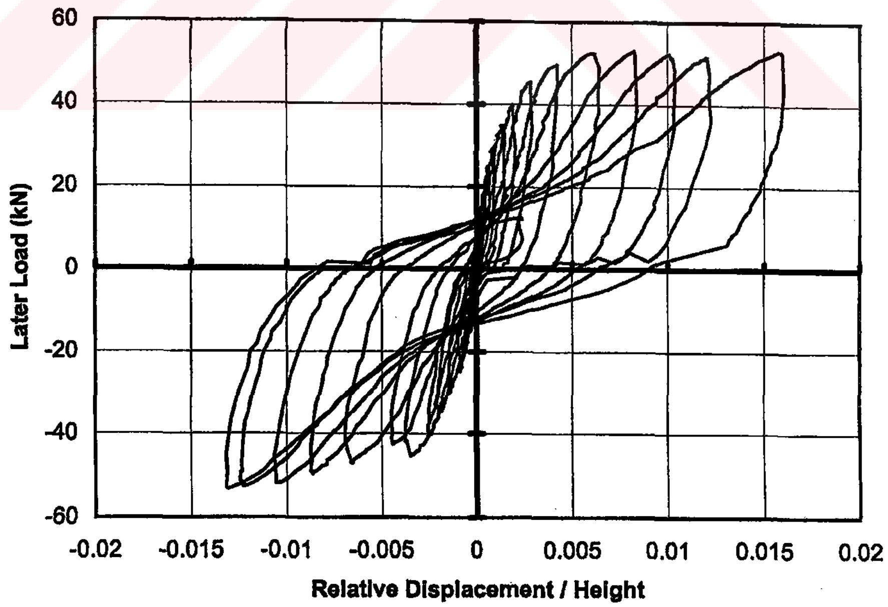

Figure 5.32 Drift ratios for the 2nd story, Specimen R1

The displacement of the infill wall due to shear can be used as an indicator of the damage level. For measuring the deformation due to shear, totally 4 dial gages were mounted on the infill wall diagonally. The details of the instrumentation were given in Figure 4.17 of the previous chapter. Figure 5.33 and 5.34 shows the displacement of the first and second stories respectively due to shear. Figure 5.34 clearly indicates that the displacement due to shear of the second story was almost zero. This behavior confirms the observed behavior of the infill wall during the test. It should be noted that displacements of the first story due to shear remained at 0.3 mm level until the yielding of the infill wall. After the yielding of the infill wall, deformations due to shear increased rapidly. This behavior also agrees with the observed behavior during the test.

The shear deformations shown in Figure 5.33 are much more than expected. This is probably due to the slip in the longitudinal bars at the boundary columns. Since deformations caused by slip were not separated, these deformations are included in Figure 5.33.

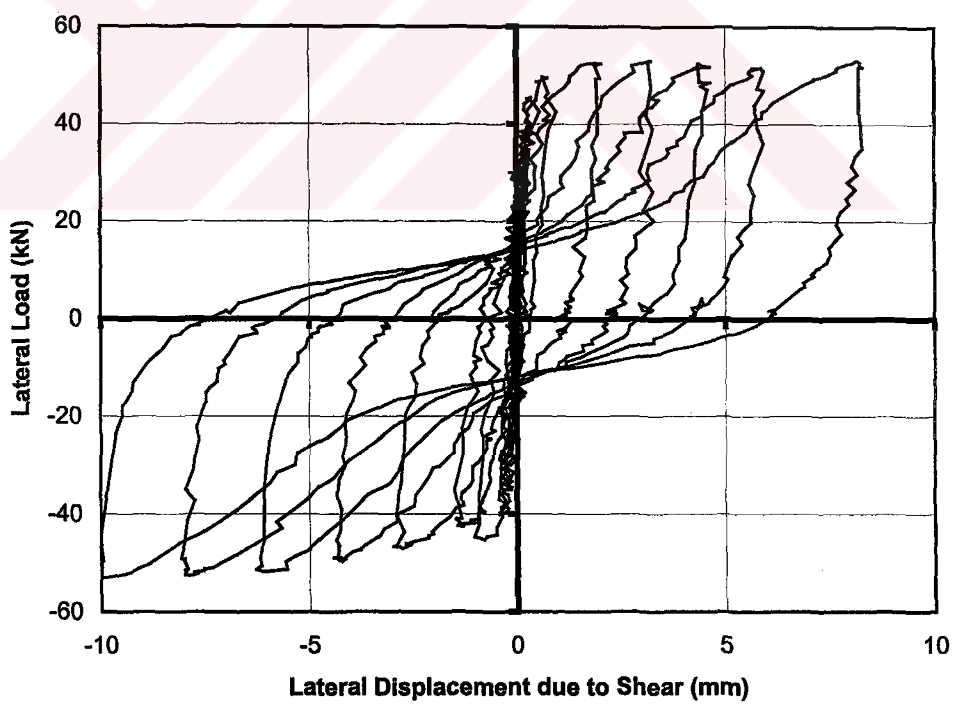

Figure 5.33 Displacement of the first story of the infill wall due to Shear, Specimen R1

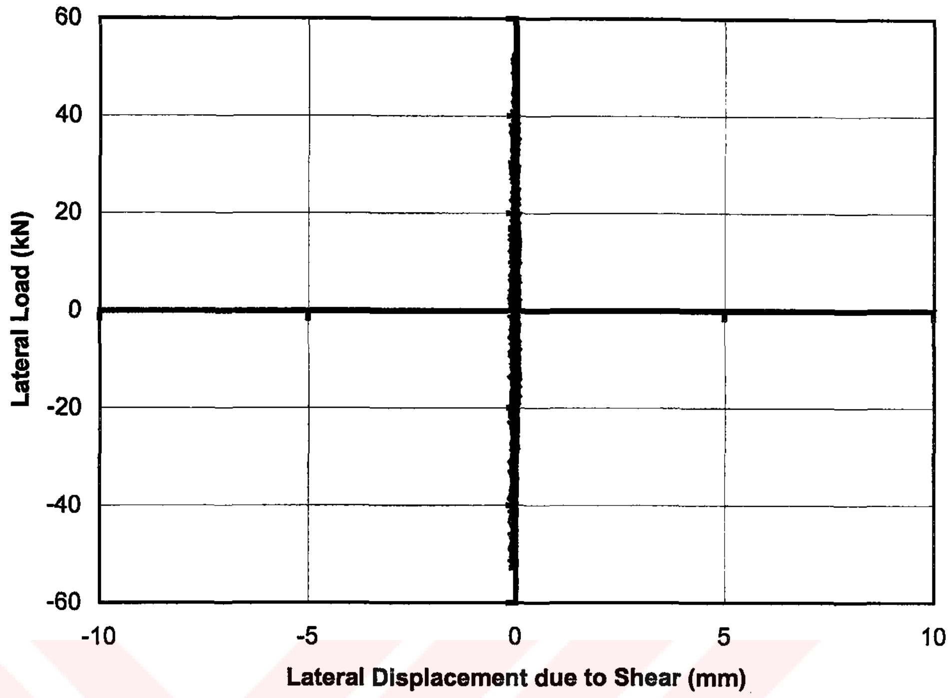

Figure 5.34 Displacement of the second story of the infill wall due to Shear, Specimen R1

The curvature at the base of the exterior columns was calculated by making use of the readings taken from the dial gages mounted on these columns. Moments were obtained from the force transducers placed at the base of the columns. Figure 5.35 and 5.36 show the moment-curvature curves for the left and right exterior columns respectively. It should be noted that, these columns were not repaired after the bare frame test, although they were damaged. Therefore, these columns did not exhibit the same behavior observed in the first test, Figure 5.11 and 5.12. These figures clearly indicate that, the stiffness of the columns in the second test was much smaller as compared to the first test. The drop in the stiffness was almost 50%. As noted before, the last six cycles were in the post yield region. If the last six cycles in these figures were overlooked, it can be said that, columns did not take significant moment and consequently did not rotate until the specimen reached the yield point.

Throughout the test, totally twelve readings were acquired from the two force transducers. After some mathematical manipulations, the internal forces were calculated at the base of the exterior columns. The details of these calculations were given in Chapter 3. Figure 5.37 through 5.42 show the internal forces developing at the ends of the columns.

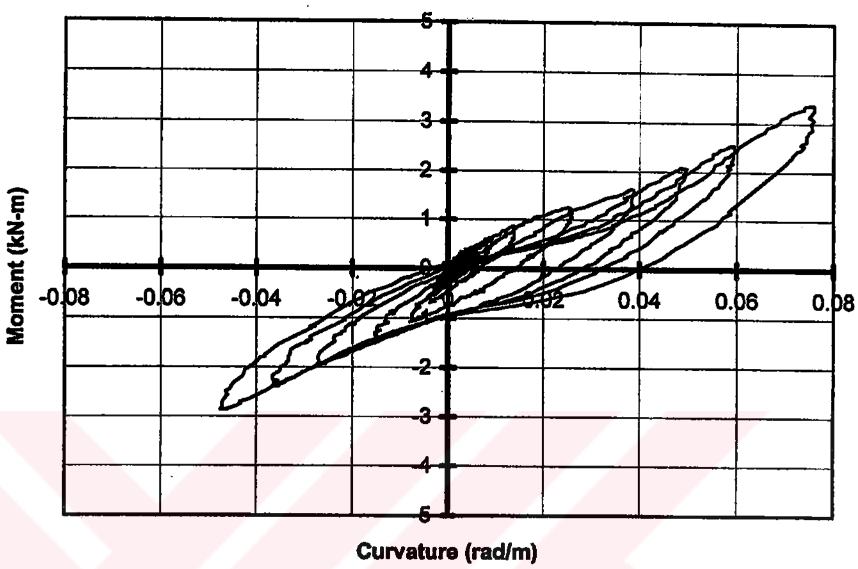

Figure 5.35 Moment Curvature curves at the base of the left exterior column, Specimen R1

An examination of the moment-lateral force curves clearly point out that, until the wall yielded the column moments were very small. After the yielding of the wall, the moments of the left and right exterior columns increased to 3 and 2kN-m respectively. Similarly, the level of the shear forces at the base of the exterior columns was very small until the yielding of the wall and they increased sharply during the plastic cycles, Figures 5.39 and 5.40. Shear force in the right exterior column was in opposite direction during the elastic cycles. But this force was very low. Therefore, it might be due to the resolution of the force transducer or due to the damaged joints formed during the previous test. Also, the specimen could have initial plastic displacements remained in the columns after the previous test. As shown in Figures 5.41 and 5.42, axial forces in exterior columns changed from compression to tension during the test.

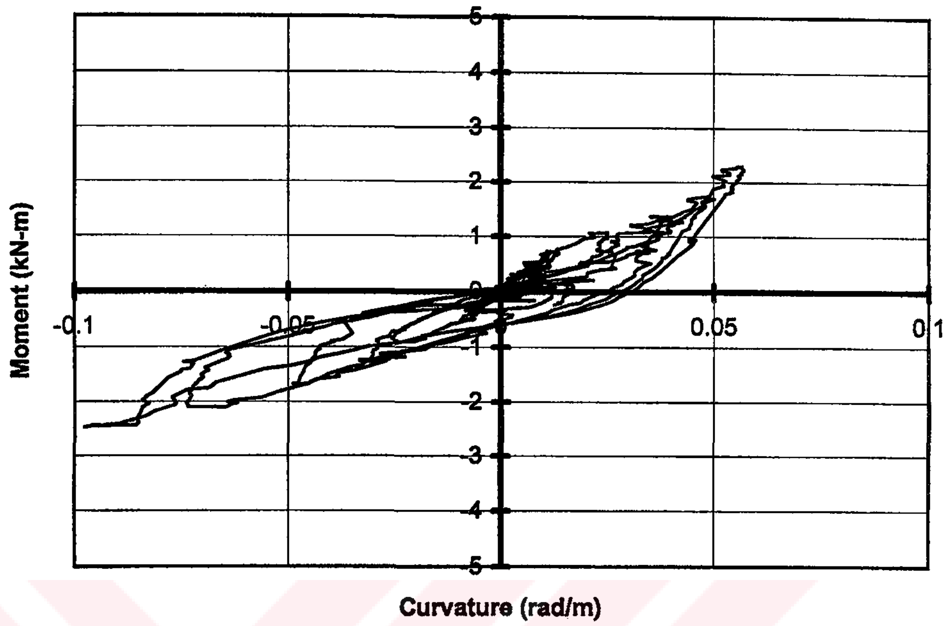

Figure 5.36 Moment Curvature curves at the base of the right exterior column, Specimen R1

Measurements taken revealed that, the wall took almost the total lateral load and releaved the columns. During the initial cycles, approximately 99 % of the lateral load was carried by infill frame. After the yielding of the wall, even at the last cycle, 90 % lateral load was carried by the infilled frame.

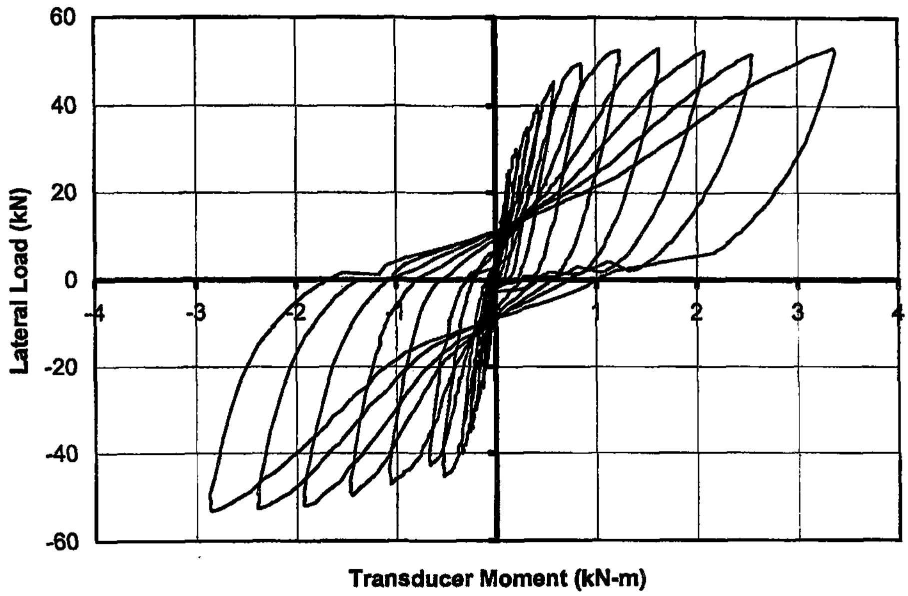

Figure 5.37 Moments at the base of the left exterior column, Specimen R1

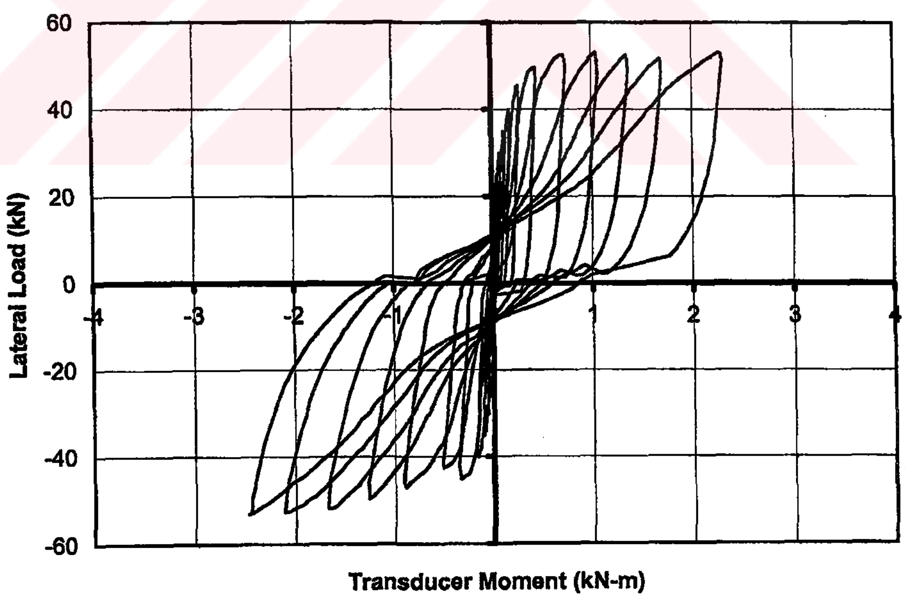

Figure 5.38 Moments at the base of the right exterior column, Specimen R1

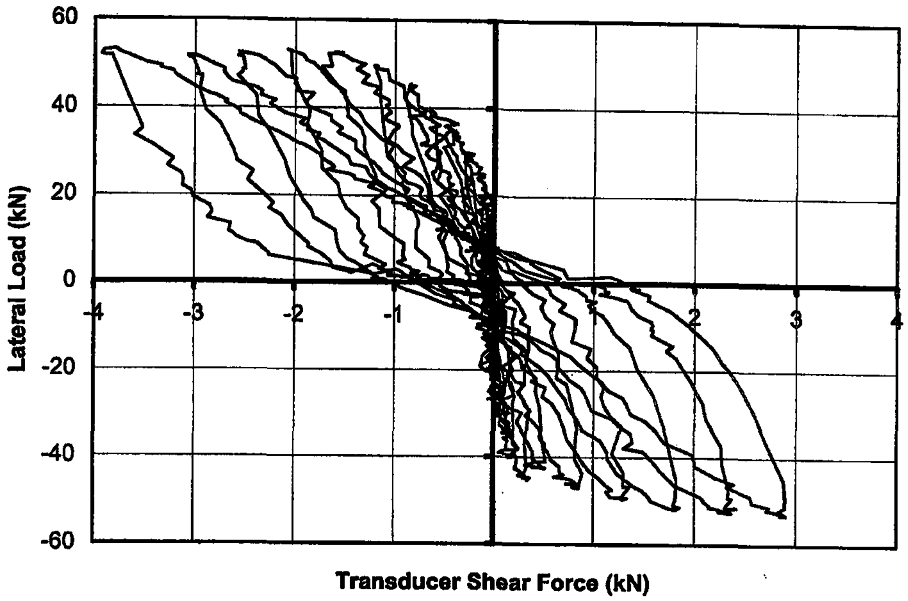

Figure 5.39 Shear force at the base of the left exterior column, Specimen R1

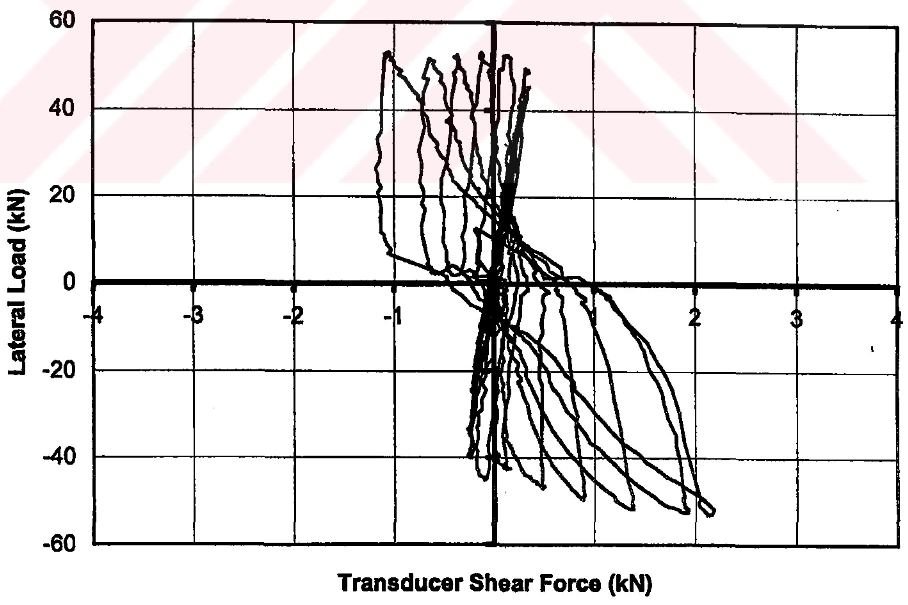

Figure 5.40 Shear force at the base of the right exterior column, Specimen R1

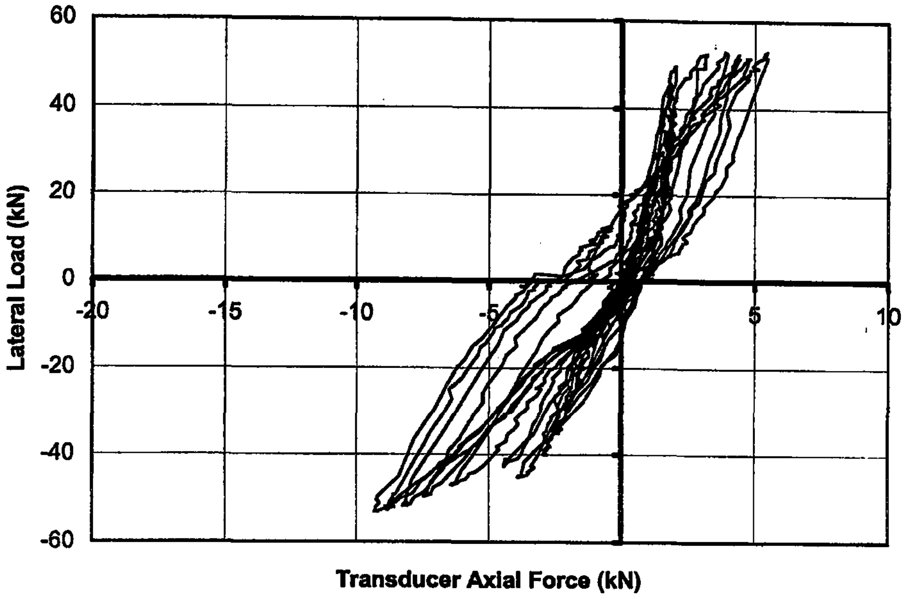

Figure 5.41 Axial force at the base of the left exterior column, Specimen R1

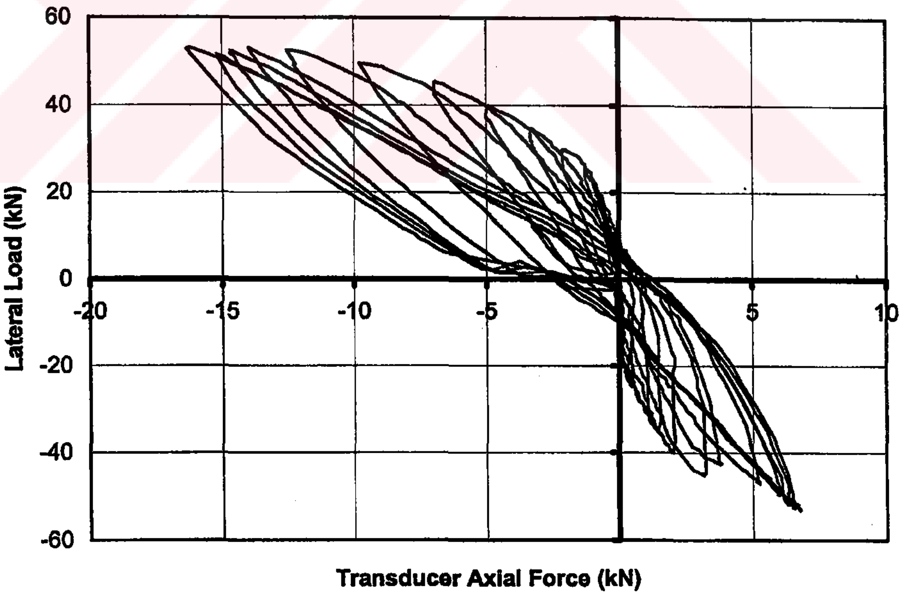

Figure 5.42 Axial force at the base of the right exterior column, Specimen R1

CHAPTER 6

DISCUSSION AND EVALUATION OF THE TEST RESULTS

6.1 GENERAL

In this chapter, the experimental results are evaluated and discussed, considering strength, stiffness, response, energy dissipation and drift characteristics of the bare frame and frame rehabilitated by infilling the middle bay.

6.2 STRENGTH

The cracking strength of the infilled specimen was calculated and compared with the test results. First, the flexural cracking strength was evaluated. For this calculation, the principles of mechanics of materials were used. Since, the failure of the infilled specimen was dominated by flexure, the shear cracking strength was not evaluated in detail. It was proved that, the cracking shear capacity was much higher than the flexural cracking capacity. The results of calculated moment-curvature relationships and of interaction diagrams were compared with the experimental values.

6.2.1 Flexural Cracking Strength

For a reinforced concrete section subjected to bending, the prediction of the flexural cracking load is important. Beyond the flexural cracking strength, the behavior of the reinforced concrete member changes from linear-elastic to nonlinear and the stiffness decreases. Assuming linear response, flexural cracking stress of a reinforced concrete section subjected to bending and axial load can be calculated using the following equation:

$$\sigma = \frac{N}{A} \pm \frac{M \cdot y}{I} \tag{6.1}$$

The cracking moment M_{cr}, can be calculated by substituting $M = M_{cr}$ and $\sigma = f_{ctf}$ into Eq. (5.1).

$$M_{cr} = \left(f_{ctf} - \frac{N}{A} \right) \left(\frac{I}{y} \right) \tag{6.2}$$

where

f_{ctf}	:	flexural tensile strength of concrete, $f_{ctf} = 0.7\sqrt{f_{ck}}$ (MPa)
I	:	moment of inertia of the gross concrete section
y	:	distance between the centroid and extreme tension fiber
N	:	total axial load applied on the section
A	:	gross cross-sectional area (web area)

The lateral load corresponding to the flexural cracking could be calculated by assuming the infill wall as a cantilever and by assuming that almost all the lateral load was carried by the infill wall. Shear measured at the base of the external columns by the transducers revealed that nearly 99% of the lateral load was carried by the wall prior to cracking.

$$V_{fcr} = \frac{M_{cr}}{H} \tag{6.3}$$

In Eq. (6.3), H is the distance between the lateral load and base of the infill wall. The strength of concrete of the boundary columns was less than that of the infill wall and the boundary columns were damaged before the infill was introduced. Therefore, for the calculations of moment of inertia, the cross-section of the infill wall was assumed to be rectangular extending from the exterior face of one column to the exterior face of the other column.

From Equations (6.2) and (6.3), shear corresponding to first flexural cracking was calculated:

$$V_{fcr} = \left(0.7\sqrt{30.8} - \frac{18000}{1110\times 70}\right)\left(\frac{70\times 1110^3/12}{1110/2}\right)/2500 \approx 21 \text{ kN}$$

During the infilled frame test, the first crack was observed at about 25 kN load level. It should be noted that, it is very difficult to determine the first crack during the testing. Also, the calculations are based on many assumptions. It is very difficult to estimate the tensile strength of concrete. It is very possible that the actual tensile strength was higher than the assumed value of $0.7\sqrt{f_{ck}}$. In calculating the moment of inertia of the wall, a rectangular section was assumed instead of the barbell shape (The flexural cracking load would be 23kN if barbell shape will be used in calculating the moment of inertia of the wall). These two factors probably reduced the calculated value of the lateral load. Therefore, the difference between the calculated and observed load is acceptable.

6.2.2 Shear Cracking Strength

In reinforced concrete structures, diagonal shear cracks occur when the principal tensile stress caused by shear alone or by shear, axial load and flexure, exceed the tensile strength of concrete. Sufficient amount of shear reinforcement must be provided in the walls in order to resist the lateral forces, since the shear strength of the concrete alone cannot be relied on.

The observation of the infilled frame test showed that, the failure mechanism of the frame was flexural. At the eighth cycle of the testing, cracks started to incline. At this stage, the lateral load applied to the specimen was 45 kN.

The shear cracking strength of a section could simply be calculated according to the equations in TS-500-2000 [30] and ACI 318-95 [53] as given below:

$$V_{cr} = 0.65\times f_{ctk}\times b_w\times d \qquad \text{(TS-500-2000)} \qquad (6.5)$$

$$V_{cr} = 0.2 \times \sqrt{f_{ck}} \times b_w \times d \qquad \text{(ACI-318-95)} \qquad (6.6)$$

The above equations give 78 kN and 69 kN for the cracking shear strength respectively. It should be reminded that lateral force corresponding to flexural cracking was much less, 21 kN. The maximum applied load on the frame during the test was 53 kN, also less than the calculated cracking load of concrete due to shear. Consequently, both the calculations and observations show that the failure was due to flexure at which stage no shear cracks would form.

6.3 STIFFNESS

Stiffness can simply be calculated as the slope of the load-deformation curve obtained from the tests. In this study, two types of stiffnesses were defined; initial stiffness and stiffness prior to failure. The initial stiffness of the specimen k_i, was calculated as the initial slope of the load-deformation curve in the first forward half cycle. "The prior to failure stiffness" of the specimen was calculated as the average slope of the load-deformation curve in the last cycle. For the calculation of the stiffness of the specimens, the lateral displacement at the top level was considered. Stiffness properties of the specimens are presented in Table 6.1.

Table 6.1 Stiffness of the test specimens

Specimen Name	Initial Stiffness (N/mm)	Prior to Failure Stiffness (N/mm)	Stiffness Degradation (%)	Ratio of Initial Stiffness of Infilled Frame to that of the Bare Frame
B1	2050	325	84.2	-
R1	31360	1460	95.4	15.3

As can be seen from the table, the stiffness reduction of the specimens near the failure stage was very severe especially in R1. The prior-to-failure stiffness and the stiffness degradation are related to the maximum displacement during the test. By increasing maximum displacement, "the prior to failure stiffness" will decrease and stiffness degradation ratios will accordingly increase. However, the maximum displacements both for the bare and infilled frame were approximately 40 mm. Therefore, one could conclude that, the stiffness degradation of the infilled frame was higher than that of the bare frame.

As can be seen from the Table 6.1, the initial stiffness of the specimen with the infill was about 15 times that of the bare frame. This is a very significant increase considering that the infill was introduced to a damaged frame.

6.4 RESPONSE ENVELOPES

Strength and stiffness characteristics of the specimens were evaluated with the help of response envelope curves. Response envelope curves were obtained by connecting the maximum points of the hysteretic load-top displacement curves of the specimens. The response envelopes of the bare frame and infilled frame were plotted together in order to see the effects of the reinforced concrete infills.

Figure 6.1 shows the response envelopes of the infilled and the bare frames. From these curves, it can be observed that both strength and stiffness have increased significantly with the introduction of the infill. Maximum lateral load carried by the bare and infilled frames were 13.9 kN and 53.2 kN respectively. The lateral load carrying capacity of the frame increased to 3.8 times the value without the infill (283 % increase) with the introduction of infill wall to the damaged frame. As given in Section 6.3, the stiffness of the infilled frame was about 15 times greater than that of the bare frame. It should also be noted that the deformation capability of the infilled frame was very high.

6.5 ENERGY DISSIPATION

The energy dissipation characteristics of the specimens strongly depend on the loading history. Therefore, it would be more meaningful to compare the energy dissipation characteristics of specimens with the same loading history. But in this study, the loading histories of the bare frame and the infilled frame were different.

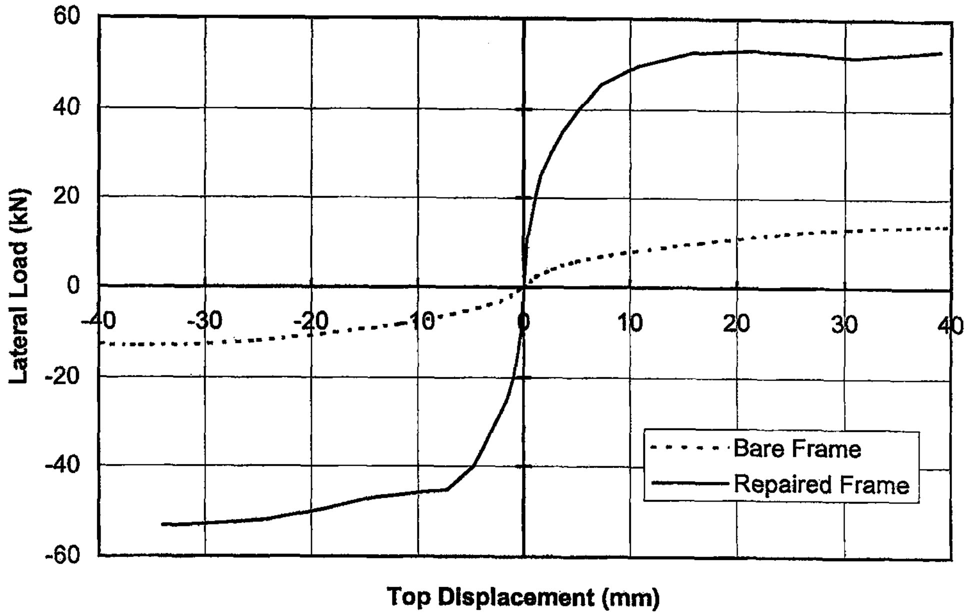

Figure 6.1 Envelope Load displacement curves of the bare and infilled frames

The amount of dissipated energy was calculated as the area under the experimental load-deformation curves. The work done by the axial load was neglected, since its contribution should be small, especially prior to yielding of the specimens. Besides, the energy dissipated by means of the friction forces was also neglected since it was also considered small. On the other hand, the cumulative displacement was calculated as the addition of absolute maximum displacements in the forward half and backward half cycles.

Cumulative energy dissipation curves of the bare and infilled frames are given in Figure 6.2. As can be seen from the figure, the infilled specimen dissipated much more energy as compared with the bare frame. It should be noted that, the bare frame dissipated energy with large amplitude inelastic displacement cycles, whereas the infilled frame dissipated energy with small amplitude inelastic displacement cycles.

It would be misleading to draw generalized conclusions from Figure 6.2, since the load histories of the two specimens were very different.

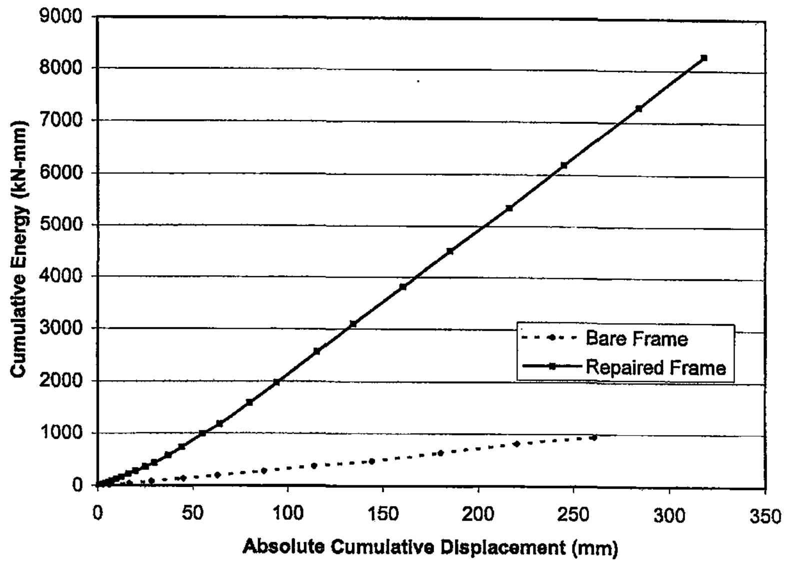

Figure 6.2 Cumulative energy dissipation curves of the bare and infilled frames

6.6 STORY DRIFT INDEX

Story drift index is a term that is frequently used in earthquake engineering. It can simply be defined as the relative displacement between the two successive floors, divided by the corresponding story height.

Generally, story drift index is not allowed to exceed a certain limit in order to prevent structural and non-structural damage. Additionally, for interstory drifts more than 1%, *P-Δ* effects lead to rapidly increasing augmentation of these drifts [28]. According to the Turkish Seismic Code [56], the maximum story drift index is limited to 0.0035 and 0.02/R based on the elastic analysis of the structure. R is the behavior factor and for frames of normal ductility R = 4.0 . On the other hand, according to UBC, the maximum story drift index for inelastic analysis is limited to 0.025 for the structures with a fundamental period less than 0.7 seconds and 0.02 for the structures with a fundamental period greater than 0.7 seconds [54]. According Sozen [55], if the drift index (inelastic) exceeds 0.01, then all types of partition walls would be totally damaged. As the numbers indicate, the Turkish Seismic Code is conservative about the amount of story drift index.

Figure 6.3 and 6.4 show envelope curves of the first and second story drift ratios for the bare and the infilled frames. The first story drift is reduced significantly by the addition of infill wall. During the first eight cycles of the infilled specimen, up to the yielding of the infill wall, the drift ratio remained at a level of 0.5%. The first and second story drifts of the infilled frame were almost the same. The reason was that this specimen behaved almost like a cantilever beam above the base. A hinge formed at the base of the infill wall and the wall rotated about this point. Therefore, the drift ratio remained almost constant along the height of the infill wall.

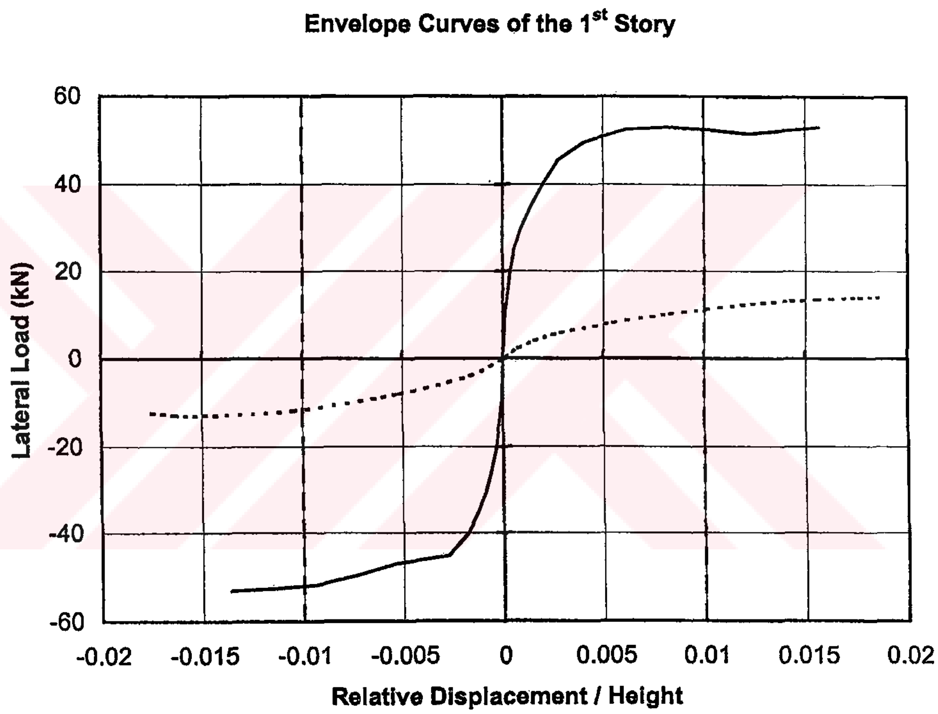

Figure 6.3 Envelope curves for the drift ratios

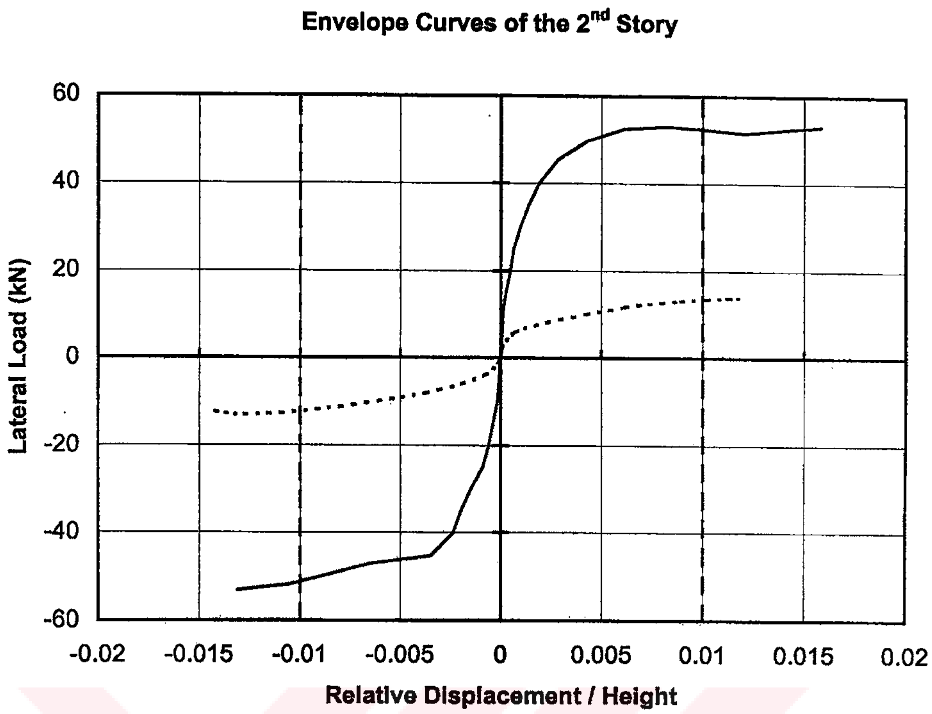

Figure 6.4 Envelope curves for the drift ratios

6.7 ANALYTICAL PREDICTION OF THE EXPERIMENTAL BEHAVIOR

The internal forces of exterior columns at the base were measured during the tests by force transducers. Additionally, the curvatures of these columns at the base were calculated by using the two strain measurements taken at the faces of the columns. By means of these data, experimental moment curvature and M-N interaction diagrams could be drawn. These curves were compared with curves predicted analytically. The computer program RESPONSE 2000 was used to calculate the analytical behavior. Additionally, simple hand calculations were performed to predict the initial slope and the slope after cracking.

For the analytical calculation of the moment-curvature diagram, the axial load on the column had to be known. However, during the test, the axial load on the column changed continuously under reversed cyclic loading. Therefore, the maximum axial load acted on the column during the test was taken as the constant load for the moment-curvature calculations. The analytical moment-curvature curves for the positive and negative half cycles were calculated separately, since the level and sign of the maximum axial load was different in these directions.

The slope of the moment-curvature curve is the EI value of the section. Therefore, the elasticity modulus "E" of concrete and moment of inertia "I" of the section have to be determined. The gross and cracked moment of inertia of a rectangular section with compression steel could be calculated as follows [64]:

$$
\begin{aligned}
I_g &= \frac{b \cdot h^3}{12} \\
I_{cr} &= \frac{b(kd)^3}{3} + n A_s (d - kd)^2 + (n-1) A_s' (kd - d')^2 \\
n &= \frac{E_s}{E_c} \\
kd &= \frac{\sqrt{2 d B \left(1 + r \frac{d'}{d}\right) + (1+r)^2} - (1+r)}{B} \\
r &= \frac{(n-1) A_s'}{n A_s} \\
B &= \frac{b}{n A_s}
\end{aligned}
\tag{6.7}
$$

The symbols used in these equations are shown in Figure 6.5.

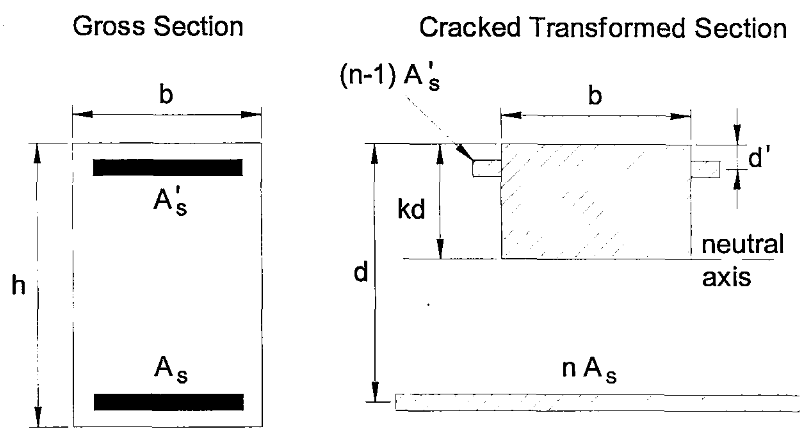

Figure 6.5 Gross section and cracked transformed section properties of a rectangular section with compression steel

Elasticity modulus of concrete was calculated using three different codes:

ACI 318: $E = 4750\sqrt{f_c} \approx 17\,000$ MPa

TS 500: $E = 3250\sqrt{f_c} + 14000 \approx 26\,000$ MPa

CEB: $E = 9500(f_c + 8.0)^{1/3} \approx 26\,000$ MPa

The modulus of elasticity given in Turkish Code and CEB are rather high, being closer to initial modulus. Therefore, elastic modulus of concrete was chosen as 20 000 MPa for beams and columns. The calculation of EI for the exterior columns are summarized in Table 6.2.

Table 6.2 Calculation of the EI

	I_{column} (mm^4)	E (MPa)	EI (kN-m^2)
Gross	12 200 000	20 000	244
Cracked	4 800 000	20 000	96

Figures 6.6 and 6.7 show the experimental and calculated moment-curvature relationships for the exterior left and right columns of the bare frame respectively. In these figures, the radial lines represent the EI values calculated. The line with a greater slope is for uncracked section and the other one for cracked section. As can be seen from these figures, analytical envelope curves agree quite well with the experimental ones.

Figure 6.8 and 6.9 show the experimental and calculated moment-curvature curves for the exterior left and right columns of the specimen with the infill. On these figures, two radial lines are shown. One of them represents the flexural stiffness calculated by using the cracked moment of inertia and the other one is drawn by connecting the origin of the axes and the peak point of the last cycle of the bare frame test. It should be pointed out that the infill was introduced after the frame was damaged and the damaged frame members were not repaired. Therefore, the experimental moment-curvature curves did not follow the analytical envelope curves due to the past load history and slope of the experimental curves was smaller than the analytical ones calculated using the cracked section. To better visualize the behavior of the column until yielding of the infill wall, the first 8 cycles were plotted separately. Figure 6.10 and 6.11 show the first 8 cycles of the moment curvature curves drawn to a larger scale. The experimental curves on these figures were almost parallel to the cracked EI or peak slope of the previous loading. These figures clearly indicated that very small moments were carried by columns until the yielding of infill wall. The curves on these figures show a great scatter. The reason of this scatter was that the level of the signal from the dial gages was almost in the noise level of the signal conditioners.

After the yielding of the infill wall, rotations of the columns increased very rapidly and the stiffness of the columns decreased considerably. At the end of the test, the outer columns could not reach their expected moment capacities under high curvatures.

The low stiffness observed from the experimental curves can be due to the following reasons:

In the infilled frame tests, the end moments in beams reached high values. Near the end of the test, plastic hinges observed at beam ends indicated that sections reached their moment capacities. High shear forces existed due to these moments. These shear forces introduced axial tension to the external columns. At later cycles, the tension force introduced exceeded the axial compression applied externally to these columns. Therefore, as axial load measurements indicated, during the cyclic loading these columns were subjected to axial tension instead of compression. The presence of axial tension reduced the stiffness of the columns.

The stiffness reduction could also be due to the slip of the column longitudinal bars. Such a slip of the column longitudinal bars could result in reduced stiffness. These bars were welded to a L-shaped steel bar which in return was welded to the base plate. It is possible that the welding between this L-shaped bar and the plate was not adequate and permitted movement of the column longitudinal bars in the vertical direction.

Another possibility which is improbable but should not be ruled out, is the possibility of error in curvature readings.

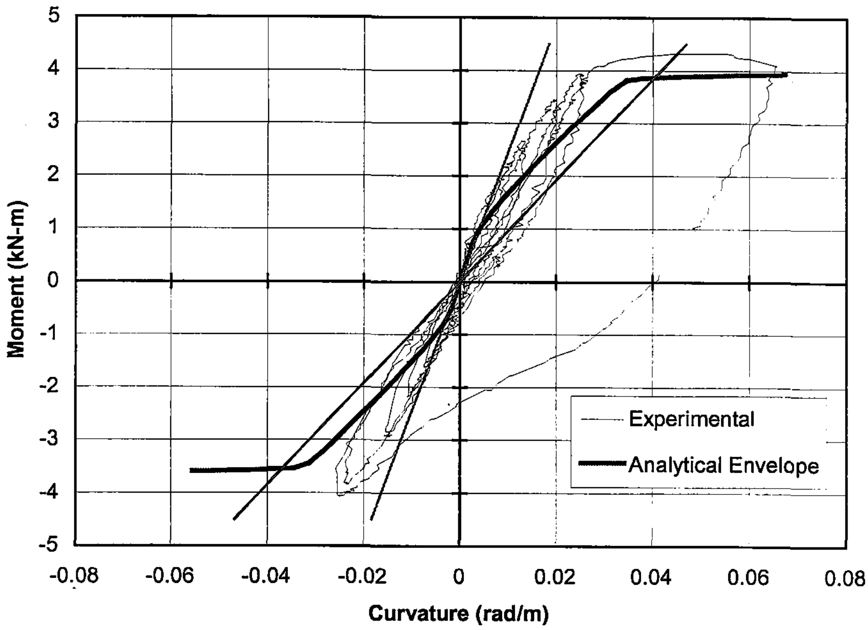

Figure 6.6 Analytical and experimental moment-curvature curves for the external left column at the base, Specimen B1 (bare frame)

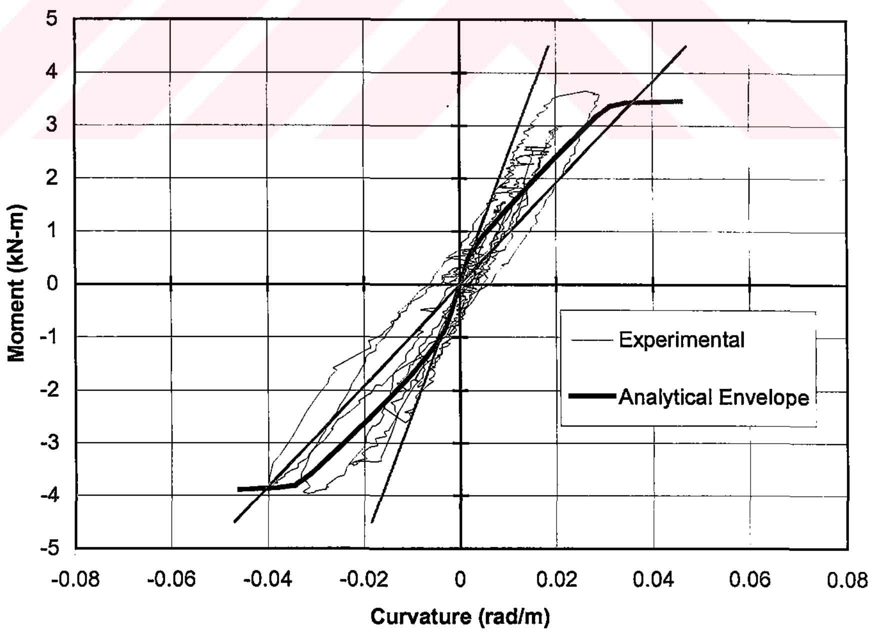

Figure 6.7 Analytical and experimental moment-curvature curves for the external right column at the base, Specimen B1 (bare frame)

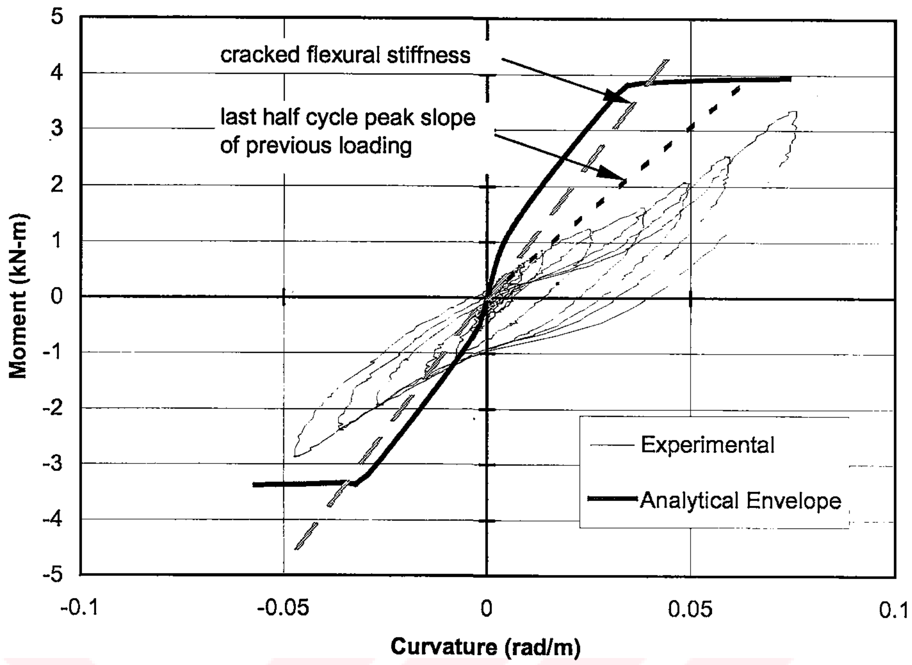

Figure 6.8 Analytical and experimental moment-curvature curves for the external left column at the base, Specimen R1 (frame with infill)

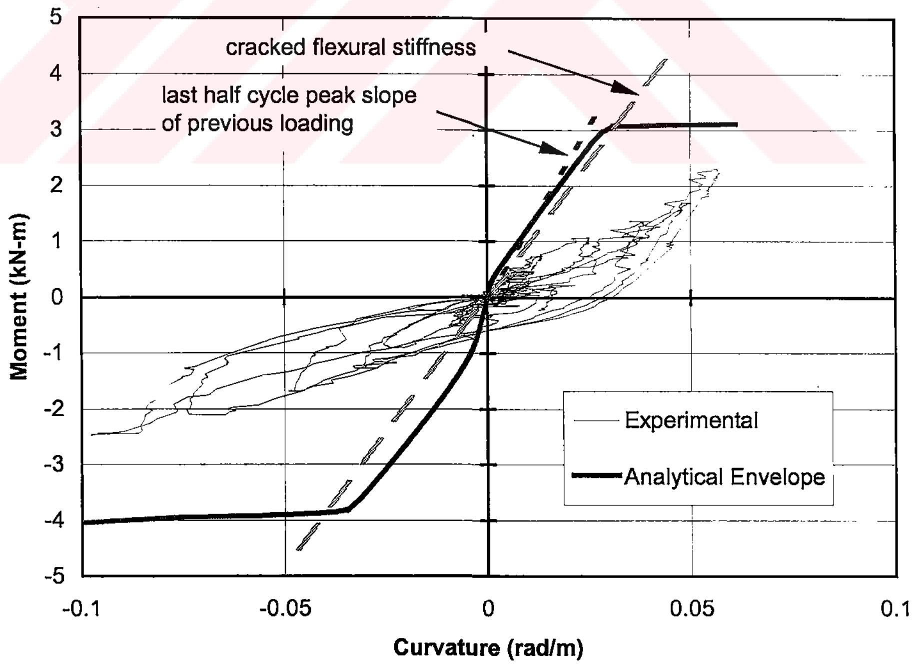

Figure 6.9 Analytical and experimental moment-curvature curves for the external right column at the base, Specimen R1 (frame with infill)

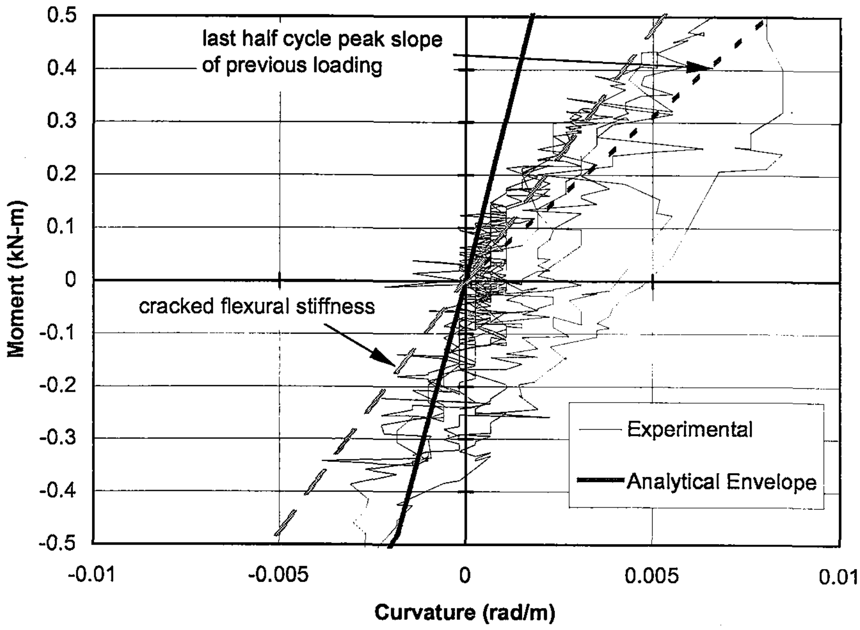

Figure 6.10 The first 8 cycles of the left external column at the base, Specimen R1 (frame with infill)

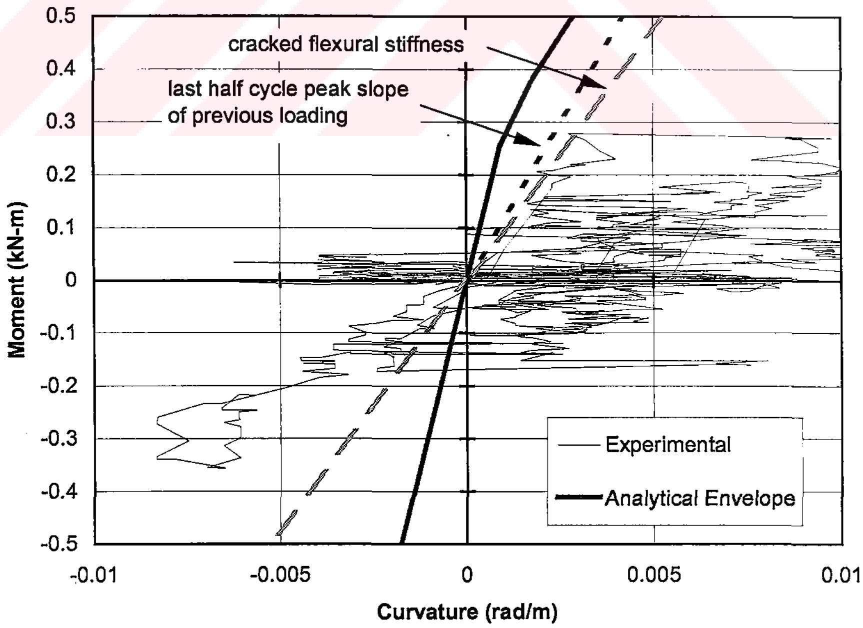

Figure 6.11 The first 8 cycles of the right external column at the base, Specimen R1 (frame with infill)

The moment and axial loads obtained from the transducers at the base of the external columns were compared with the values obtained from calculated interaction diagrams. The interaction curves were calculated by means of a computer program written by the author. Two analytical curves were computed; one considering the strain hardening of reinforcement and the other by neglecting the strain hardening of the reinforcement.

Figure 6.12 shows the interaction curves of the external columns of the bare frame. On these plots, the experimental M-N responses of the external columns were superimposed. Two interaction diagrams constitute a band for the strength envelope. Measured moment and axial load values indicate that, the observed strength of the columns remained in this band. For better visualizing the failure region of the diagram, this section was enlarged and reproduced in Figure 6.13. On the interaction curves, $N = 0.1\, f_{ck}\, A_c$ was shown with dashed lines. These figures clearly show that the level of the axial load applied on the columns was very low. Figure 6.14 shows the same interaction curves for the external columns of the infilled frame. The moment and axial load combination at the end of the test remained within the two interaction diagrams.

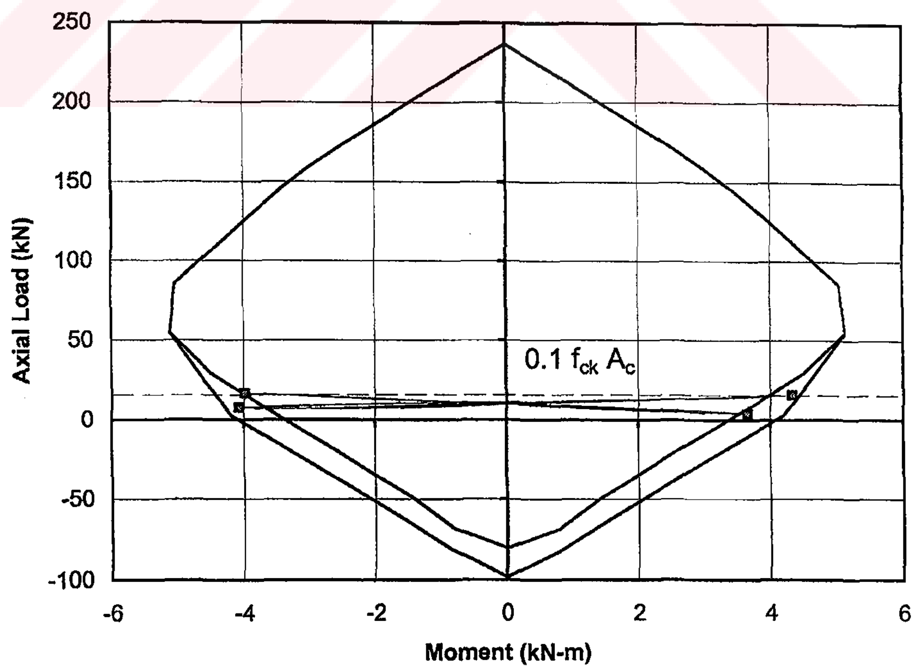

Figure 6.12 Analytical interaction curves and experimental M-N response of the external columns for the bare frame, Specimen B1

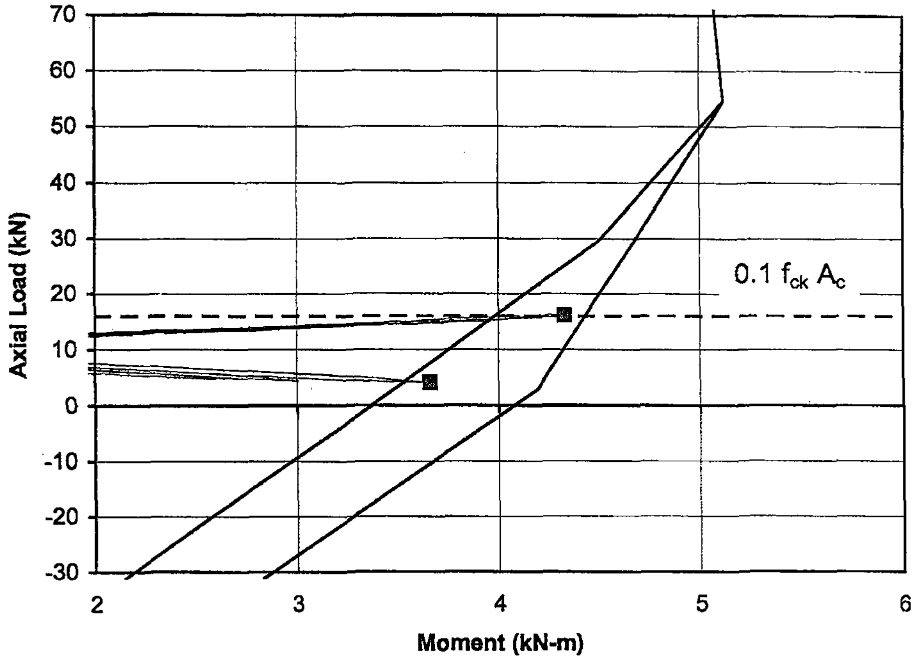

Figure 6.13 Analytical interaction curves and experimental M-N response of the external columns of the bare frame, Specimen B1

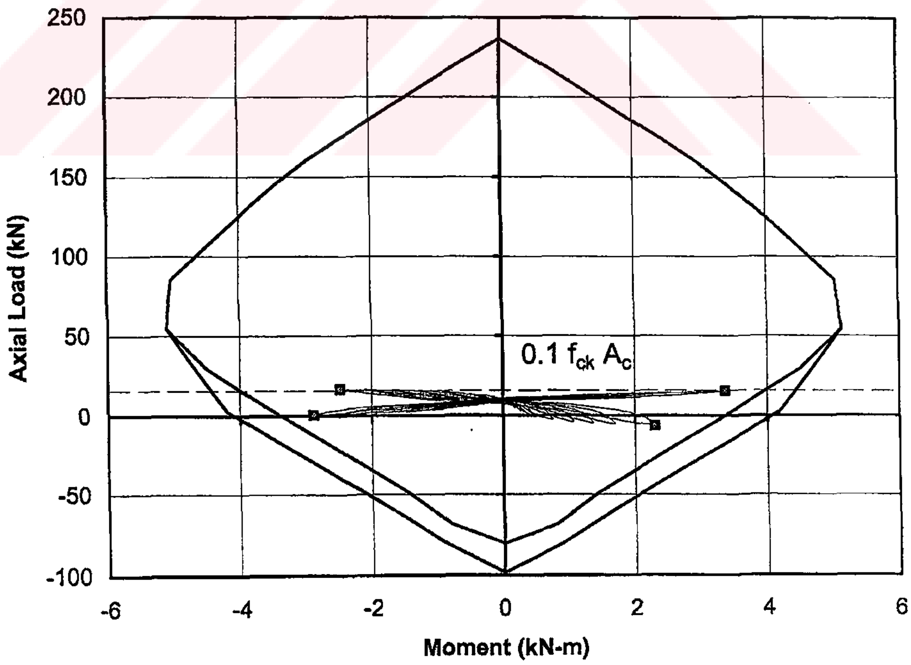

Figure 6.14 Analytical interaction curves and experimental M-N response of the external columns of the infilled frame, Specimen R1

Simple calculations were made to predict the experimental behavior of the two test specimens. To calculate the slope of the force deflection curves, the values given in Table 6.3 were used. The calculation of the moment of inertia of cracked sections was explained in detail during the discussion of moment-curvature curves. By means of the values given in Table 6.3, linear analysis was performed on both frames. For this analysis, computer program SAP2000(*) was used.

Table 6.3 E and I values used in the calculations

	I_{column} (mm^4)	I_{beam} (mm^4)	I_{infill} (mm^4)	$E_{column,beam}$ (MPa)	E_{infill} (MPa)
Gross	12 200 000	30 900 000	10 200 000 000	20 000	28000
Cracked	4 800 000	10 600 000	3 400 000 000	20 000	28000
Reduced	4 800 000	10 600 000	3 400 000 000	13 000	16 000

As a result of the linear analysis, three lines were drawn to predict the slope of the experimental envelope curves. Figure 6.15 and 6.16 compares the experimental envelope curves and analytical curves for the bare and infilled frame respectively. The steepest line (stiffness) was calculated using the values in the first row of Table 6.3. The second line represents the cracked section behavior in which only the moment of inertia was reduced. For the calculation of the third line, elastic modulus of concrete was also reduced due to the effect of cyclic loading. The reduced elastic modulus of concrete was determined as the half of the elastic modulus calculated according to TS-500.

The horizontal line in each figure at the top of the curves represent the lateral load capacity calculated from the limit analysis which will be discussed later.

At stages near the maximum load, the stiffness obtained from the experimental curve is less than the stiffness of the cracked section. This observation can be attributed to the slip of the column longitudinal bars.

(*) licensed by METU

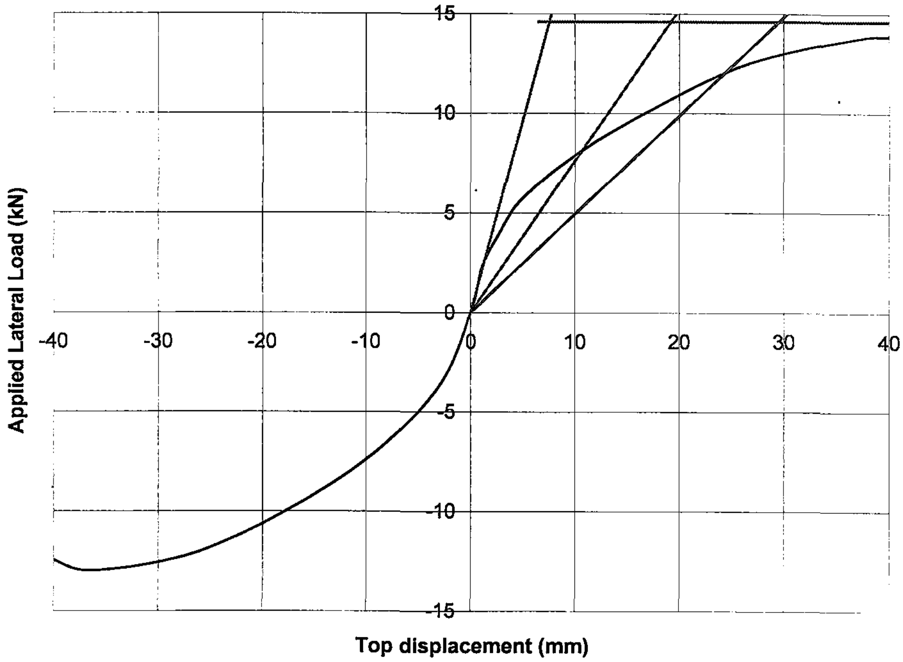

Figure 6.15 Comparison of the analytical stiffness curves and capacity with experimental envelope curve for Specimen B1

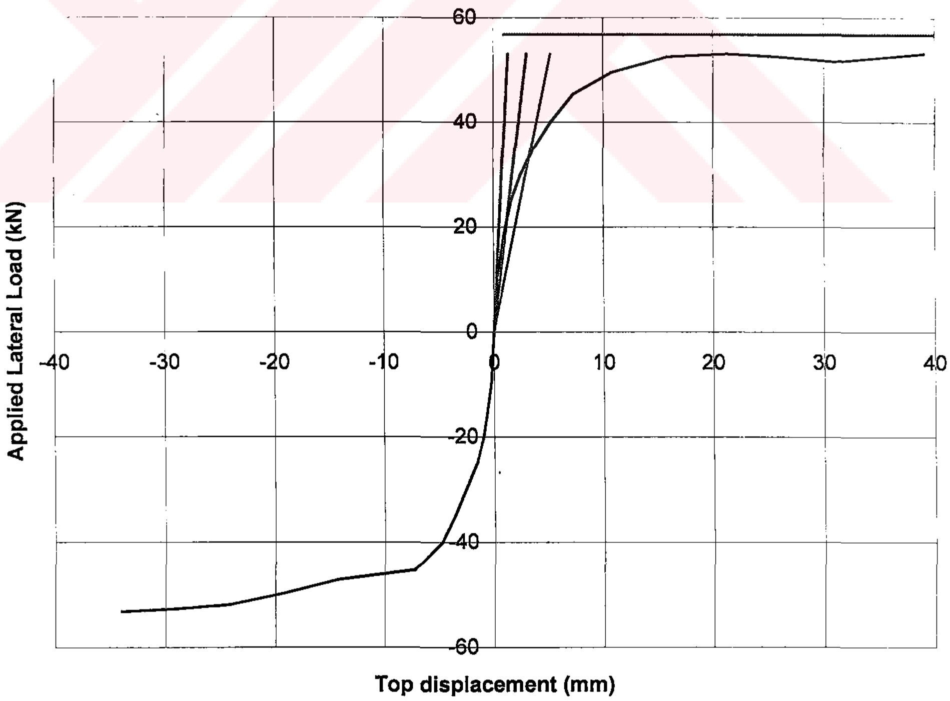

Figure 6.16 Comparison of the analytical stiffness curves and capacity with experimental envelope curve for Specimen R1

For the prediction of the maximum lateral load capacity, a limit analysis was performed. First, adequate numbers of plastic hinges were selected for the limit state of the frames. Then, the moment capacities of the columns, beams and infill wall were calculated. The lateral load P was calculated by equating the work done by internal forces to the work done by external loads. The axial deformations of the members were ignored. The collapse limit states of the bare and the infilled frames are shown in Figure 6.17. The rotation of the beam, θ_2 for the infilled frame was not equal to the rotation of columns, θ_1 due to the finite width of the columns and infill wall. The relation between θ_1 and θ_2 can be written as follows:

$$\theta_2 = \theta_1 \frac{L}{L_{eff}} = 1.36\theta_1$$

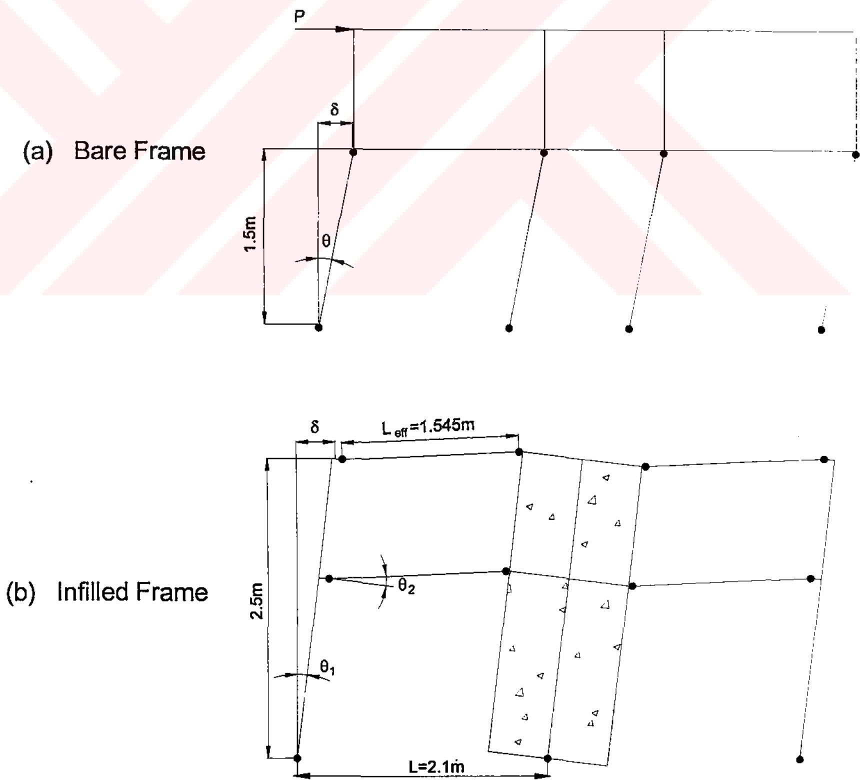

Figure 6.17 Collapse limit state of the bare and infilled frame for the limit analysis

The moment capacities of the columns change with the level of axial load on that column. But, a constant moment capacity was taken for simplicity. The axial load for moment calculations was taken as the load prior to application of the lateral load. Table 6.4 shows the moment capacities of the members, thus calculated.

Table 6.4 Calculated moment capacities of the members

	Column	Beam	Infill Wall
Moment Capacity (kN-m)	3.5	4.9	145

The analytical prediction of the lateral load P is given below for the bare and infilled frame.

Bare Frame (Figure 6.17 a):

$$P \cdot \delta = 8 \cdot M_{col} \cdot \theta$$
$$P \cdot 1.5 \cdot \theta = 8 \cdot M_{col} \cdot \theta$$
$$P = 18.7 \text{ kN}$$

Infilled Frame (Figure 6.17 b):

$$P \cdot \delta = 2 \cdot M_{col} \cdot \theta_1 + M_{wall} \cdot \theta_1 + 8 \cdot M_{beam} \cdot \theta_2$$
$$P \cdot 2.5 \cdot \theta_1 = 2 \cdot M_{col} \cdot \theta_1 + M_{wall} \cdot \theta_1 + 8 \cdot M_{beam} \cdot 1.36 \cdot \theta_1$$
$$P = 82.7 \text{ kN}$$

During the tests, the maximum lateral load applied to the bare and infilled frames were, 13.9 kN and 53.2 kN respectively. The experimental values were significantly lower than the calculated values. The reason for these differences was concluded to be the bond problem in the longitudinal reinforcement of the members. Therefore, analyses were repeated by taking into account the bond problem. It was intended to compute the member capacities considering the maximum forces developed in members using the actual anchorage lengths. To do this, a nominal bond stress had to be assumed. However, bond has been a very complex phenomenon and studying the bond stress was out of the scope of this thesis. Bond stresses vary along the length of the bar and therefore, using a nominal average bond stress seems to be more reasonable [60]. According to the bond tests on beams reinforced with plain bars, conducted by Mylrea [61], it was concluded that the average bond stress was about 1.7 MPa (250 psi). Additionally, ACI 318-56 [62] limited the allowable bond stress to $0.045f_c'$ (psi) for plain bars. If a factor of safety 2.0 is inherit in this formula, then for a concrete strength of 20 MPa, the formula gives approximately 1.7 MPa. Therefore, 1.7 MPa nominal bond stress was used in calculations.

The maximum stresses in the splice bars were calculated using a nominal bond stress of 1.7 MPa. The bond stress value was also checked using the results of the experimental studies of Sonuvar [59]. The bond stress multiplied by the surface area of the bar (length × perimeter), divided by the bar area would give the reduced stress in the bar. The stress in the bar was calculated using the following relationship:

$$\sigma_{s,bond} = \frac{(Splice\ Length)\cdot(\pi * \phi)\cdot \tau_{bond}}{\frac{\pi\phi^2}{4}}$$

The lapped splice length at the base of the inner columns was 40ϕ. The diameter of the longitudinal reinforcement of the columns was 8 mm. Therefore, the maximum stress developed in column longitudinal bars would be:

$$\sigma_{s,bond} = \frac{(40*8)*(\pi*8)*1.7}{\frac{\pi*8^2}{4}} = 272\ MPa$$

The capacity at the base of internal columns was calculated using the reduced bar stress given above.

Although, calculated moment capacities were used in analysis, for the external columns the measured values were used. In the bare frame test, maximum moments measured at base of the external columns were 3.5 kN-m and 4 kN-m. At the first story level, the lapped splice length of the first story columns was about 40ϕ. The lateral load capacity can be calculated by using the reduced strength of the columns. Assuming that the collapse mechanism is as shown in Figure 6.17 (a). The lateral load could be calculated using the following relationship:

$$P = \frac{M_{ext,left,bottom} + M_{ext,right,bottom} + M_{\mathrm{int},bottom} + M_{top}}{Height}$$

$$P = \frac{4 + 3.5 + 2 * 3.5 * 0.68 + 4 * 3.5 * 0.68}{1.5} = 14.5\ kN$$

Other types of mechanisms were studied in addition to mechanism given in Figure 6.17. In such mechanisms, reduction in strength due to bond was also considered. Lateral load capacities obtained from these mechanisms were not very different. Therefore, the simplest mechanism was taken as basis for the calculation of lateral load.

Reinforced concrete infill walls were used for the rehabilitation of the damaged bare frame. The force transfer between the infill wall and existing frame was achieved by means of dowels embedded into the frame members. During drilling of the holes for dowels, the bottom regions of the inner columns, where the lapped splices exist, were severely damaged. At this region, Hilti was used for drilling the holes, which was very strong for a 1/3 scale concrete column. Therefore, the concrete at the bottom regions of the inner columns were damaged. Afterwards, a small hand drill was used for making the holes which kept the damage at a minimum level. Therefore, it was decided to reduce the bond stress at base of inner columns for the infilled frame test. For this region, the bond stress was decreased from 1.7 MPa to 1.0 MPa (60% reduction). This reduced the bar stresses calculated, to 160 MPa.

During reversed cyclic loading, moments at the ends of the beams at external joints changed from negative to positive. Therefore, both the top and bottom longitudinal reinforcements could be in tension in these cycles. But, the bottom reinforcement of the beams were intentionally improperly detailed to represent the typical existing buildings. Bottom bars extended into the column and were terminated by 180° hooks. The anchorage lengths of these bottom bars were only 11ϕ. Also, the anchorage length of the top reinforcement was not fully adequate. At external beam-column joints, there was lack of confinement which if existed could improve the bond. The length of the anchorage was only 32ϕ for the top reinforcement of the beams at external joints. Since the longitudinal reinforcements were continuous along the length of the beams, there was no splice problem at the inner beam-column joints.

The reinforcement of the infill wall was also studied for the bond problem. It was found out that the dowels were stronger than the mesh reinforcement, considering the development lengths. The splice length of the mesh reinforcement was 50ϕ.

The moment capacities of the members thus calculated are summarized in Table 6.5. The moment capacities of the left and right outer joints of the beams swapped during the reversed loadings.

Table 6.5 Moment capacities of the members considering the bond problem (infilled frame)

	Moment Capacity (kN-m)	Yield Strength of Steel (MPa)	Assumed Bond Stress (MPa)	Splice Length (ϕ)	Developed Stress along the Splice (MPa)	Ratio of Actual to Yield Stress (%)	Actual Moment Capacity (kN-m)
Left External Column	Measured	-	-	-	-	-	3.3
Right External Column	Measured	-	-	-	-	-	2.4
Beam Internal Supports	5	400	No Bond Problem	-	-	-	5
Left Beam External Support	5	400	1.7	11	75	19	0.9
Right Beam External Support	5	400	1.7	32	218	54	2.6
Infill: Boundary Column	145	400	1.0	40	160	40	100
Infill: Wall Reinforcement		378	1.7	50	340	90	

The calculation of the lateral load capacity using limit analysis taking the reduced moment capacities given in Table 6.5 is given below (in limit analysis the mechanism shown in Figure 6.17 (b) is used):

$$P = \frac{M_{column,ext,left,bottom} + M_{column,ext,right,bottom} + M_{beam,\text{int}} + M_{beam,ext,left\&right} + M_{wall}}{Total\ Height}$$

$$P = \frac{3.3 + 2.4 + 4*5*1.36 + 2(0.9 + 2.6)1.36 + 100}{2.5} = 57.0 \text{ kN}$$

The maximum lateral load measured during the infilled frame test was 53.2 kN. The difference between the experimental and analytical values is quite small. Lateral load capacities of the frames calculated analytically were drawn in Figures 6.15 and 6.16. The agreement between the experimental curves and analytical lines were quite acceptable.

The advantage of the limit analysis was that the behavior of the test frame could be clearly understood. Many types of mechanisms were studied. All possible regions of bond failure were examined carefully. All these investigations helped to explain the behavior of the test structure during the experiments.

The load-deflection behavior of the test specimens was also studied using the computer program Drain-2DX. In this manner, push-over analysis was conducted on the analytical models to predict the experimental envelope behaviour of the test frames. Push-over analysis is a kind of nonlinear static analysis procedure that is generally used to evaluate the performance of structures under lateral loads. Displacement controlled loading was used during the analysis.

First, the analysis was performed ignoring the bond problems at the joints. In this case, the computer analysis gave much higher lateral load capacities as compared to the experimental values. Therefore, calculations were repeated considering the reduced moment capacities, calculated using the bar forces obtained for that development length.

Drain-2DX accepts axial load-moment interaction curve or just yield moment as the yield capacity of the members. In this study, interaction curves were used both for the columns and beams. Longitudinal reinforcement was 4ϕ8 bars both for columns and beams. The yield stress of the ϕ8 bars was 400 MPa. However, due to the inadequate development length and insufficient lapped splice lengths, the yield stress could not be developed at some regions. At the joints, where bond problem could occur, the yield stress was decreased proportional to the splice length of the reinforcement and interaction curves of those sections were calculated with reduces yield stresses. The reduced yield stresses were given in Table 6.5. Figure 6.18 shows the interaction curves of the columns, beams and infill wall considered in the computer program.

Elastic modulus "E" and moment of inertia "I" of the members used in the computer program were tabulated in Table 6.3. In the computer program cracked section inertia was used.

Infilled frame was modelled as a column element. To include the width of the infill wall in wire frame modelling, the ends of the beams connecting to the infill wall was modelled with rigid end zones. This type of modelling of the shear walls has been extensively used in the analysis of such structures.

In Figure 6.19 and 6.20, the experimental hysteretic curves and calculated push-over curves are presented for the bare and infilled frame respectively. According to these figures, the analytical models adequately simulated the behavior of the tests specimens. The initial stiffness and the lateral load capacities were simulated quite well. However, the decrease in the stiffness due to the reversed cyclic loading could not be well simulated. The reason was that the computer program could not consider the stiffness degradation due to the reversed cyclic loading and also does not take into account the reduction in stiffness due to axial tension.

The plastic hinge regions formed during the analysis are marked in Figure 6.21. The circles on the figure symbolize the plastic hinges. The size of the circles represents the amount of the accumulated plastic hinge rotations. The plastic hinge regions, which were found from the computer program, did not fully match with the predicted plastic hinge regions in limit analysis. However, the configurations of the plastic hinges from the computer program did not significantly change the results found in limit analysis.

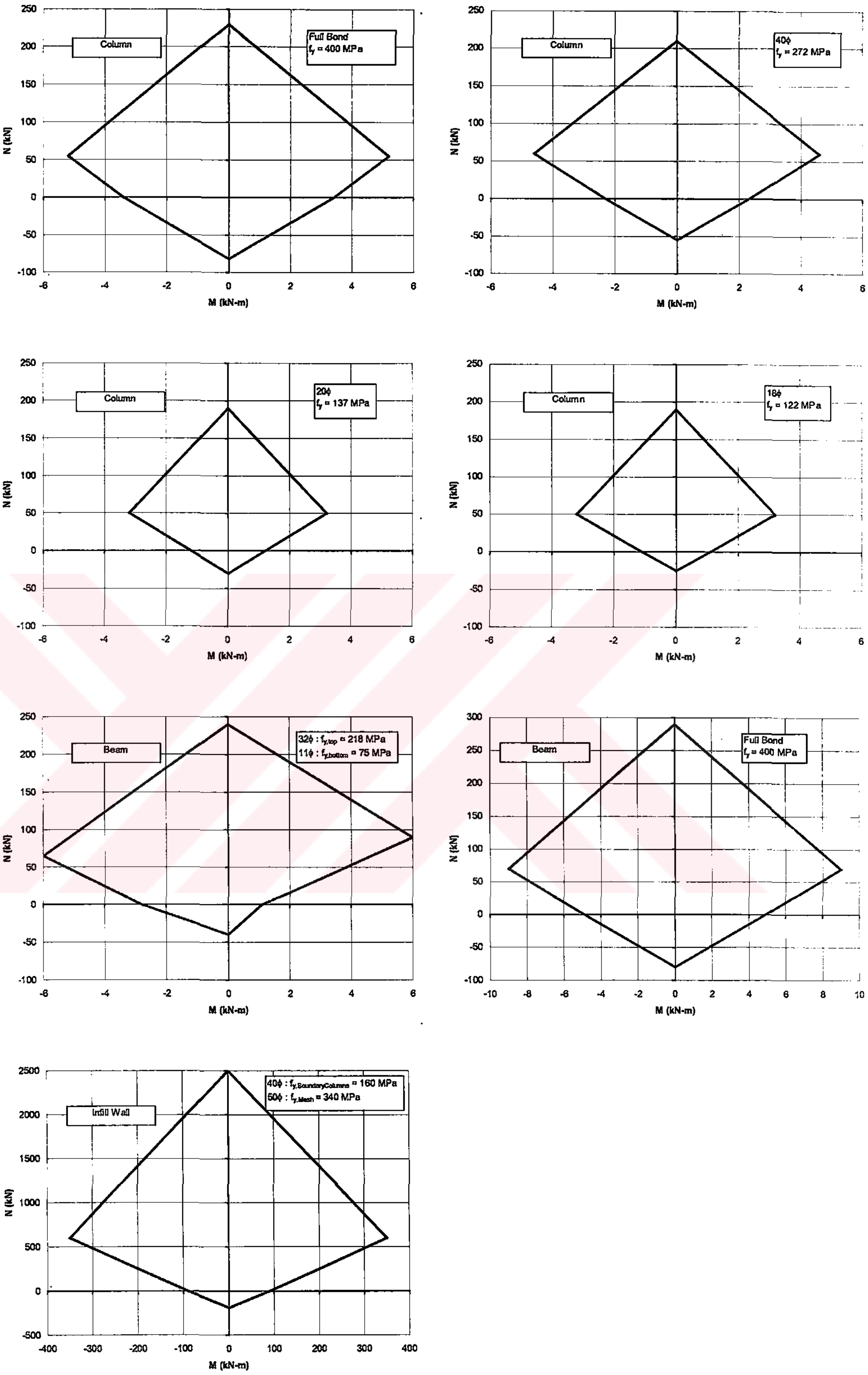

Figure 6.18 Axial load- moment interaction curves of columns, beams and the infill wall

Figure 6.21 indicates that the rotations at the bases of exterior columns were relatively small according to the results of the analysis. However, the measured values were much higher. In the evaluation of the moment-curvature relationships, high curvatures at low moment levels were discussed in detail. The difference between the measured and calculated rotations can be explained with probable slip in the longitudinal bars.

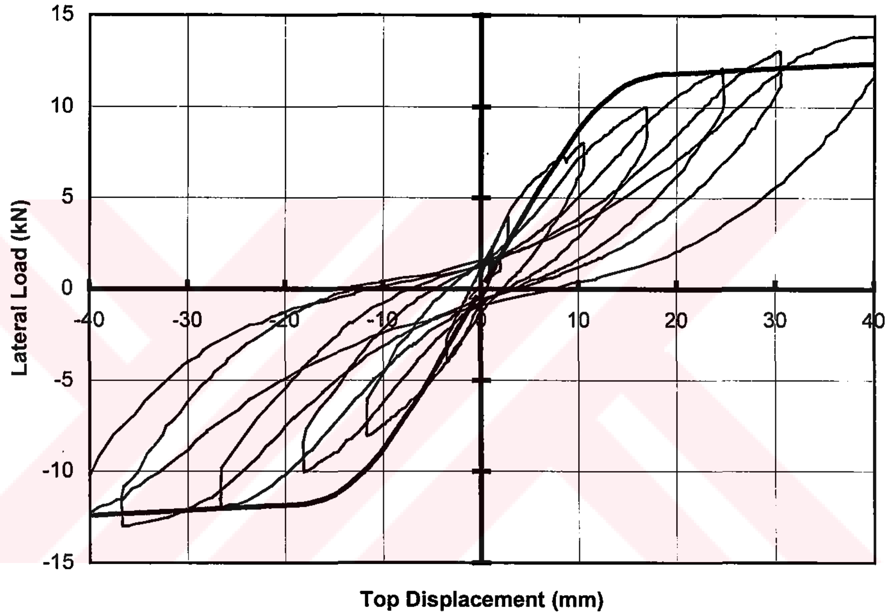

Figure 6.19 Push over analysis and experimental curves, Specimen B1 (bare frame)

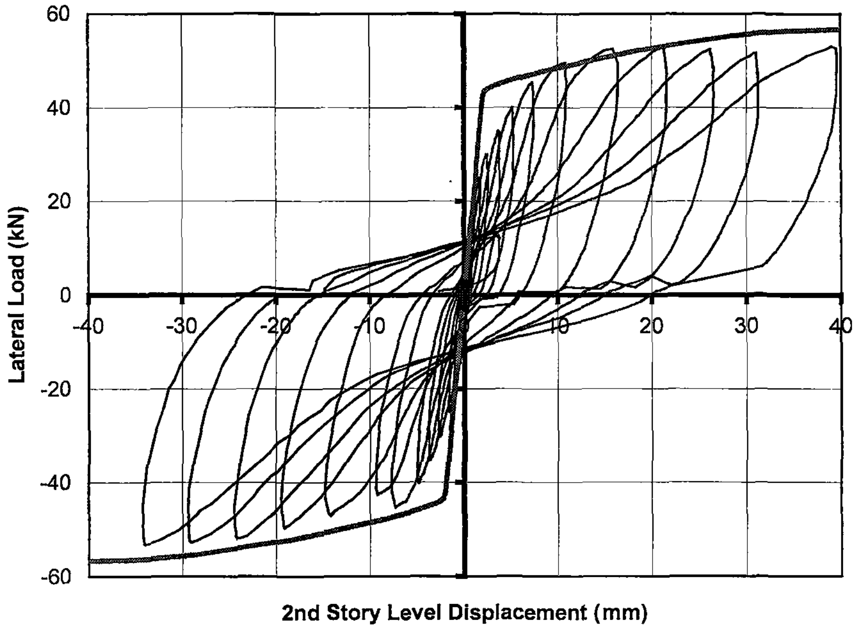

Figure 6.20 Push over analysis and experimental curves, Specimen R1 (infilled frame)

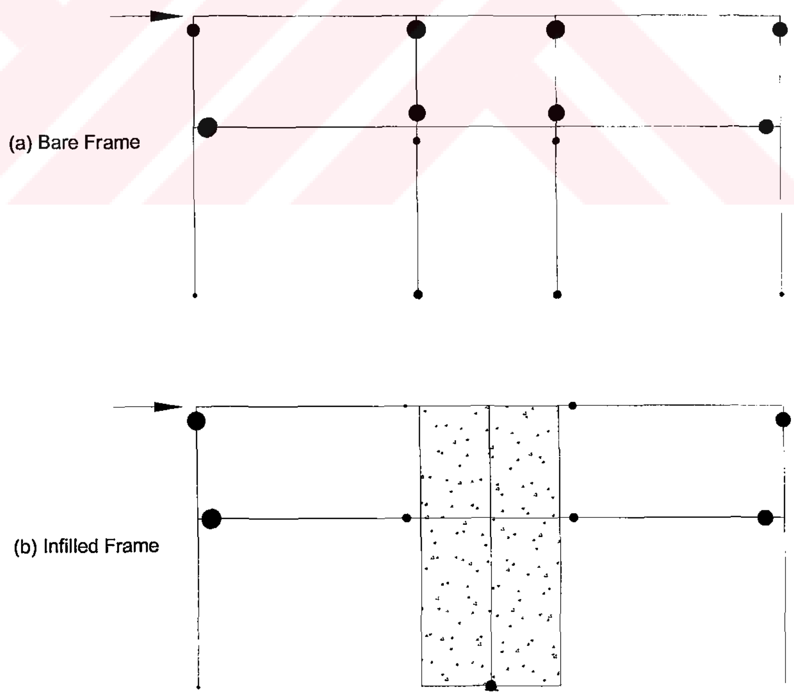

Figure 6.21 The plastic hinge regions and the intensity of the accumulated plastic hinge rotations

CHAPTER 7

CONCLUSIONS AND RECOMMENDATIONS

7.1 SUMMARY

The design and the construction quality of reinforced concrete buildings in Turkey are quite poor and therefore, these buildings have suffered considerable damage during the recent earthquakes. After these earthquakes, the large stock of damaged buildings had to be rehabilitated effectively in a short time. One of the major causes of damage in buildings was the inadequate lateral stiffness.

In practice, several approaches have been used in rehabilitation studies. The simplest and the most effective way of improving the behavior of such buildings, where unsatisfactory seismic behavior is inherent in the system, is to provide an adequate number of structural walls in both direction. Such walls not only increase the lateral stiffness significantly, but also relieve the existing frames from the lateral loads.

In the experimental studies at METU in the past twenty years, two-story, one-bay infilled frames were tested. In the study reported here, a three-bay, two-story frame in which only the middle bay was infilled was used as the test specimen. With such a test specimen, it was possible to study the sharing of the lateral force between the frame and the infilled panel (wall). In the test specimen, the frame members had most of the common weaknesses encountered in buildings in Turkey.

The infill was applied to the frame which was damaged under reversed-cyclic lateral load. The ratio of the wall to the total tributary area (assuming 0.7 m on each side of the frame) at the base was approximately 0.01. Special transducers were developed to measure the axial load, moment and shear at the base of the exterior columns.

The scope was limited to testing and analyzing one type of structure designed and built at the Structural Mechanics Laboratory of METU. The design of the force transducer for accurately measuring the internal forces in the first story columns of the test specimen was one of the most important accomplishments of this research. This involved the design, fabrication, calibration and installation of the force transducers.

7.2 CONCLUSIONS

The results presented in this thesis were obtained from one set of tests; bare frame and infilled frame having certain dimensions, reinforcement and material strength. Therefore, the generalization of the results obtained from such an experimental study can be misleading. It should be clearly pointed out that the test has been conducted to obtain trends and guidelines for rehabilitation process and the analytical studies have been conducted to understand the behavior of the test frame. The behavior of the prototype structures can be different from that of the sub-assemblages tested. Quality of materials, scale effect, workmanship, detailing of the reinforcement and experimental errors may affect the test results. Hence, the conclusions that are presented below should be evaluated in the light of these constraints and should not be generalized without making proper evaluation and judgement.

1. The test setup and instrumentation proved to be satisfactory for the investigation of framed structures rehabilitated by introducing infills to certain bays.

2. The axial load, shear and moments were measured at the base of exterior columns by the special transducers developed. With these measured values, it was possible to observe the distribution of lateral force to the wall and columns.

3. The infill wall introduced to the damaged frame carried almost the entire lateral load applied to the frame prior to yielding. Prior to failure stage, 90% of the lateral load was carried by the infill wall. The ratio of the wall area to the floor area at the base was approximately 1%.

4. The initial stiffness of the specimen with the infill was about 15 times that of the bare frame. This is a very significant increase considering that the infill was introduced to a damaged frame.

5. The lateral load carrying capacity of the frame increased approximately 4 times with the introduction of infill wall to the damaged bare frame. It should be also noted that the deformation capability of the infilled frame was quite high.

6. Energy dissipation capacity of the frame increased considerably as a result of the introduction of the infill wall. Moreover, such an increase in the energy dissipation capacity was obtained with smaller displacement amplitudes and much higher lateral loads.

7. The story drift of the infilled structure was very small up to the level where the wall reached its capacity. After this stage, the infilled frame specimen showed a ductile behavior. The drift ratio increased up to 1.6 % towards the end of the test, without any collapse.

8. The moment-curvature behavior of the undamaged columns could be calculated satisfactorily. But, the moment-curvature of a damaged section could not be calculated accurately, because of the past load history.

9. Interior columns had lap splice length of 40 bar diameters. Even with this length, there were slip problems. This was probably caused by the ill behavior of plain bars under reversed cyclic loading.

10. By means of limit analysis and of simple stiffness calculations of the gross section and cracked section, the behavior of the frame was quite well calculated. In the limit analysis, the reduction of the moment capacities of the members due to the bond problem was taken into account.

11. The pushover analysis revealed that after yielding of the wall, plastic hinges would develop in the first story beams, since at the exterior joints summation of column capacities are greater than that of the beam. This was also observed in the test. In the second story, pushover analysis indicated hinging at the top of the exterior column. However, in the test, hinging was at the exterior end of the beam. This was probably due to the premature failure of the beams at exterior beam-column connections. This premature failure was caused by the slip of the beam bottom bars which had inadequate anchorage length. Test results indicated that inadequate anchorage of beam bottom bars, as commonly done in practice, can cause problems under reversed loading.

12. The analysis could not predict the behavior even of the bare frame specimen with reasonable accuracy. This was mainly due to the local bond problems and severe cracking at the beam-column joints. Therefore, in the analysis of the real structures, it should be kept in mind that the results obtained are merely approximate.

13. Comparison of calculated and experimental results revealed that the infill wall can be modeled as "column" with rigid arms at story levels. The moment capacities of the members at probable yield regions have to be reduced considering their bond characteristics. In this manner, the push over analysis estimated the envelope behavior of the frames reasonably well.

14. Analysis resulted in relatively small rotations at the bases of exterior columns. However, the measured values were much higher. This is probably due to the slip in the longitudinal bars.

15. An analysis of the test results indicated that the wall capacity was also reduced due to inadequate anchorage length of longitudinal bars of columns located at the boundaries of the infill. To get the full capacity, it will be necessary to apply partial strengthening to the boundary columns at regions where anchorage problems exist.

7.3 RECOMMENDATIONS

The following recommendation can be made for future research, using the same test set-up:

1. In this study, the lateral load was applied at second story exterior beam-column joint. The load was changed from compression to tension at each cycle. Applying tension to the joint damaged the joint and the second story beams. In the future studies the lateral load can either be applied to the interior beam or can be applied as compression to the right and left exterior joints.
2. The axial load level of the columns should be increased.
3. It would be desirable to measure the curvatures at the base of the wall. Also, if the rigid body rotation of the wall at the base due to the bar slip was measured, the behavior could be better understood.
4. Members with inadequate lap spliced bars should be carefully investigated. Tests can be performed after partial strengthening of the columns in regions where anchorage problem exists.

REFERENCES

1. Sugano, S., "Aseismic Strengthening of Existing Reinforced Concrete Buildings", Proceedings of the first Seminar on Repair and Retrofit of Structures, US/Japan Cooperative Earthquake Engineering Research Program, May, 1980, pp.13-40
2. Wyllie, L.A.Jr., "Strengthening Strategies for Improved Seismic Performance", Proc. of the 11th WCEE, Paper No. 1424, 1996
3. Ersoy, U., "Seismic Rehabilitation - Applications, Research and Current Needs", Proc. of the 11th WCEE, Paper No. 2099, 1996
4. Sugano, S., "State - of - the - Art in Techniques for Rehabilitation of Buildings", Proc. of the 11th WCEE, Paper No. 2175, 1996
5. Üzümeri, Ş.M., Tankut, T., Özcebe, G., Atımtay, E., "Assessment, Repair/Strengthening of Moderately Damaged Reinforced Concrete Buildings in Ceyhan Earthquake (1998)", Uğur Ersoy Symposium on Structural Engineering, Proceedings, METU-Department of Civil Engineering, Ankara, Turkey, July 1999)
6. Vintzeleou, E., "Behaviour of Infilled Frames Subject to Lateral Actions (A State-of-the-Art Report)", CEB-IMOIS-METU Seminar on Assessment and Redesign of Reinforced Concrete Structures, İzmir, Turkey, April, 1989, pp.1-60
7. Ersoy, U., Uzsoy, S., "The Behavior and Strength of Infilled Frames", Report No. MAG-205 TUBITAK, Ankara, Turkey, 1971, In Turkish
8. Higashi, Y., Kokusho, S., "The Strengthening Method of Existing Reinforced Concrete Buildings", U.S.-Japan Cooperative Research Program in Earthquake Engineering, 1975, Honolulu H1
9. Kahn, L.F., Hanson, R.D., "Infilled Walls for Earthquake Strengthening", Proc. of the ASCE, Vol. 105, No. ST2, February, 1979, pp. 283-296
10. Hanson, R.D., "Repair and Strengthening of Buildings", Proc. of the 7th WCEE, İstanbul, Vol. 9, 1980, pp. 71-74
11. Higashi, Y., Endo, T., Okhubo, M., Shimizu, Y., "Experimental Study on Strengthening Reinforced Concrete Structure by Adding Shear Wall", Proc. of the 7th WCEE, İstanbul, Vol. 7, 1980, pp.173-180
12. Endo, T., Adachi, H., Nakanishi, M., "Force-Deformation Hysteresis Curves of Reinforced Concrete Shear Walls", Proceeding of the 7th World Conference on Earthquake Engineering, Vol. 6, İstanbul, 1980
13. Sugano, S., Fujimura, M., "Aseismic Strengthening of Existing Reinforced Concrete Buildings", Proc. of the 7th WCEE, İstanbul, 1980 Vol.4

14. Ohki, K., Bessho, S., "Experimental Investigation on Aseismic Strengthening for Existing Reinforced Concrete frames", Proceedings of the 7th World Conference on Earthquake Engineering, Vol. 6, Istanbul, 1980

15. Hayashi, Y., Niwa, H., Fukuhara, M., "The Strengthening method of the Existing R/C Buildings", 7th World Conference on Earthquake Engineering, Vol. 4, Sept. 1980, Istanbul, Turkey

16. Sugano, S., "Aseismic Strengthening of Existing Reinforced Concrete Buildings", Proceedings of the first Seminar on Repair and Retrofit of Structures, US/Japan Cooperative Earthquake Engineering Research Program, May 1980

17. Higashi, Y., Endo, T., Shimizu, Y., "Effects on Behaviors of Reinforced Concrete Frames by Adding Shear Walls", Proceedings of the third Seminar on Repair and Retrofit of Structures, Ann Arbor, 1982 May

18. Higashi, Y., Endo, T., Shimizu, Y., "Experimental Studies on Retrofitting of Reinforced Concrete Building Frames", 8th World Conference on Earthquake Engineering, Vol. 1, pp. 477-484, 1984, San Francisco CA

19. Aoyama, H., Kato, D., Katsumata, H., Hosokawa, Y., "Strength and Behavior of Postcast Shear Walls for strengthening of existing R/C Buildings", 8th World Conference on Earthquake Engineering, 1984 July, San Francisco CA, Vol. 1, pp.485-492

20. Liauw, T.C., Kwan, K.H., "Unified Plastic Analysis for Infilled Frames", ASCE Journal of Structural Division, Vol. 111, No 7, July 1985, pp. 1427-1449

21. Jirsa, J.O:, Kreger, M.E., "Recent Research on Repair and Strengthening of Reinforced Concrete Structures", ASCE Structures Congress, Vol. 1, 1989

22. Altın, S., "Strengthening of R/C Frames with R/C Infills", A Doctor of Philosophy Thesis in Civil Engineering, Middle East Technical University, February 1990.

23. Altın, S., Ersoy, U., Tankut, T., "Seismic Strengthening of Reinforced Concrete Frames with Reinforced Concrete Infills", Report No. METU/SML-90/01, Ankara, Turkey, June, 1990

24. Altın, S., Ersoy, U., Tankut, T., "Hysteretic Response of Reinforced Concrete Infilled Frames", Journal of Structural Engineering, Vol. 118, No. 8, Aug., 1992

25. Valluvan, R., Kreger, M.E., Jirsa, J.O., "Strengthening of Column Splices for Seismic Retrofit of Nonductile Reinforced Concrete Frames", ACI Structural Journal, Vol. 90, No.4, July 1993

26. Miller, J.T., Reaveley, L.D., "Historic Hotel Utah Remodel and Seismic Upgrade", SP. 160-5, 1996

27. Gregorian, Z.B., Gregorian, G.B., "Seismic Upgrading of Hospital Building No. 6 and 7, VA Medical Center, Bedford, Mass.", SP 160-6, 1996

28. Paulay, T., Priestly, M.J.N., "Seismic Design of Reinforced Concrete and Masonry Buildings", John Wiley & Sons, Inc., 1992

29. Phan, L.T., Lew, H.S., "Strengthening Methodology for Lightly Reinforced Concrete Frames", Proc. of the 11th WCEE, Paper No. 1896, 1996

30. TS-500, Requirements for Design and Construction of Reinforced Concrete Structures, Ankara, 2000

31. Wyllie, Jr.L.A., "Strengthening Strategies for Improved Seismic Performance", Proc. of the 11th WCEE, Paper No. 1224, 1996

32. Hidalgo, P., Clough, R.W., "Earthquake Simulator Study of a Reinforced Concrete Frame", Report No. UCB/EERC-74/13, University of California, Berkeley, 1974

33. Oliva, M.G., "Shaking Table Testing of a Reinforced Concrete Frame with biaxial Response", Report No. UCB/EERC-80/28, University of California, Berkeley, 1980

34. Aktan, A.E., Bertero, V.V., "The Seismic Resistant Design of R/C Coupled Structural Walls", Report No. UCB/EERC-81/07, University of California, Berkeley, 1981

35. Aktan, A.E., Bertero, V.V., Chowdhury, A.A., Nagashima, T., "Experimental and Analytical Predictions of the Mechanical Characteristics of a 1/5-Scale Model of a 7-Story R/C Frame-Wall Building Structure", Report No. UCB/EERC-83/13, University of California, Berkeley, 1983

36. Sause, R., Bertero, V.V., "A Transducer for Measuring the Internal Forces in the Columns of a Frame-Wall Reinforced Concrete Structure", Report No. UCB/EERC-83/05, University of California, Berkeley, 1983

37. The Technical Staff of Measurements Group, "Strain Gage Based Transducers, Their Design and Construction", Measurements Group, Inc., 1988

38. "Transducer-Class Strain Gages, Bondable Resistors, Installation Accessories", Micro-Measurement Division, Catalog TC-116-4, 1992

39. Wilson, E.L., Habibullah, A., "SAP90 Structural Analysis Users Manual", Computers and Structures, Inc., 1992

40. Prakash, V., Powell, G.H., Campbell, S., "DRAIN-2DX Base Program Description and User Guide", Version 1.10, Report No. UCB/SEMM-93/17, 1993

41. Perry, C.C., Lissner, H.R., "The Strain Gage Primer", McGraw-Hill Book Company, Second Edition, 1962

42. Potma, T., "Strain Gauges, Theory and Application", Philips Paperbacks, 1967

43. Neubert, H.K.P., "Strain Gauges, Kinds and Uses", MacMillan & Co. Ltd., 1967

44. Dally, J.W., Riley, W.F., "Experimental Stress Analysis", McGraw-Hill, Inc., Third Edition, 1991

45. "Optimizing Strain Gage Excitation Levels", TN-502, Tech Note, Measurements Group, 1979

46. "Strain Gage Thermal Output and Gage Factor Variation with Temperature", TN-504-1, Tech Note, Measurements Group, 1993

47. "Strain Gage Selection Criteria, Procedures, Recommendations", TN-505-4, Tech Note, Measurements Group, 1989

48. "Surface Preparation for Strain Gage Bonding", Instruction Bulletin B-129-7, Measurements Group, 1996

49. "Strain Gage Installations with M-Bond 200 Adhesive", Instruction Bulletin B-127-14, Measurements Group, 1999

50. Tankut, T., "Experimental Stress & Strain Analysis", Lecture Notes, Middle East Technical University, 1978

51. "Rehabilitation of Moderately Damaged R/C Buildings after the 1 October 1995 Dinar Earthquake", Report No: METU/EERC 99-01, Ankara, 1999

52. Ersoy, U., Özcebe, G., Tankut, T., Türk, M., Sonuvar, M.O., "Behavior of RC Infilled Frames, an Experimental Study", Proceedings of the 2nd Japan-Turkey Workshop on Earthquake Engineering, Volume 1, İstanbul, Turkey, 1998

53. ACI, American Concrete Institute, Committee 318, Building Code Requirements for Reinforced Concrete (ACI 318-95) and Commentary (ACI 318-R-95), Michigan, 1995

54. UBC, 1997 Uniform Building Code, 5360 Workman Mill Road, Whittier, California 90601-2298, USA, 1997

55. Sozen, M.A., "Toward a Behavior Based Design of Reinforced Concrete Frames to Resist Earthquake", Proceedings of the 9th Technical Conference of Turkish Society of Civil Engineering, Vol.1, Ankara, Turkey, Nov. 1987 (in Turkish)

56. Turkish Seismic Code, Ministry of Public Work, Ankara, 1998

57. Mayes, G.T., Sozen, M.A., Siess, C.P., "Tests on a Quarter-Scale Model of a Multiple-Panel Reinforced Concrete Flat Plate Floor", Structural Research Series No. 181, Department of Civil Engineering, University of Illinois, 1959

58. Tankut, A.T., "The Behaviour of the Reinforced Concrete Flat Plate Structures Subjected to Various Combinations of Vertical and Horizontal Loads", Ph.D. Thesis, Imperial College, 1969

59. Sonuvar, M. O., "Hysteretic Response of Reinforced Concrete Frames Repaired by Means of Reinforced Concrete Infills", A Doctor of Philosophy Thesis in Civil Engineering, Middle East Technical University, June 2001

60. ACI 408, "Bond Stress – The State of the Art", reported by ACI Committee 408, Journal of the American Concrete Institute, V.63, 1966

61. Mylrea, T. D., "Bond and Anchorage", Journal of the American Concrete Institute, V.44, 1948

62. ACI 318-56, "Building Code Requirements for Reinforced Concrete", Journal of the American Concrete Institute, V.52, 1956

63. Türk, A. M., "Rehabilitation of Reinforced Concrete Infill Walls", A Doctor of Philosophy Thesis in Civil Engineering, Boğaziçi University, 1998

64. PCA, "Notes on ACI 318-99 Building Code Requirements for Structural Concrete", Portland Cement Association, 1999

65. ATC-43 Project: FEMA Reports 306-8, "Evaluation and Repair of Earthquake Damaged Concrete and Masonry Wall Buildings", Applied Technology Council, 1998

APPENDIX A

EVALUATION OF SHEAR DEFORMATIONS

In this appendix, the computation of shear displacement is presented. Shear deformations on the panels were measured by means of diagonally placed dial gages. Since two displacement readings were taken along the diagonals, it is possible to determine the deformed shape of the wall panel. Approximate deformed shape of the panel is presented in Figure A.1.

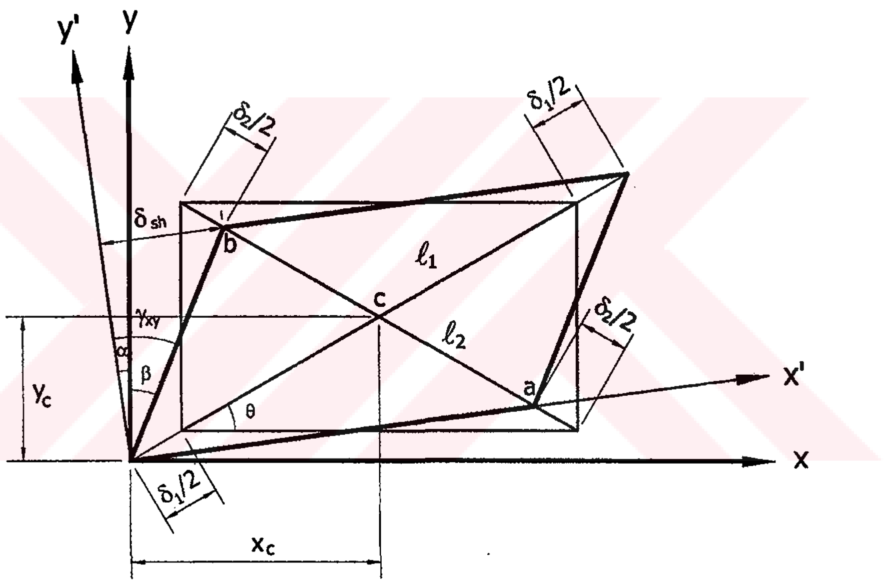

Figure A.1 Rectangular Shape Distortion

According to the geometry shown above, shear deformations can be computed approximately as follows.

$$\theta = \arctan\left(\frac{h}{w}\right)$$

h height of the rectangle

w width of the rectangle

$$\ell'_1 = \ell_1 + \delta_1 = \ell_1(1+\varepsilon_1)$$

$$\ell'_2 = \ell_2 + \delta_2 = \ell_2(1+\varepsilon_2)$$

ℓ_1 length of diagonal 1

ℓ_2 length of diagonal 2

ℓ'_1 length of diagonal 1 after deformation

ℓ'_2 length of diagonal 2 after deformation

ε_1 strain in diagonal 1 direction

ε_2 strain in diagonal 2 direction

δ_1 total elongation in diagonal 1 direction

δ_2 total elongation in diagonal 2 direction

$$x_c = \frac{\ell'_1}{2}\cos(\theta)$$

$$y_c = \frac{\ell'_1}{2}\sin(\theta)$$

$$x_a = x_c + \frac{\ell'_2}{2}\cos(\theta) = \left(\frac{\ell'_1 + \ell'_2}{2}\right)\cos(\theta)$$

$$y_a = y_c - \frac{\ell'_2}{2}\sin(\theta) = \left(\frac{\ell'_1 - \ell'_2}{2}\right)\sin(\theta)$$

$$x_b = x_c - \frac{\ell'_2}{2}\cos(\theta) = \left(\frac{\ell'_1 - \ell'_2}{2}\right)\cos(\theta)$$

$$y_b = y_c + \frac{\ell'_2}{2}\sin(\theta) = \left(\frac{\ell'_1 + \ell'_2}{2}\right)\sin(\theta)$$

Shear deformation γ_{xy} is defined as the sum of the angles α and β shown in Figure A.1. Angles α and β can be obtained easily from the following equations.

$$\alpha = \arctan\left(\frac{y_a}{x_a}\right) = \arctan\left(\frac{\left(\frac{\ell'_1 - \ell'_2}{2}\right)\sin(\theta)}{\left(\frac{\ell'_1 + \ell'_2}{2}\right)\cos(\theta)}\right) = \arctan\left(\frac{\ell'_1 - \ell'_2}{\ell'_1 + \ell'_2}\tan(\theta)\right)$$

$$= \arctan\left(\frac{\ell'_1 - \ell'_2}{\ell'_1 + \ell'_2}\left(h/_w\right)\right) = \arctan\left(\frac{\varepsilon_1 - \varepsilon_2}{2 + \varepsilon_1 + \varepsilon_2}\left(h/_w\right)\right)$$

$$\beta = \arctan\left(\frac{x_b}{y_b}\right) = \arctan\left(\frac{\left(\frac{\ell'_1 - \ell'_2}{2}\right)\cos(\theta)}{\left(\frac{\ell'_1 + \ell'_2}{2}\right)\sin(\theta)}\right) = \arctan\left(\frac{\ell'_1 - \ell'_2}{\ell'_1 + \ell'_2}\cot(\theta)\right)$$

$$= \arctan\left(\frac{\ell'_1 - \ell'_2}{\ell'_1 + \ell'_2}\left(w/_h\right)\right) = \arctan\left(\frac{\varepsilon_1 - \varepsilon_2}{2 + \varepsilon_1 + \varepsilon_2}\left(w/_h\right)\right)$$

$$\gamma_{xy} = \alpha + \beta$$

δ_{sh} shown in Figure A.1 could easily be obtained from geometry. The shear-displacement values could than be computed using the following equation.

$$\delta_{sh} = \gamma_{xy} \cdot h$$

Shear-displacement value (δ_{sh}) measured for each panel was the interstory shear-displacement for that story. Total shear-displacement curve can be calculated by summing the shear-displacements of each panel.

It must be realized that the sensitivity and placement of the instrumentation was not sufficient to obtain accurate values of the shear distortions at infill panel. It is difficult to get accurate measurements of shear deformations due to uncertainties introduced by panel cracking.

VITA

Erdem CANBAY was born in Karabük on August 11, 1970. He received his B.Sc. degree from İstanbul Technical University in 1992 and M.Sc. degree from Middle East Technical University in 1995. His main area of interest is rehabilitation of the structures.

EDUCATION

September 1995- present : Middle East Technical University, Ankara, Turkey Civil Engineering, PhD, GPA: 3.63/4.00

February 1993- June 1995 : Middle East Technical University, Ankara, Turkey Civil Engineering, Master of Science GPA: 3.64/4.00

September 1988- June 1992: İstanbul Technical University, İstanbul, Turkey Civil Engineering, Bachelor of Science GPA: 82.78/100

EXPERIENCE

March 2001-present PROJECT ENGINEER (Researcher):

Department of Civil Engineering, Division of Structural Mechanics, Middle East Technical University, Turkey. He has been working as engineer in different projects.

October 1993-March 2001 RESEARCH ASSISTANT(involves teaching also)

Department of Civil Engineering, Division of Structural Mechanics, Middle East Technical University, Turkey. Have been responsible for the following courses (teaching assist): CE382-Reinforced Concrete Fundamentals, CE481-Reinforced Concrete Structures, CE221-Engineering Mechanics I and CE520-Graduate Seminar (Structures). Taught "Civil Engineering Drawing with AutoCAD" course for one year. Responsible assistant for the structural mechanics laboratory for the last four years. Conducted experimental and analytical research on High Strength Concrete Columns during the masters program. Presently, conducting experimental and analytical studies on the contribution of R/C infills on the seismic behaviour of structural systems as part of the PhD study.

Earthquake Engineering Research Center, Middle East Technical University, Turkey. Part of the team that carried out repair and strengthening projects of both masonry and reinforced concrete structures after 1995 Dinar Earthquake, 1998 Ceyhan Earthquake and 1999 Marmara Earthquake.

May 1993-September 1993 DESIGNER

Part of the team that carried out structural design of Underground Stations of Ankara Underground Transportation Network at TABAR Engineering Consultancy Service.

COMPUTER SKILLS

Use of Finite Element program SAP, nonlinear inelastic dynamic analysis program DRAIN

Development of softwares using BASIC, FORTRAN, PASCAL, DELPHI, DBASE.

Several editing, graphical and spreadsheet programs.

MS-DOS and Windows-2000 Operating Systems.

Many Internet Applications

LANGUAGES

English and German

LIST OF PUBLICATIONS

Canbay, E., "Behaviour of High-Strength Concrete Columns under Eccentric Compression - Tied Columns", Master of Science Thesis, Middle East Technical University, 1995.

Türel, G., Canbay, E., Cumhur, K., and Sucuoğlu, H., "Capacity Analysis of a Moderately Damaged Reinforced Concrete Building before and after Strengthening", Proceedings of 4^{th} National Earthquake Engineering Conference, Ankara, Turkey, pp. 341-348, 1997, (in Turkish)

Canbay, E., Sucuoğlu, H., "Seismic Assessment of Damaged-Repaired Reinforced Concrete Buildings", Proceedings of 2nd Japan-Turkey Workshop on Earthquake Engineering, İstanbul, Turkey, Vol.1, pp.132-151, 1998

Editors:Wasti, S.T., Sucuoğlu, H., Contributors: Ersoy, U., Özcebe, G., Tankut, T., Utku, M., Canbay, E., Gür, T., Kaur, C.,"Rehabilitation of Moderately Damaged R/C Buildings after the 1 October 1995 Dinar Earthquake", Report No: METU/EERC 99-01, April, 1999, Ankara

HONORS

Award for being second best among 213 students during undergraduate study in İstanbul Technical University (1992)